高効率プラズマロボット溶接システムの開発

Development of High Efficiency Plasma Robotic Welding System

２０１７年3月

埼玉大学大学院理工学研究科（博士後期課程）

理工学専攻（主指導教員　山根　敏）

王　維西

PREFACE

This thesis treats the problem which is concerning the development of high efficiency plasma robotic welding system by means of several kinds of image processing.

It is commonly thought to be important of acquiring stable back bead for joining in butt welding of thick plate so as to achieve welded metal joint of high quality. Since the current of high density has been employed in plasma arc welding (PAW), it will be more appropriate for thick material in energy saving and efficiency promoting, provided that welding conditions are applicably supplied and torch guidance is under an exact control during welding process. Known as keyhole welding, the keyhole in PAW depends on the orifice gas and welding current, directly corresponding to the back bead, and owing to the strong pressure of plasma arc, keyhole will come into being under the electrode.

In PAW, welding quality and efficiency is further improved by the process control, which is being widely applied and broadly divided into two strategies: seam tracking (also known as joint tracking) and weld formation control. Seam tracking involves real-time tracking just ahead of where the weld is being deposited. Besides shifting the robot or machine trajectory, this technique alters

the weld bead formation by adaptive control. And the weld formation control can be divided into the penetration control and deposited metal control.

While the electrode hides in large plasma torch, it is difficult to teach the welding robot and trace the weld line exactly by human eyes during the welding process. Moreover, on account that arc length, which is related to welding voltage and current, almost keeps constant in PAW, conventional arc sensor making a measurement of voltage and current won't be effective in an automatic welding. And there is no corresponding on-line tracking and real-time standoff control method in PAW at the same time.

It is sometimes necessary to observe welding situation in real-time to make an automatic control so as to assure welding quality. Thus, visual sensor is considered to be more appropriate and direct to make an exact observation of welding conditions. Through extraction of image characteristic of fusion zone photographed by visual sensor, it is capable of obtaining the torch position to make an automatic seam tracking of weld line in the welding process.

Generally speaking, a high efficiency robotic PAW system with mature process control technology, especially the visual sensing technology is urgently needed in the industrial manufacture of nowadays society.

CONTENTS

CHAPTER 1. INTRODUCTION

1.1 Background and purpose of researches on visual robotic PAW system

Plasma arc welding (PAW) and cutting process were invented by Robert M. Gage in 1953 and patented in 1957. The process was unique to achieve precision welding and cutting on both thin and thick metals. It was also capable of spray coating and hardening metals onto other metals, so that the spray coating was adopted in the turbine blades of the moon bound Saturn rocket [1].

PAW is an arc welding process wherein coalescence produced by the heat obtained from a constricted arc between the tungsten electrode and water-cooled nozzle (non-transferred arc process) or between the electrode and work piece (transferred arc process). The process usually employs two inert gases, one forms the arc plasma and the other shields arc plasma. In PAW, the filler metal may or may not be added [2, 3].

On the other hand, PAW is a kind of gas tungsten arc welding (GTAW), often compared with the Tungsten Inert Gas welding (TIG). The key difference from TIG welding is that in PAW, by positioning the electrode within the body of the torch, the plasma arc is constrained [4]. The plasma is then forced through a

fine-bore copper nozzle which constricts the arc and the plasma exits the orifice at high velocities (approaching the speed of sound) and a temperature approaching 28,000 °C or higher. Just as oxy-fuel torches can be used for either welding or cutting, so too can plasma torches, which can achieve plasma arc welding or plasma cutting [5-7]. Torch structure and the principle of PAW is shown in Fig 1.1.

Arc plasma is the temporary state of a gas. The gas gets ionized after passage of electric current through it and it becomes a conductor of electricity. In ionized state atoms break into electrons (−) and cations (+) and the system contains a mixture of ions, electrons and highly excited atoms. The degree of ionization may be between 1% and greater than 100% i.e.; double and triple degrees of ionization. Such states exist as more electrons are pulled from their orbits. The energy of the plasma jet and thus the temperature is dependent upon the electrical power employed to create arc plasma [8, 9].

Working efficiency and environment of welding can be improved by means of PAW. And welding quality and efficiency is further improved by carrying out process control, which has been widely applied in PAW and which is broadly divided into two strategies: seam tracking (also known as joint tracking) and weld formation control [10-12]. Seam tracking involves real-time tracking just ahead of

where the weld is being deposited. Besides shifting the robot or machine trajectory, this technique alters the weld bead formation by adaptive control such as adjustments to voltage, wire feed rate, or travelling speed.

Weld formation control includes penetration control and deposited metal control. Autonomous welding robots based on weld formation control have been investigated in several significant studies. Shen employed weld formation control in a “teach and playback” robot to handle gap variations in a multi-pass welding process [13]. Zhou et al. presented a system that measures and controls the weld pool size of the upper surface in real-time [14]. Trushnikov considered ways to control the formation of welds with periodic effects on the electron beam [15]. He found that the density distribution is closely linked to the nature of the beam–metal interaction and can be exploited in remote control of the technology process [16]. Zhang [17] and Fan [18] improved prediction models by including seam gap measurements in the model.

Sensing methodology is essential for seam tracking and weld formation control. Without reliable signal sensing, the control becomes difficult. A few sensing, detecting, and monitoring methods have been already developed for PAW. Welding conditions in the PAW process were adjusted by measuring such as the

efflux plasma voltage signal, sound signal, light signal, or plasma cloud charge. Sensing methods can also be based on visual imaging. In PAW, the efflux plasma exits through an open keyhole, generating an electrical voltage. In methods that detect the efflux plasma signal, this voltage is measured to characterize the establishment and size of the keyhole. The reliability of sound and light sensors is degraded by interference from environmental noises and the difficulty in distinguishing the statuses of the stable keyhole from weld cutting status. Plasma cloud charge sensors predict the angle of the plasma cloud from the voltage between the probe and work piece. However, this sensing approach is also indirect and cannot quantify the shape and size of an open keyhole [19, 20].

Vision sensor provides more direct information on the welding condition and size, enabling better sensing of the fusion zone, than other sensor types. Therefore, visual sensing has been increasingly applied to PAW processes and is commonly combined with the sensing of electrical signals (such as the efflux plasma voltage). Considering the need for close attention and real-time control during the welding process, visual sensors are considered the most appropriate for exact observation of the welding conditions in the establishment of robotic PAW system [21-23].

1.2 Construction of the present thesis

In the present thesis the problems concerning the construction of the establishment and development of the high efficiency robotic PAW system are studied in detail.

In order to achieve the high efficiency of plasma robotic welding system, this thesis has focused on two aspects shown in Fig. 1.2. One is coming up with a series of image processing for solving the mentioned problem in different conditions, which is inspected to be useful for the welding engineers to make a visible automatic control of the weld line instead of human sight. The other is to develop a welding system on the basis of PAW and gas metal arc welding (GMAW) so that the filler metal can be added in one-pass procedure for overlay welding to save the working hours required in PAW. The seam tracking of weld line has also been realized in this case.

The thesis consist of six chapters. Chapter 1 as this chapter introduces the background of the PAW and two strategies of traditional process control with several significant studies. Since sensing methodology is essential for the process control, it has brought in the outstanding visual sensing technology for the purpose of establishing a high efficiency robotic PAW system in this research.

Chapter 2 introduces the principle of the PAW, and deals with the problem concerning the controlling and visual sensing system employed in the robotic welding system. Since there is time delay of the motion of welding robot due to strong inertia force, a specially designed digital controller is capable of tracking of the weld line and standoff control of the standoff to approximate with a second order system.

Since the plasma electrode hides in plasma torch, it is difficult to teach the welding robot and trace the weld line exactly during the welding process. In the chapter 3, image processing methods have been proposed to solve the mentioned problem in different welding conditions. The proposed system is useful for the welding engineers by making a visible automatic control instead of human sight. In this case, visual sensor is fixed on the jig in the rear of welding torch to monitor the fusion zone. Above all, it has attempted to pay attention to the triangle groove of base metal by using template matching technique. The performance of the proposed method was verified under normal circumstance.

However, it is at the expense of no keyhole to find the characteristic of the weld line existing in the fusion zone. Since welding quality in PAW is considered depending on the performance of tracking results and maintenance of keyhole.

Making assurance of welding quality, it needs to monitor the real-time status of keyhole area. The Image processing for automatic tracking of the weld line has been developed. The method is available to monitor the keyhole and weld pool. Numerous fundamental experiments and analyses have been carried out to find the characteristic of weld line in keyhole area.

Moreover, gap which easily causes a burn-through may sometime exist in the groove along the weld line. Then, under the circumstances whether there is a gap or not, an image processing for automatic tracking of the weld line has been developed. It has efficiently integrated the previous means under normal condition and a boundary detection method in the case of existing gap into the image processing, and make real-time tracking and analysis of variable gap to ensure the welding quality in the whole experiments.

In chapter 4, a brand new PAW system integrating plasma arc welding (PAW) and gas metal arc welding (GMAW) has been proposed. In this system, PAW is leading torch with high current density and GMAW tailing torch using consumable electrode has been developed to improve the welding quality at a higher level. Since arc under 100% Ar shielding gas becomes unstable in the mild

steel welding, by using the welding system of PAW and GMAW, it confirms that the arc of GMAW becomes stable due to the interference of PAW.

Because two kinds of different welding are processing on the same base metal in the meantime, it has discussed about the concrete system structure, especially the polarity and distance of both electrodes. It is available to make a clear observation of welding phenomena by means of high-speed video camera, and the interference between two electrodes has been investigated with respect to weld pool and metal transfer. The metal transfer has become smooth by its result. Since the combination of PAW and GMAW are employed, there're a lot of welding parameters due to the complexity of welding conditions, which has resulted in several welding defects due to the improper welding condition. In this chapter, the cause of the welding defect was investigated by analysis of cross section of weld bead, corresponding waveform and arc condition in the welding process. The keyhole size and distance are important parameters as the results, and appropriate welding condition were found to make an improvement of the welding defects. During hybrid optimization process for the combination of PAW and GMAW, it is available to perform the keyhole welding and building up of groove at the same time, which leads to an improvement of high work efficiency and welding quality.

Since the GMAW is employed as a tailing torch in the welding system of PAW and GMAW, it is difficult to realize the seam tracking from the rear of consumable electrode. In this case, the visual sensor is going to be fixed on the jig in front of plasma torch to monitor the gouging area of plasma keyhole. In chapter 5, an image processing for automatic tracking of the weld line and self-regulated standoff of the torch has been developed in plasma robotic welding. The multiple thresholds in the image processing are proposed so as to raise the precision of boundary detecting and improve the welding quality, and standoff control method effectively keep the standoff of plasma torch in a constant value determined by lots of basic experiments in order to maintain the keyhole and make a stable and optimal welding in the meantime.

The concluding remarks was described in chapter 6.

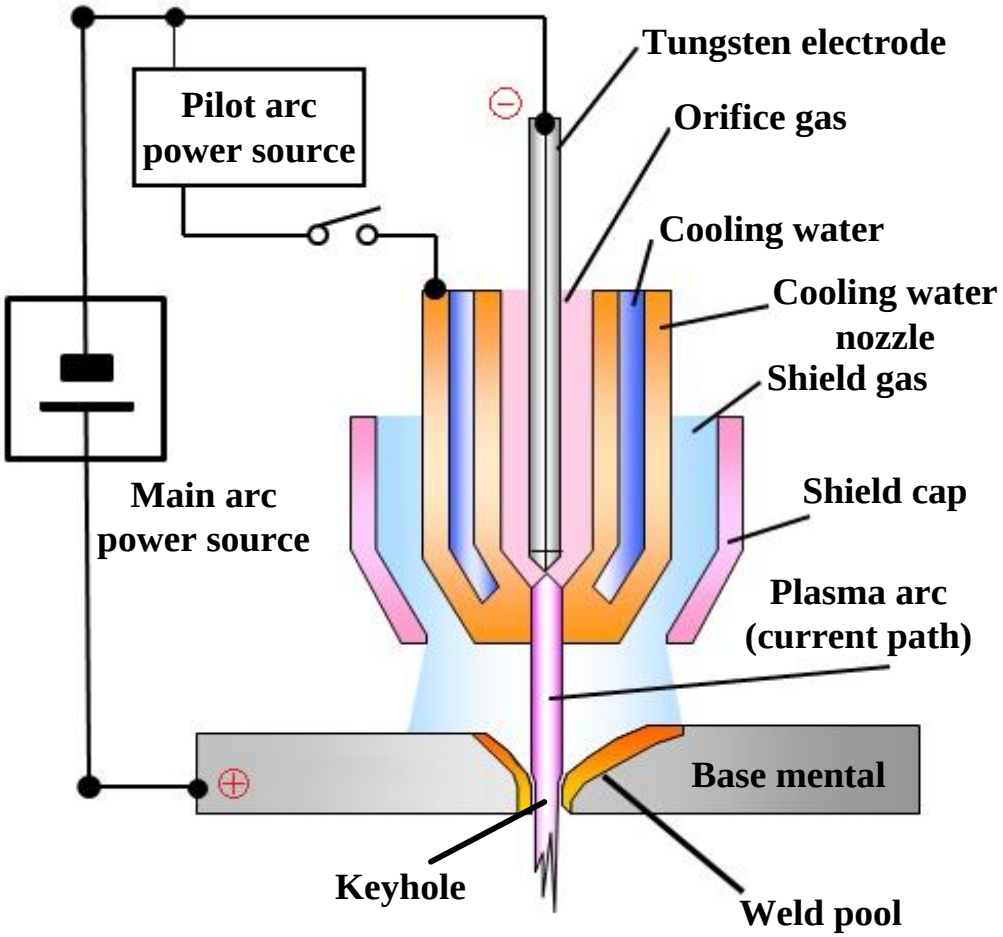

Fig. 1.1 Torch structure and principle of PAW

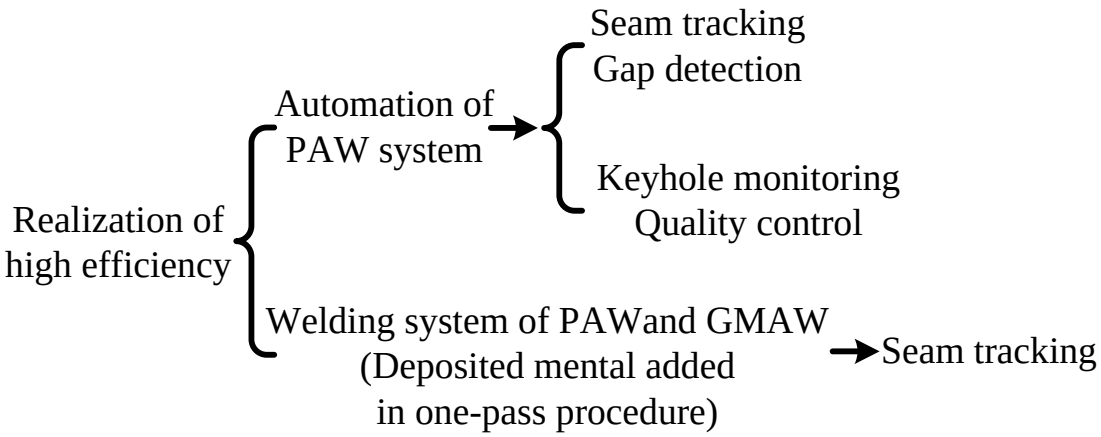

Fig. 1.2 Realization of high efficiency

CHAPTER 2. PLASMA ROBOTIC WELDING SYSTEM WITH VISUAL SENSOR

2.1 Introduction

This chapter will introduce the principle of the PAW, and deals with the problem concerning the controlling and visual sensing system to construct the robotic PAW system. Since there is time delay in the motion of welding robot due to strong inertia force in robot axes, a digital controller has been specially designed to trace the weld line and control the standoff of plasma torch. The model of robot was approximated with a second order system.

2.2 Robotic welding system

The PAW system has been shown in Fig. 2.1a. It mainly consists of a PAW robot with its movement controller, imaging processing PC, an industrial camera and its shutter timing is controlled by dsPIC of 16-bit digital controller. Moreover, communication between welding robot and its movement controller makes use of Ethernet and welding conditions will be sent to dsPIC through RS-232C.

Plasma power source emits strong electrical noise during the welding. Once the plasma power supply is connected to PC controller directly, electrical noise

from the power source may be transmitted to control terminal, as a consequence, working program of PC controller is going to stop due to the electrical noise, and even the computer is possible to restart without control of the welding current. In order to eliminate the effect from electrical noise, it applys dsPIC to make a control of power source together with the invertor, and additionally the dsPIC has been operated owing to the program saved in its EPROM, where the welding condition has been stored. The dsPIC may receive strong electrical noise emitted from power source once connected to it and lead to automatically restarting of the dsPIC program. PC controller makes a control of welding robot through Ethernet and sends the welding conditions to dsPIC due to RS-232C, which guards strongly against the electrical noise and welding process can continue without the bad influence of electrical noise.

As the torch structure introduced in the Fig. 1.1, through a small-bore nozzle, heat of plasma arc will be produced between a tungsten electrode and base metal. In PAW, the power source for main arc and high frequency power source igniting pilot arc have been assembling together. Owing to the applied voltage between electrode and tip, pilot arc occurs after orifice gas is supplied, and plasma, ionized by the supplying gas, comes into being. The state of main electric current flowing

through the base metal is shown as Fig. 2.1b. On account of plasma gas and nozzle of small diameter, an arc of high current density has taken place.

Base metal of thick plate with groove have been employed in this research. After partially heats the fusion zone, it is depressed by plasma gas deeply. The heat of plasma arc melts the base metal in front of keyhole, and melted metal fills in the posterior region [24, 25]. By adjusting the electric current, it is available to control plasma pressure. Pulsed current waveform has been used, and the base metal melts during the pulse peak. On the other hand, the cooling and solidification of weld pool is carried out during the base current. Since the pulsed waveform will be adjusted, appropriate welding condition becomes complicated.

2.3 Visual sensing system

It is necessary to observe the fusion zone during the welding process. Usually by using the hand shield, it is possible to obtain a similar image so as to make a recognition of the fusion zone. For that reason, it should understand the optical characteristic of the fusion zone based on choosing the suitable tool like visual sensor, filter and so on [26]. That is, because high brightness and low brightness exist on the fusion zone at the same time, it needs to choose the visual sensor with the ability maintaining the observation of dark parts and not being

saturated in the radiance; it needs to choose a suitable filter depending on spectrum properties of the fusion zone.

In this research, CCD camera was ever employed. Because the radiant intensity of arc is strong, the CCD camera with general performance may give rise to smear and halation on the characteristic of fusion zone, and replaced by the CMOS camera with response capacity. On the other hand, as it is shown in Fig. 2.2, which is the radiant intensity of arc and weld pool. Arc produces strong radiant light from the ultraviolet area to infrared area, and in the fusion zone, the radiant light has centered on the near-infrared area (800 nm ~ 2500 nm). In order to make an observation of the fusion zone and nearby the groove, it ought to select the wavelength of near-infrared area to decrease the radiant intensity of arc light and increase that of the weld pool. In this way, when a filter with wavelength more than 800 nm, it is basically available to interrupt the arc light, and only allow the light of weld pool to transmit. In addition, the cognitive domain and photographic condition changes along with the transmitted wavelength and fusion zone where is expected to be emphasized [27]. Due to fundamental experiment, by adjusting the visual sensor with a filter of IR 950-nm, it is available to obtain the appropriate images and execute processing results more exactly by image processing software.

In the sensing system, visual sensor equipped with infrared (IR) 950-nm filter corresponding to near-infrared area intercepting all the visible light has been set in front or in the rear of the plasma torch in different cases. It has been fixed on the jig and pays attention to the fusion zone from the topside of work piece at a variable angle from the horizontal position. Due to the strong light of plasma arc, the taken image will become too bright even during the base current as it is shown in Fig. 2.3a, and the molten pool cannot be recognized.

The arc light depends on the welding current. In order to reduce the effect of excess arc light, welding current decreases for a short time synchronized with the trigger signal and the clear image of the molten area can be taken. Since the shutter of CCD camera opens for 3 ms, it is required that welding current descends to the specified value in the short time. It can sometimes achieve the same welding result by using pulse current and corresponding effective current, which will be higher than the base current and normally takes a longer time for effective current to descend to the specified value (30A). Furthermore, the welding current descends for a short time during the base current will not affect the welding result too much unlike in the period of peak current, since the welding phenomena such as the flow of molten pool is slower than 3ms.

Controlled wave pattern of welding current is shown in Fig. 2.4, which the peak current is 350A and base current is 150A. As mentioned, welding current will fall to 30A when the shutter of CCD camera opens for 3 ms synchronizing with the waveform, In this way, it will be effective of reducing the excess arc light in order to make a clear image shown in Fig. 2.3b.

Signal transmission between PCs is sometime disturbed by the electric noise from power source in practical field. Since conventional CCD camera sends out video signal to the frame grabber after receiving the trigger signal, it will convert the signal to digital signal with AD converter and stores into image memory. Thus, PC processes the image in its memory as illustrated in Fig. 2.5a.

However, electrical noise will probably enter the transmission line between analog CCD camera and frame grabber. As a consequence, it is going to use digital CCD camera of camera link interface to prevent the possible electrical noise. Image signal is converted to the digital signal by the AD convertor into CCD camera after taking images, and then sends out through RS-232C interface. At this moment, disturbance of noise will be neglected due to the noise margin as illustrated in Fig. 2.5b.

2.4 Design of digital controller

Since there is time delay of the motion of welding robot due to strong inertia force in each axis, it is unable to move the torch to the target position immediately when the robot controller receives pulse signal. Control of the torch position is performed by feeding the pulse to a manipulator. Indicial response to the pulse in the torch motion is shown in Fig. 2.6.

Since the response is approximated by the second order delay system, dynamic behaviors of welding robot for tracking of the weld line and standoff control of the standoff are approximated with a second order system shown as follows:

$$G_t(s) = \frac{X_t(s)}{U_t(s)} = \frac{\omega^2}{s^2 + 2\delta\omega s + \omega^2} \times \frac{1}{s} \quad \text{for tracking of the welding line}$$

$$G_s(s) = \frac{Y_s(s)}{U_s(s)} = \frac{\omega^2}{s^2 + 2\delta\omega s + \omega^2} \times \frac{1}{s} \quad \text{for control of standoff} \tag{2.1}$$

There δ is 0.9, ω is 40 rad/s, X_t (s) and U_t (s) are the position with respect to weld line and operating value of plasma torch, and Y_s (s) and U_s (s) are the standoff and operating value to adjust the height of welding torch. In addition, parameters of plant G_t (s) and G_s (s) are the same on account of the same robot axes.

By using digital control theory, the plants are transferred to the discrete time system, which G_t (s) and G_s (s) is transferred by Z-transform as follow.

$$G_t[z] = \frac{dz^2 + ez}{(z-1)(z^2 + bz + c)}$$
$$G_s[z] = \frac{dz^2 + ez}{(z-1)(z^2 + bz + c)} \tag{2.2}$$

where

$$\varphi = \omega_n \sqrt{1-\zeta^2}$$
$$b = -2e^{-\zeta_n \omega_n T} \cos \varphi T$$
$$c = e^{-2\zeta_n \omega_n T}$$
$$d = 1 - \frac{\zeta \omega_n}{\varphi} e^{-2\zeta_n \omega_n T} \sin \varphi T - e^{-2\zeta_n \omega_n T} \cos \varphi T$$
$$e = e^{-2\zeta_n \omega_n T} + \frac{\zeta_n \omega_n e^{-\xi_n \omega_n T}}{\varphi} \sin \varphi T - e^{-\zeta_n \omega_n T} \cos \varphi T$$
$$f = e^{-2\zeta_n \omega_n T} + \frac{\zeta_n \omega_n e^{-\zeta_n \omega_n T}}{\varphi} \sin \varphi T - e^{-\xi_n \omega_n T} \cos \varphi T$$
$$T = 0.05$$

Deviations e_t [i] and e_s [i] from the reference of weld line and standoff at the i th sampling can be calculated by

$$e_t[i] = R_t - X_t[i]$$
$$e_s[i] = R_s - Y_s[i] \tag{2.3}$$

Illustrated in Fig. 2.7, z transfer for the desired responses, X [z] and Y [z], to the reference value are determined in the 10 sampling and given by

$$
\begin{aligned}
X[z] &= 0.05Z^{-1} + 0.15Z^{-2} + 0.25Z^{-3} + \cdots + 0.95Z^{-10} + 1.0Z^{-11} + Z^{-12} + \cdots \\
&= p_1 Z^{-1} + \cdots + p_{10} Z^{-10} + \frac{Z^{-11}}{1 - Z^{-1}} \\
Y[z] &= 0.05Z^{-1} + 0.15Z^{-2} + 0.25Z^{-3} + \cdots + 0.95Z^{-10} + 1.0Z^{-11} + Z^{-12} + \cdots \\
&= p_1 Z^{-1} + \cdots + p_{10} Z^{-10} + \frac{Z^{-11}}{1 - Z^{-1}}
\end{aligned}
\tag{2.4}
$$

Moreover, controller to acquire the finite setting response has been designed. The block diagram is shown in Fig. 2.8. In this case, two digital controllers, D_t [z] and D_s [z], are required to trace the weld line and make a control of the standoff independently. The controllers are given by the following equation.

$$
\begin{aligned}
D_t[z] &= \frac{1}{Gt[z]} \frac{X_t[z]}{R[z] - X_t[z]} \\
D_s[z] &= \frac{1}{Gt[z]} \frac{Y_s[z]}{R[z] - Y_s[z]}
\end{aligned}
\tag{2.5}
$$

Characteristic of the controller is found by substituting the deviations of Eq. 2.3 and desired responses of Eq. 2.4 by

$$
\begin{aligned}
D_t[z] &= \frac{a_0 + a_1 Z^{-1} + a_2 Z^{-2} \cdots + a_{12} Z^{-12}}{1 + b_1 Z^{-1} + b_2 Z^{-2} + \cdots b_{12} Z^{-12}} \\
D_s[z] &= \frac{a_0 + a_1 Z^{-1} + a_2 Z^{-2} \cdots + a_{12} Z^{-12}}{1 + b_1 Z^{-1} + b_2 Z^{-2} + \cdots b_{12} Z^{-12}}
\end{aligned}
\tag{2.6}
$$

where

$$
\begin{aligned}
a_0 &= p_1 / d \\
a_1 &= \left(\left(p_2 - p_1\right) + p_1 b\right) / d \\
a_2 &= \left(\left(p_3 - p_2\right) + \left(p_2 - p_1\right) b + p_1 c\right) / d \\
a_3 &= \left(\left(p_4 - p_3\right) + \left(p_3 - p_2\right) b + \left(p_2 - p_1\right) c\right) / d \\
a_4 &= \left(\left(p_5 - p_4\right) + \left(p_4 - p_3\right) b + \left(p_3 - p_2\right) c\right) / d \\
&\vdots \\
a_{10} &= \left(\left(1 - p_{10}\right) + \left(p_{10} - p_9\right) b + \left(p_9 - p_8\right) c\right) / d \\
a_{11} &= \left(\left(1 - p_{10}\right) b + \left(p_{10} - p_9\right) c\right) / d \\
a_{12} &= \left(1 - p_{10}\right) c / d
\end{aligned}
$$

$$
\begin{aligned}
b_1 &= 1 + e / d \\
b_2 &= \left(1 - p_1\right) + e / d \\
b_3 &= \left(1 - p_2\right) + e\left(1 - p_1\right) / d \\
b_4 &= \left(1 - p_3\right) + e\left(1 - p_2\right) / d \\
&\vdots \\
b_{11} &= \left(1 - p_{10}\right) + e\left(1 - p_9\right) / d \\
b_{12} &= e\left(1 - p_{10}\right) / d
\end{aligned}
$$

The reference $R[z]$ is z transfer of step function recorded as follows

$$R[z] = \frac{1}{1 - z^{-1}} \tag{2.7}$$

Sampling period is 150ms with respect to the interval of image processing.

The manipulating variables u_t [i] and u_s [i] of the welding robot at i th sampling period are found by transforming Eq. 2.6 to discrete time system. That is,

$$u_t[i] = a_0 e_t[i] + a_1 e_t[i-1] \cdots - b_1 u_t[i-1] \cdots b_{12} u_t[i-12]$$
$$u_s[i] = a_0 e_s[i] + a_1 e_s[i-1] \cdots - b_1 u_s[i-1] \cdots b_{12} u_s[i-12] \quad (2.8)$$

Above equation means that the manipulating values are calculated from the weighted average of deviations. Even if the error is caused in the image processing, the affection of its error becomes small. According to Eq. 2.8, tracking of the weld line is carried out by the digital controller.

2.5 Conclusions

Robotic PAW system with its controlling and visual sensing system has been established. The digital controller can be applied to tracking of the weld line and standoff control of the standoff. The controllers are designed by approximating the plant as a second order system. It is going to introduce the specific application of digital controller in the following chapters.

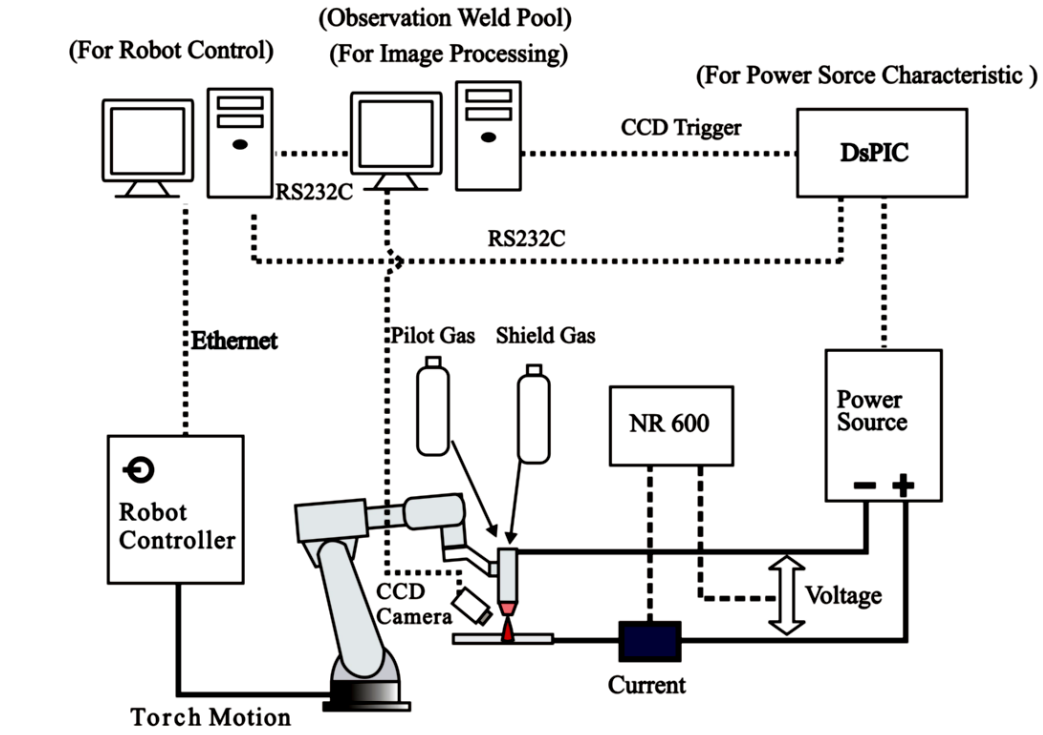

(a) Robotic welding system

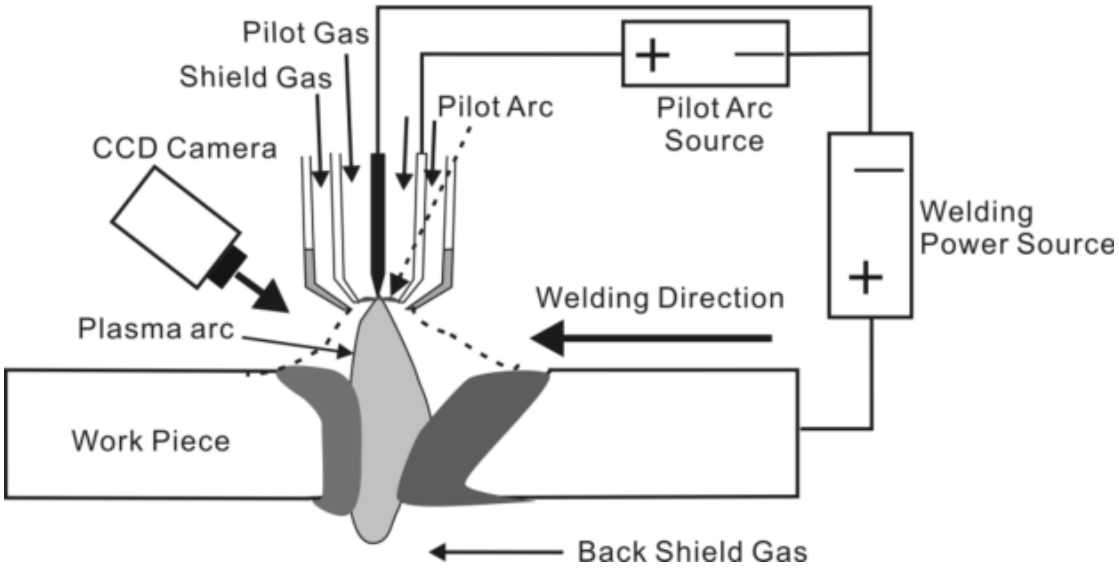

(b) Relationship between torch and keyhole.

Fig. 2.1 System configuration of plasma arc welding.

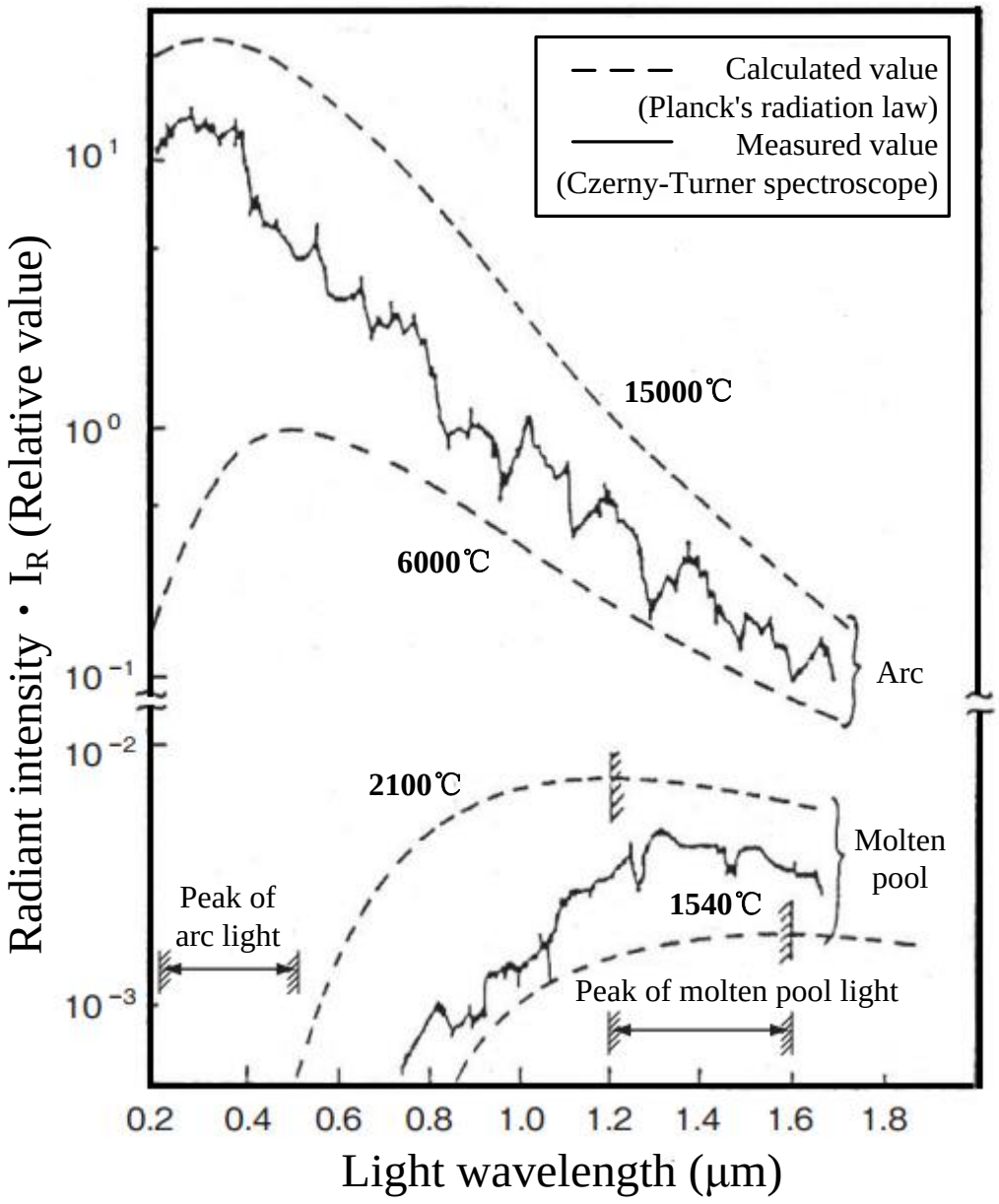

Fig. 2.2 Radiant intensity of arc and weld pool [27]

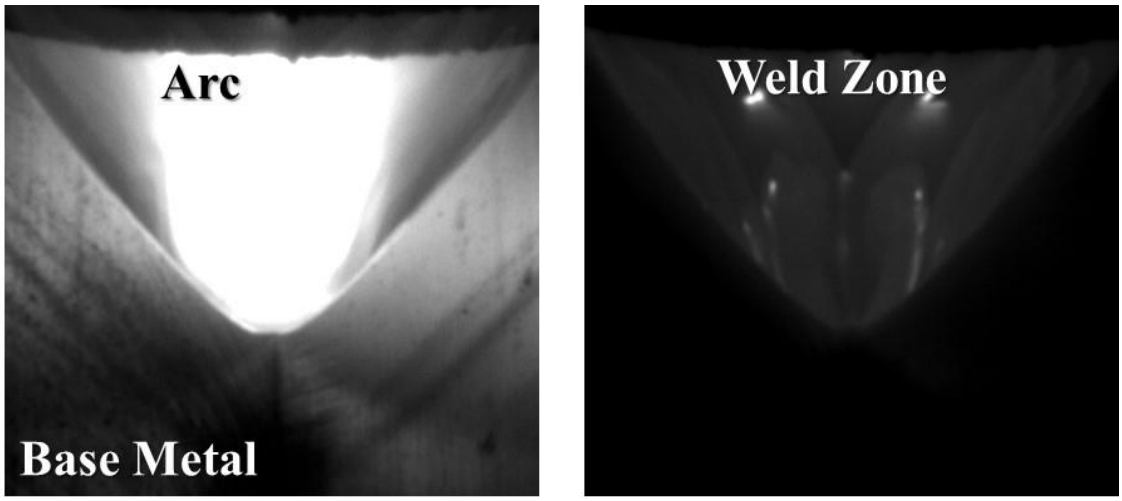

(a) During base current. (b) During 30A.

Fig. 2.3 Typical fusion zone images.

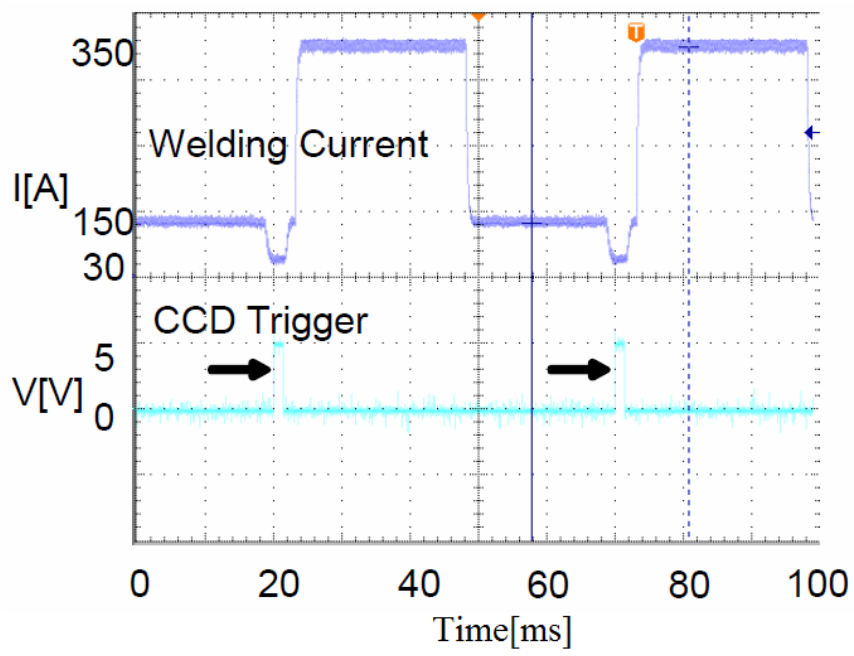

Fig. 2.4 Relationship between waveform of the pulse current and the trigger timing of the CCD camera

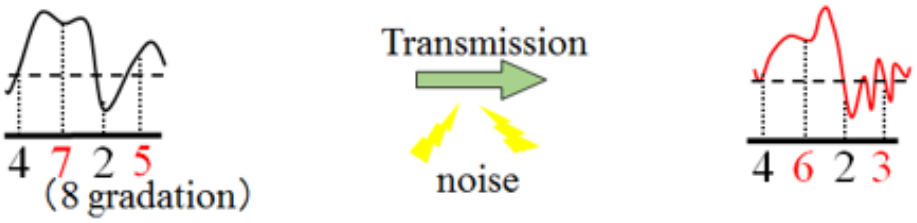

(a) Effect of noise for analog transformation with NTSC interface

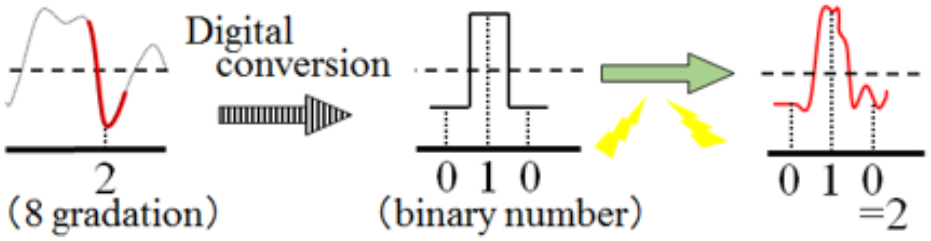

(b) Effect of noise for digital transformation with camera link interface

Fig. 2.5 Difference of transmission between analog and digital system.

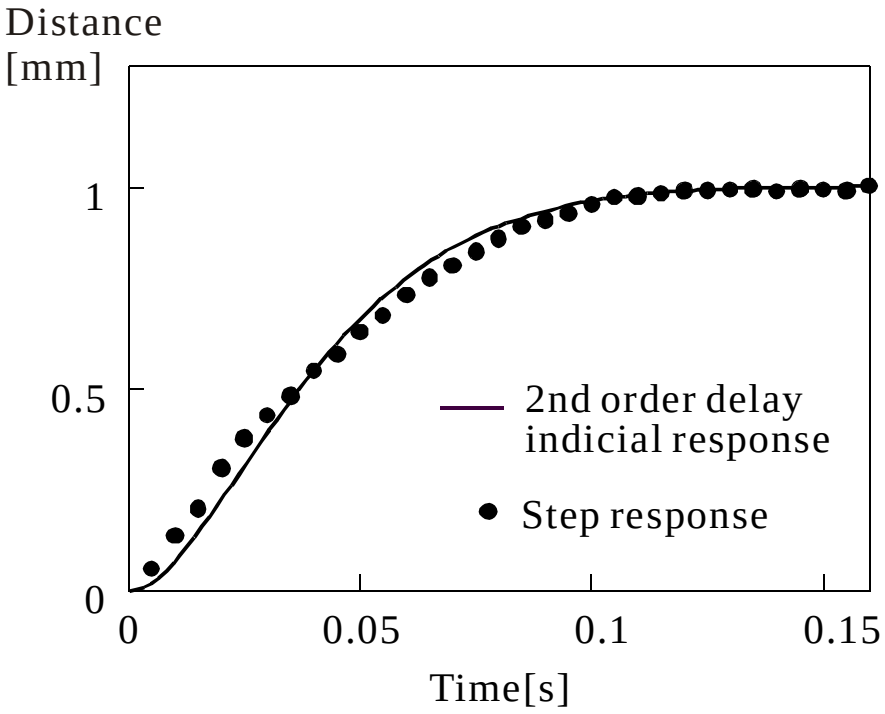

Fig. 2.6 Indicial response of the torch axis

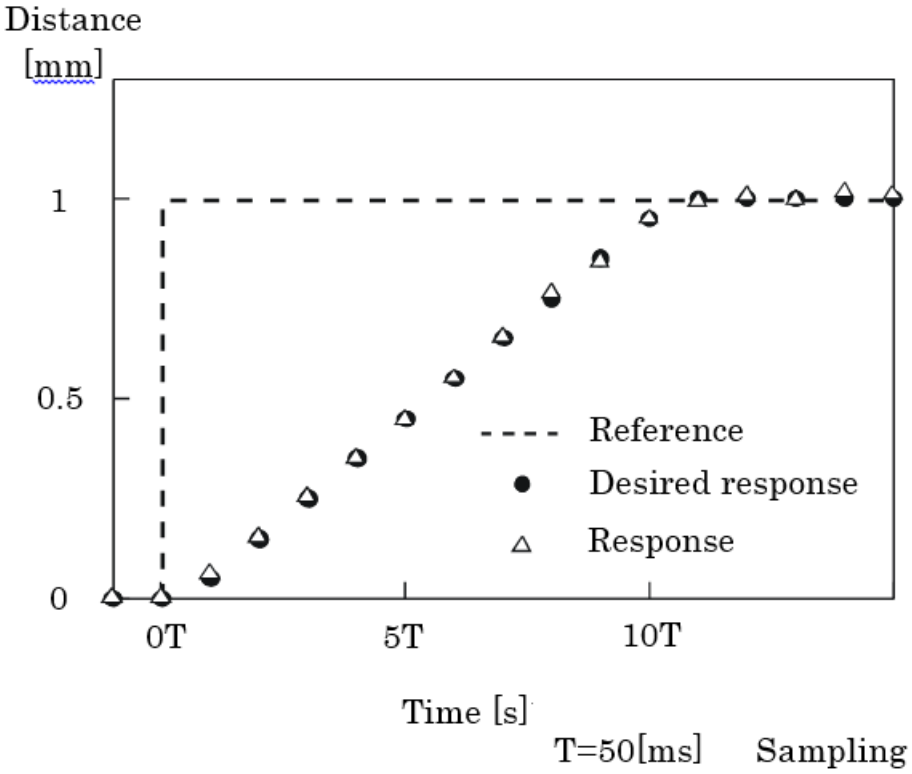

Fig. 2.7 Desired response of the torch axis.

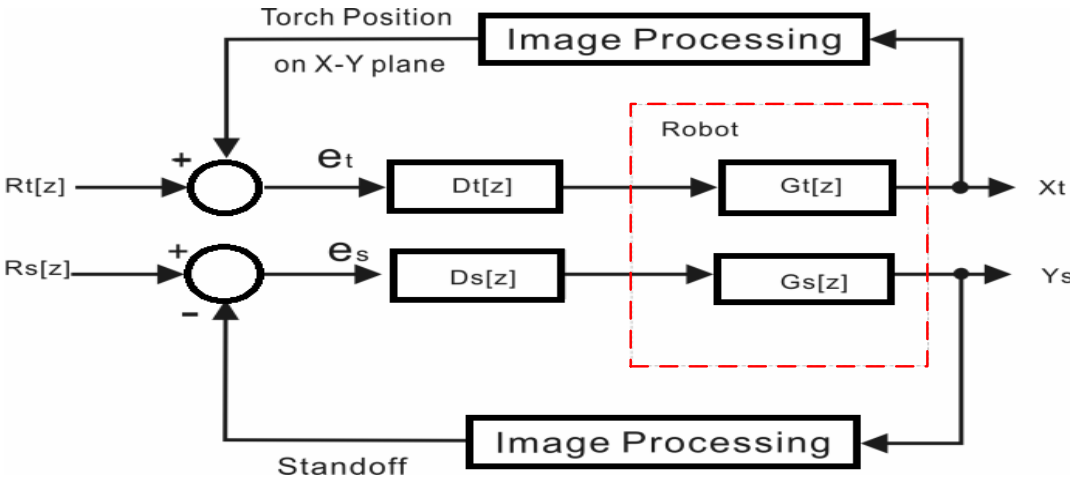

Fig. 2.8 Digital control block diagram for the tracking of the weld line and the control of the standoff.

CHAPTER 3. IMAGE PROCESSING FOR AUTOMATIC TRACKING OF WELD LINE

3.1 Introduction

As mentioned, the length of plasma arc, related to welding voltage and current, almost keeps constant in PAW. Conventional arc sensor making a measurement of voltage and current won't be effective in an automatic welding. And because the visual sensor provides information more directly on the welding condition, it enables better sensing of the fusion zone than some other sensor types.

An ultra-high shutter speed vision system was used to image the keyhole and the weld pool from the backside of the work-piece [28]. As shown in Fig. 3.1, the camera system includes a strobe-illumination unit (pulse laser), camera head and system controller. The keyhole and the weld pool could be imaged clearly as shown in Fig. 3.2. In spite of high precision and sensitivity, such a laser-strobe system is complicated and very expensive in practical applications, which cannot be widely used in the normal industrial manufacture. Besides that, it is important to ensure that laser systems are clean and free from dirt and other foreign materials, otherwise accuracy will be affected. In the production field with complex and poor environment, the safety and reliability of the high precision instrument will be

questioned. Since laser heads have electronic components that are highly sensitive, the operating temperature is somewhat restricted [29].

A low-cost visual sensor like industrial camera is more attractive for sensing keyhole in PAW process. To this end, Wu's team developed a cost-effective vision system for observing the keyhole from the backside of work-piece, and clear images of keyhole are obtained [30, 31]. Fig. 3.3 shows the experimental system for observing the keyhole image from the backside of the test plates. And if the work-piece is fully penetrated and an open keyhole is formed, the keyhole image is captured by the CCD. Because of the large volume of the PAW torch, it has obstructed the view of observing the keyhole image from the topside of work piece in some degree. In Wu's study, the CCD camera aims at the back-side of the work piece to observe the keyhole image. But in this way, it is not convenient to make the visual sensor moving together with the plasma torch for a real-time monitoring. And it is also not available to observe the welding state and fluid flow of molten metal in the fusion zone. On the other hand, only modeling and simulation has been realized without corresponding on-line tracking and real-time standoff control method in this study.

In this study, the visual sensor has been fixed on the jig in the rear of plasma torch to observe fusion zone from the topside of work piece and moving together during the welding process. In order to achieve high efficiency and welding quality in PAW, image processing for automatic tracking has been designed for the butt welding of thick plate with a V-groove in normal case by template matching, which is to find out the small parts of welding characteristic image matching the template image. Template matching can be used in manufacturing as a part of quality control [32]. And it is also very useful in the PAW by matching the template images of the fusion zone taken in the steady state with the real-time images during the welding process. Based on that, it is able to reappear the steady-state welding in the fundamental experiments by controlling the welding conditions. Above all, it has paid attention to the front part of fusion zone to detect the triangular groove of work piece. By matching the template image of triangular groove where characteristic of the weld line exists, image processing has been performed to conduct an automatic seam tracking.

In keyhole plasma arc welding, the stability of keyhole is an important factor that affects the stability of the welding process and the quality of the weld joint [33-35]. Thus, monitoring of the keyhole status are very important to achieve

defect-free and high-quality welds. Because of a large size of plasma torch, there is only a small operation scope for the visual sensor, shooting from the topside of the work piece to make an observation of the keyhole in the fusion zone. Image processing by template matching of triangular groove is easy and direct to find out the characteristic of the weld line. However, it is not available to monitor the keyhole at the shooting angle for the groove in front of the fusion zone. Since welding quality in PAW is considered depending on the performance of tracking results and maintenance of keyhole, it is tried to monitor the real-time status of keyhole area to make an assurance of welding quality. In this way, it is going to pay close attention to the keyhole to ensure the weld quality and realize the seam tracking by finding out the characteristic of the weld line in keyhole area at the same time.

Gap may exist in the groove along the weld line. False teaching of welding robot may cause a burn-through in this case. Image processing with a boundary detection method has been proposed in order to solve such problem. As a result, the gap are effectively detected by the image processing with its central position and width calculated. Furthermore, the central position of variable gaps as position

of weld line are sent to the PC controller in real-time for a seam tracking to ensure welding quality in PAW.

3.2 Groove detection under normal conditions

To realize automatic control of a welding robot, the author experimentally investigated the welding phenomena and the real-time image processing has been discussed based on the experimental results by using our proposed system. As a basic technique of image processing, the author employ template matching by calculating the similarity between a template and a given image. The simplest similarity degree is the sum of the absolute or squared differences in the gray values between the template and each pixel in the image. The summed absolute and squared differences are denoted as SAD and SSD, respectively. Provided that the brightness in the image is fixed, the performance of SAD is similar to SSD.

However, if the average brightness changes during the welding process, both will return a large value even when the image and template contain the same object. This occurs because the gray value of the searched image has altered from its value at the time of template construction. Therefore, it requires a different similarity standard that is robust to linear average brightness change. Here, the author adopts the normalized cross correlation (NCC) by $M \times N$ pixels are

selected as template image [36, 37]. The NCC similarity degree is then calculated by

$$R_{NCC} = \frac{\sum_{j=0}^{N-1}\sum_{i=0}^{M-1}(I(i,j)T(i,j))}{\sqrt{\sum_{j=0}^{N-1}\sum_{i=0}^{M-1}I(i,j)^2 \times \sum_{j=0}^{N-1}\sum_{i=0}^{M-1}I(i,j)^2}} \tag{3.1}$$

where T(i, j) and I(i, j) at pixel (i, j) are the values of the template and target images, respectively.

The brightness of each pixel from the template image and target image is regarded as the element of vector. The smaller the angle difference between the vectors is, the higher the similarity will be, and the value of NCC similarity degree is approaching 1. It is also available to calculate the cos θ of inner product of vectors through the transformation between the vector and trigonometric function. Expression here is as same as the inner product expression, and the change of gain is like the length of vector which is difficult to be affected by the change of brightness. As a consequence, it is appropriate to take advantage of pattern matching in the fusion zone on account of the confusion of various brightness.

During the actual welding process, a steady-state image was selected as the template. This image captures the nozzle and border of the weld pool, along with

the triangular domain of the groove as shown in Fig. 3.4. In this way, the template matching is carried out in real time.

Since the CCD camera and plasma torch are fixed on the same robot axis, the image is centered at the center of the weld line under the torch. During the welding, the high-pressure plasma arc forms directly under the electrode; thus, the center lines of the plasma arc and torch are almost in the same line shown in the image. As the plasma arc should weld the center of the groove between two pieces of base metal, the welding robot should maintain vertical line at the center in the CCD camera image to the weld line.

3.3 Quality control by using pattern matching of keyhole

Numerous fundamental experiments and analyses have been carried out for the acquisition of characteristic of the weld line from keyhole area. To analyze the welding situation in fundamental experiment, fusion zone image was observed by high speed video camera with 5000 frames per second. The observed image is shown in Fig. 3.5. Since the normal filter was used to find out the material existence in weld pool and fluid flow situation, high light effect of plasma arc has not been eliminated.

Base metal employed here has a V-type groove. After partial heating, the groove is deeply depressed by plasma gas. It can also be confirmed that some oxide on the surface appears from the base metal by the plasma arc, and is flowing in the direction of virtual arrow to form boundary lines and finally converge behind. Cooling and solidification of the molten metal forms the rear boundary of weld pool. According to the simplification and efficiency of manufacture process, topside surface of base metal is thought to be seldom polished in the practical field of welding [38].

Since CMOS camera has a higher sensitivity in the near-infrared region (NIR), it has been utilized in this study rather than CCD camera used before. A CMOS camera equipped with an infrared (IR) 950-nm filter, which intercepts all of the visible light down to NIR, has been set on the jig in the rear of plasma torch. As mentioned above, because of the huge size of plasma torch, the adjustment range of exposure angle is limited. Thus, it is not easy to take a clear image of the keyhole. To make an assurance of welding quality, monitoring of the real-time status of keyhole is needed. In this way, characteristic of weld line from keyhole area has been obtained, and an image processing for automatic tracking of the weld line has been developed.

3.3.1 Acquisition of characteristic from fusion zone

Fundamental experiments have been carried out without tracking process to find the characteristic of weld line from keyhole area. Typical image of fusion zone taken by CMOS camera is shown in Fig. 3.6a. Since CMOS camera equipped with an infrared (IR) 950-nm filter, the image is clear regardless of strong light from plasma arc. It is possible to make an observation of keyhole just under the cap of plasma torch.

Since heat is spreading around the plasma arc in the center, molten metal with higher temperature is bright in the groove. On the other hand, cooling and solidification is from the surrounding. The temperature of solidified metal in the rear boundary is dropping. Its brightness become dark as shown in Fig. 3.6a. It is noticeable of the boundary line of weld pool and due to the symmetry, center line of weld pool and welding image almost coincide with each other.

Image with a deviation from the endpoint of weld line has been shown in Fig. 3.6b. Weld seam has been deliberately left as white line to determine the position of weld line and related characteristic. Yellow line in the center of image is electrode position and gradually deviating from the weld line.

Based on the analysis of welding images in fundamental experiments, it is determined that as long as the center line of image is still in the V-type groove, weld line passes through the keyhole. Moreover, the center of keyhole deviates along with center line of the image to some extent, and keyhole's area grows bigger. As the characteristic of weld line, it's worth noting that the center between boundary lines behind keyhole almost coincides with the weld line in Fig. 3.6b. And according to a large number of experiments with endpoint deviated, it is found out not to be an individual phenomenon, which certainly matches the pervious result when transfer path of plasma torch following the weld line.

Fig. 3.7 shows welding result that the endpoint is 3 mm apart from weld line. When the electrode was deviating from the weld line, keyhole would be too big to maintain its circular shape. Molten metal flow became unstable and it led to a strong vibration of keyhole. Once the deviation became bigger over the critical value, maintenance of keyhole's shape will be out of control and it result in burning through. The result was confirmed from the bead shown in Fig. 3.7a. The bead on the rear side surface is shown in Fig. 3.7b. Along with the travelling of torch, keyhole grew bigger and unstable leading to an abnormal formation of the back bead.

Model of welding state has been shown in Fig. 3.8 and it assumes that the starting point *s* is located in weld line and end point *e* is 3 mm distance apart from the weld line. During the welding process, the standoff of the plasma torch restricts the plasma arc to in the V-type groove and *c* denotes the keyhole. The groove is melted and torn oxide firm on the surface. Oxide on the top surface of the base metal has been melted and flows with the molten metal to rear of weld pool in the direction of dotted line as shown in Fig. 3.8a. α plane shown in Fig. 3.8b is the projection of fusion zone in the cross section of base metal, which is in a moment during the welding process. Corresponding to the Fig. 3.6b, the line *a* represents the center of the image, line *b* represents the weld line, and *c* is the projection of keyhole.

Since weld line of base metal is minimally heat-conducting, it is more easily melted by plasma arc to form a keyhole than other zones. The keyhole is limiting the movement of molten metal in V-type groove, so it is available to detect the weld line whether the travelling direction deviate to left or right. Due to analysis result of characteristic image, the author infers that the center of left and right boundary of fusion zone fundamentally coincides with the weld line.

3.3.2 Tracking of weld line by image processing

In image processing, the size of taken image is 1280×1024 pixels. Before the image was taken, the center line of image was set as electrode position. Since it will take image processing time even if keyhole does not exist, it is needed to identify whether there is a keyhole or not at the beginning. The brightness of the pixel on a centerline in vertical direction is investigated to find the existence of keyhole. And if the average brightness is less than 10, it is considered that keyhole doesn't exist. As mentioned above, it is possible to remove the images of welding start and end. On the other side, the 100th pixel from the bottom up in the centerline as average brightness is to make a binarization processing on the centerline. If continuous pixels brighter than average brightness from the bottom up are more than 300, it is considered that keyhole is generated and the welding gets into the steady state. The image are neglected before the steady state.

Since keyhole's shape is maintained in a stable welding, template matching has been used for the detection of keyhole. In this method, the similar degree between a template image and target image is calculating to detect an object in the image. Above all, a rectangle area containing keyhole center is selected as a template, and a relatively larger area containing the both boundary lines shown in Fig. 3.9 is also used as a template. Template matching for recognition of keyhole

are applied, and the size of template image is $M \times N$. Normalized cross correlation here after NCC was used as template matching method as introduced in chapter 3.2. Similarity degree in NCC is given by Eq 3.1.

Provided that similarity of the template in the target image is less than 0.5, another different template is required. This is because the keyhole shape in steady state is different from the current. And if similarity is still less than 0.5, the keyhole disappears. By calculating the difference of size and angle between the template image and target image, affine transformation is carried out to denote both rectangles of the target image.

Since the right part of image will be brighter than the left due to a deviation of arc, brightness distribution is not the same in the target image. Two rectangular domains of 100 pixel height region of interest (ROI) are appointed in both sides below the center of keyhole to outer side of keyhole. It is to make a detection area for finding out the black boundary lines in Fig. 3.10a. There is often more than one black line in the domain which needs to prevent the false detection of boundary line. Since edge detection is on the basis of looking for the area with big change of brightness, the noise with topical change of brightness is eliminated by the filter using Gaussian as follow:

$$f(x) = A \exp\left\{ - \frac{(x - \mu)^2}{2\sigma^2} \right\} \tag{3.2}$$

with constants A, μ, and σ controlling the peak value, center and width, respectively. According to Eq. 3.2, the pixels near target pixel will be more significant than the distant ones and the noise will leave from the target pixel becoming non-significant to make the image smoothly. In the image processing, σ in Eq. 3.2 also expresses the standard deviation which will increase or decrease along with the smoothing quantity nearby the target pixel. In this way, the pixel in transverse direction will become smooth to emphasize the possible edge including the boundary line in vertical direction.

Inflection point, which is the cross point between brightness curve and horizontal axis of pixel, will be used for extraction of the edge. If length of detected edge is shorter than 150, the detected edge is regarded as the noise. In addition, average brightness of edge is calculated. And if minimum value of brightness on the edge is bigger than the average brightness of ROI, which the edges seem brighter, it is considered lowering smoothing quantity to acquire the dark edge easily. And if there is no other edge with length from 100 to 2000, the next image will be taken.

In ROI, there are more than one edges such as edge A, B, C, D and E, in which differential of the brightness are equal to zero. Edge B with smallest average brightness was selected as the boundary line in Fig. 3.10b. The central abscissa of both ends of edge B to determine the boundary is calculated in one side. The boundary in other side is detected in the same way. ROI corresponds to black area such as F shown in Fig. 3.10. Since the change of brightness here is not acute, i.e. the differential of brightness in area F is not equal to zero. F is not considered as an edge by the differential filter. Furthermore, weld line is located in the center of connecting line by two boundaries. Integer part of x coordinate of weld line will be written in the serial communication. The flowchart of image processing is shown in Fig. 3.11.

3.4 Image processing in case of gap

Since the plasma electrode is embedded inside the torch, human operators cannot exactly guide the plasma torch to the weld line, whose pilot arc ejects from a tip with a base width of 10 mm. The performance of the tracing depends on the training of workers, and poor training will negatively affect the welding quality. Therefore, the author tried to make a gap detection by the image processing.

The taken image comprises 700×750 pixels, and the model of the image is established shown in Fig. 3.12. Because the brightness of pixels corresponding to plasma torch becomes dark, and the brightness of weld pool becomes high. The acquired image has been binarized by the threshold along a vertical line. 0 is corresponding to the plasma torch, and 1 is corresponding to the weld pool, respectively. From the black–white boundary, it appointed 50 lines as the gap area. The image is divided into two subdomains separated by the row center. It is also the reference line that the electrode has located.

Boundaries between the gap and base metal are detected by the binarization in the horizontal direction, because the brightness of gap becomes dark than base metal. Gap center and width are calculated by the average and difference of the x-coordinates at each boundary, respectively. A flowchart of the image processing is shown in Fig. 3.13. As the above mentioned mechanism, the welding robot trace the gap center to the horizontal center line in the image and is automatically controlled by the real-time image processing.

Clear images of the fusion zone are taken by the CCD camera as shown in Fig. 3.14. The strong highlight of the plasma arc must be reduced to capture the weld pool situation under the electrode. For this purpose, the author applies a

pulsed welding current. Fig. 3.15 shows a block diagram of the image processing. The image of gap is automatically captured, and the width and centroid of the gap are simultaneously acquired. The approximate gap location is clarified in the brightness distribution under normal conditions. Moreover, a histogram along a vertical line through the brightness profile reveals two distinct brightness peaks. From this histogram, the gray-level threshold is determined. Pixels are binarized by the threshold as 0 corresponding to the gap, and 1 corresponding to the weld pool, respectively.

Molten metal in front of fusion zone is reduced with expanding the gap during the welding process, the brightness of taken image declines as shown in Fig. 3.17a. A histogram through the brightness profile of the vertical line exhibits three peaks, as shown in Fig. 3.17b. In this case, the threshold value is obscured by a possible error in the numerical calculation, which presents between the right and center peaks. The average brightness is in the dark part of the weld pool. Above-average brightnesses are lowered to the average and the peaks of the weld pool are merged into a single peak so as to determine the threshold value, as shown in Fig. 3.18. This figure was generated by implementing the image processing in Matlab/Simulink as shown in Fig. 3.15.

3.5 Results and Discussion

The work piece was a 9-mm-thick plate of mild steel with a 3-mm butted section and a groove corner of 90° in normal condition. The supplied gas was pure argon, and the other welding conditions are listed in Table 1.

Table 1 Experimental data of plasma arc welding

Diameter of nozzle	3.2 mm
Electrode setback	3.5 mm
Flow quantity of orifice gas	3.2 l/min
Flow quantity of Shielding gas	10 l/min
Standoff	6 mm
Pulse frequency	20 Hz
Duty ratio	40 %
Peak current	300 A
Base current	200 A
Travelling speed	15 cm/min

In the experiments, the start and end points were on the groove center and at a 2-mm away from the groove center, respectively, and automatic tracking of the PAW was performed. The tracking result of template matching by the image processing program is presented in Fig. 3.19. The PAW was started after an initial 4-s stop period, and the automatic tracking began at 10 s. The weld line was

properly tracked by the template matching procedure as mentioned in chapter 3.2. Figure 3.20 shows the weld bead on the base material. Near the start point, before the control was applied, the weld line deviated from the reference. Once the control was applied, the tracking was successfully accomplished.

In the case of template matching procedure of keyhole as mentioned in chapter 3.3, the welding condition is as same as before. But it has adopted a 235A of constant current as the welding current. Tracking result is shown in Fig. 3.21. This time, automatic tracking of PAW was monitored. In processing program, deviations $e_t[i]$ calculated by Eq. 2.3, is the difference between reference positions Rt and abscissa value of central point. Simultaneously, command pulse of the position in robot axis is calculated by Eq. 2.8 and it is sent to the robot. After fundamental experiments, desired positions Rt of welding torch was determined as 640 pixels (Ref 0 mm) in vertical direction. A deviation of 1 mm corresponds to 70 pixels in the target image. Welding robot was started after an initial 4-s stop period for the generation of keyhole, and automatic tracking began at about 10 s. It can also confirm that detection points of the torch distance from weld line were approaching the reference after tracking started.

Welding robot was controlled by using the image processing result. Specifically, plasma torch is located to learned the approximately correct position before starting fundamental experiment. Tracking of weld line was carried out during the experiment. Figure 3.22 shows the weld bead on base material. Near start point, before the control was applied, the torch was deviated from the weld line. From the corresponding images in Fig. 3.22b, a deviation between the controllable yellow center as torch position and objective red center point of boundaries growing bigger before tracking starts. Once control was applied, two points coincides with each other in steady state to exhibit a successful tracking in the welding experiment. Stable formation of back bead can be confirmed at the same time.

Figure 3.23 shows the tracking performance in the presence of a gap. The width, which increases with the weld length, is properly detected as shown in Fig. 3.23a. Ten seconds after the start of tracking, the welding position followed the gap center of the base metal shown in Fig. 3.23b. The threshold between the gap and base metal was determined by binarizing the vertical histogram acquired along the center of the image. The image was trimmed to accelerate the image processing.

The image processing in chapter 3.4 is intended for control of a welding robot. Prior to the control experiments, weld line is taken by CCD camera and the welding position is recorded in preliminary experiments. The profile control was then implemented by tracking the weld line of the gap center. The position order pulses calculated by Eq. 2.8 were conveyed to the robot. Figure 3.24 shows the topside weld bead on the base material. The image processing result of the weld line under the profile control is shown in Fig. 3.25. In this case, the control was started at 10 s after the begining of welding. The back bead closely corresponded to the gap. The experiments yielded a good tracking result with no false teaching data. Therefore, the image processing and the utility of the profile control were well confirmed.

3.6 Conclusions

In the image processing for automatic tracking, template matching is a technique used digital image processing for finding small parts of welding typical image which match the template image, serving as a part of quality control in general case.

Since welding quality in PAW depends on the performance of tracking results and maintenance of keyhole, it has integrated automatic tracking control of

weld line by using an image processing under monitoring of keyhole. Welding results has proved that an efficient, high-quality, and stable welding process has been achieved in this study.

Moreover, boundary detection method effectively detect the existence and boundary of the gap, and make real-time tracking and analysis of variable gap to ensure the welding quality in particular case.

In general, the image processing for automatic tracking of the weld line in plasma robotic welding has been considered in the case whether there is a gap or not. Template matching technique is efficient under normal circumstance.

In verification trials, proposed method demonstrated efficient welding work as follows:

1. Weld pool images were clearly obsereved by the CCD camera on the camera link transmission.

2. Lots of fundamental experiments have been conducted to make an acquisition of characteristic of weld line with monitoring keyhole condition.

3. Relationship between center of the boundary line and weld line has been investigated by high speed video camera and the change of state in V-type groove.

4. Patten matching of characteristic image and detection of boundary line in the fusion zone have been achieved by image processing, and weld line was accurately detected by a hybrid optimization process of image processing in the case whether there is a gap or not.

5. Seam tracking were successfully performed with designed digital control system. Image processing and control system were validated in a real-time welding experiment.

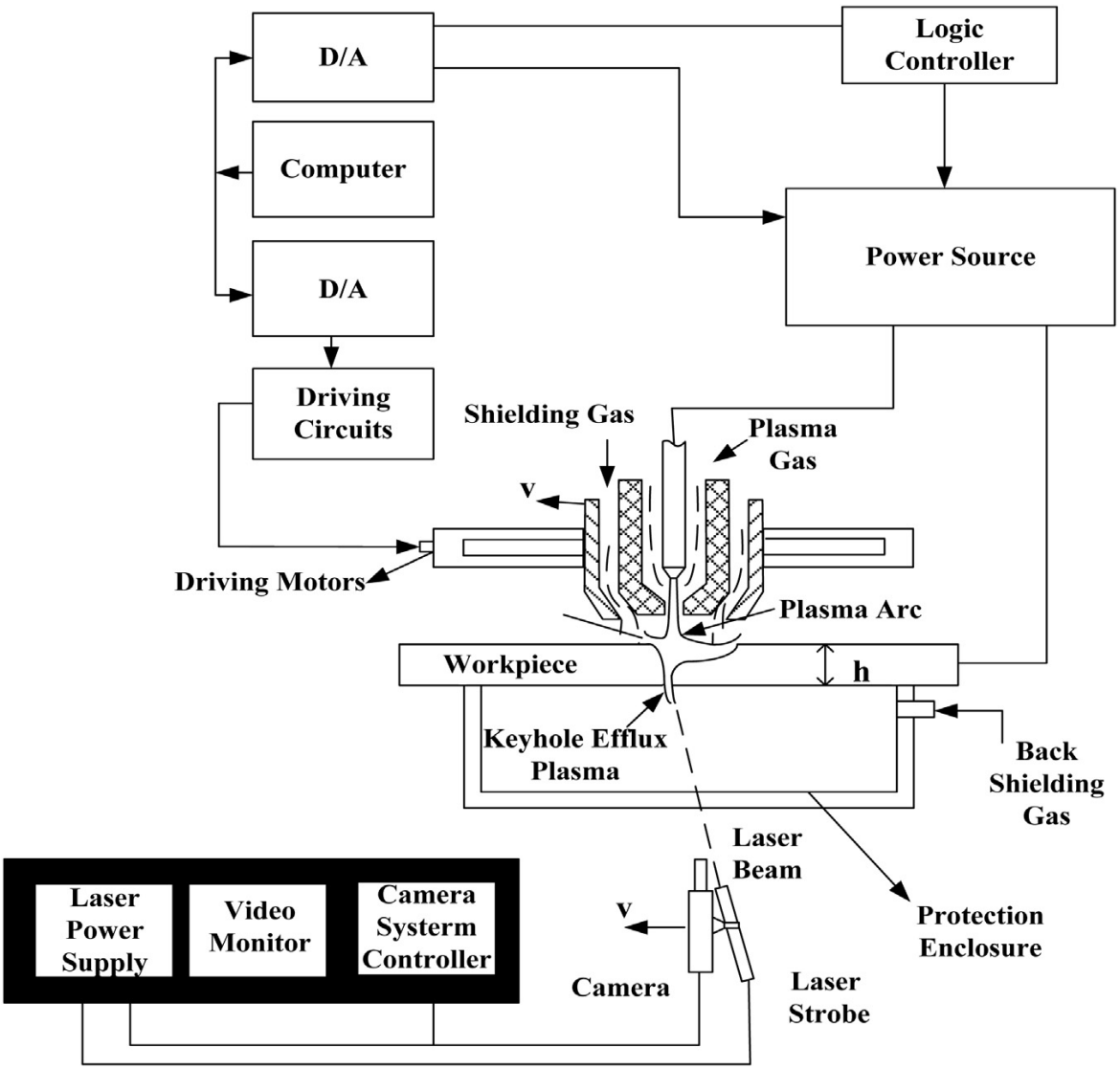

Fig. 3.1 Schematic of the laser-strobe system [28]

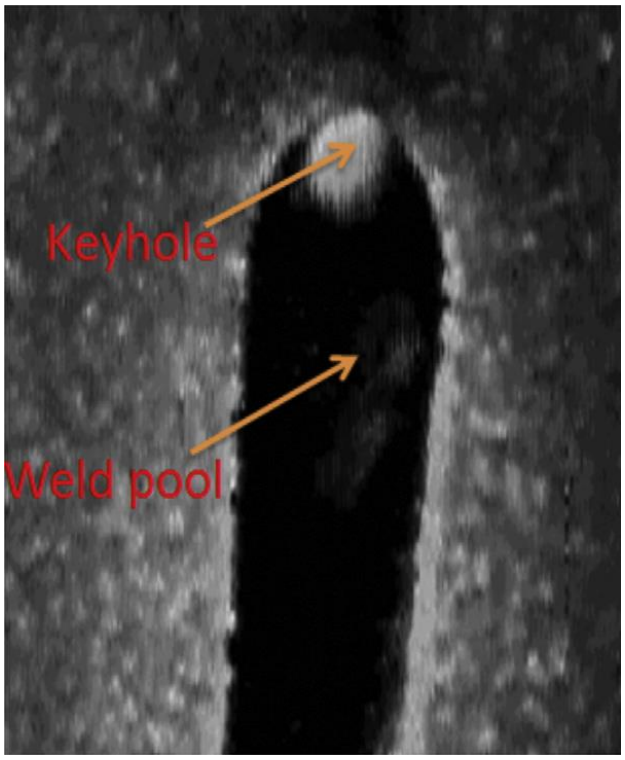

Fig. 3.2 Simultaneous imaging of weld pool and keyhole from backside

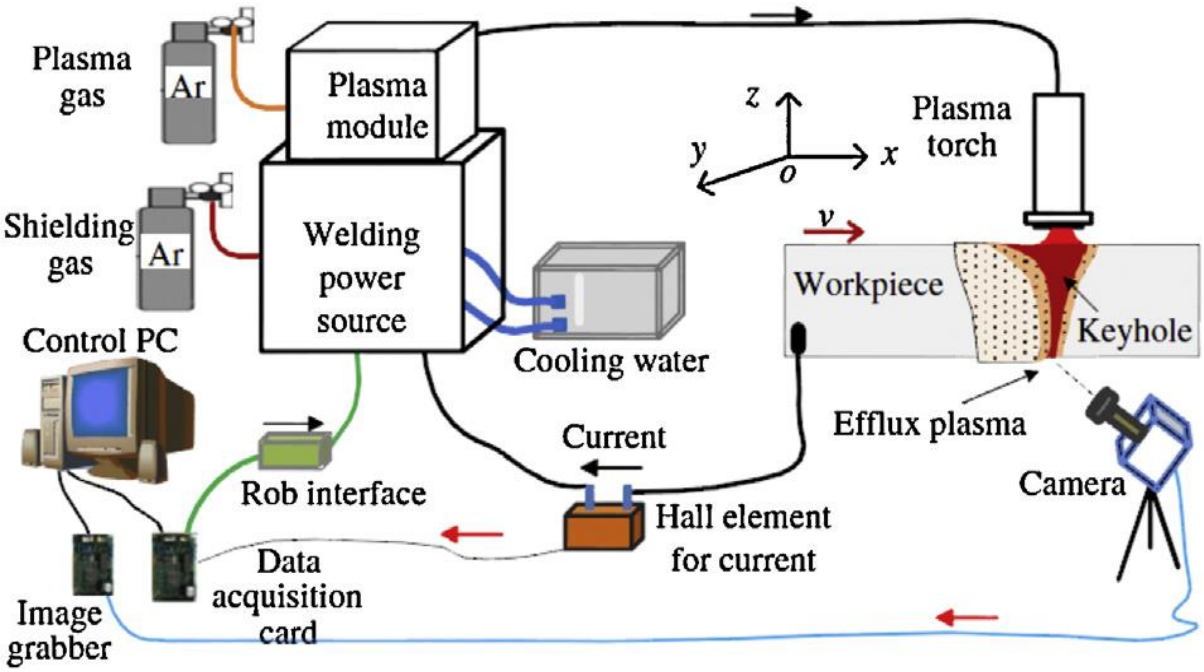

Fig. 3.3 Schematic of the cost-effective vision system [29]

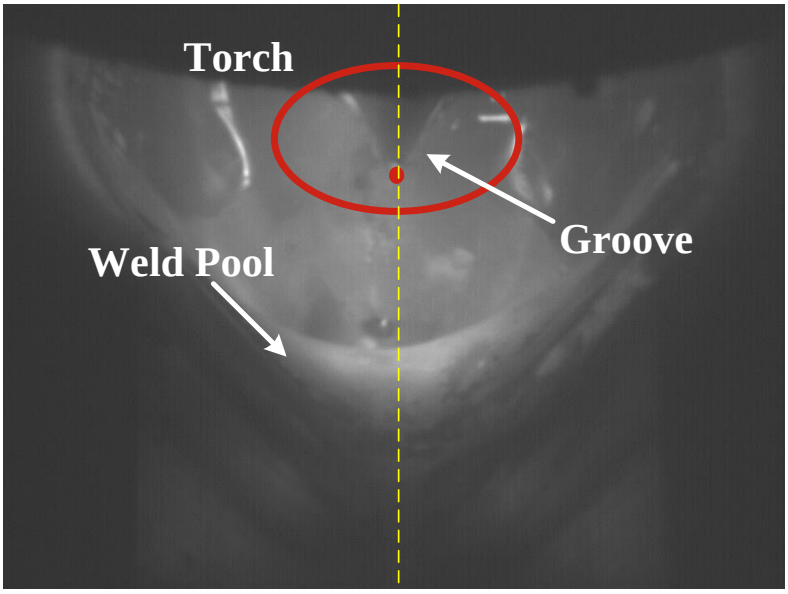

Fig. 3.4 Proposed template matching in the welding process

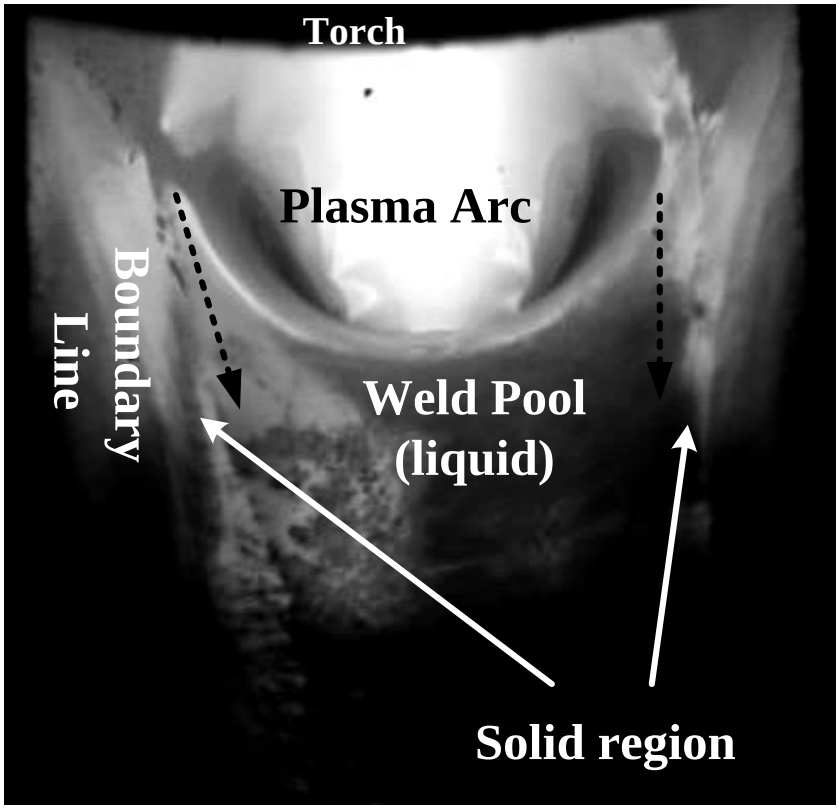

Fig. 3.5 Fusion zone image of high speed video camera

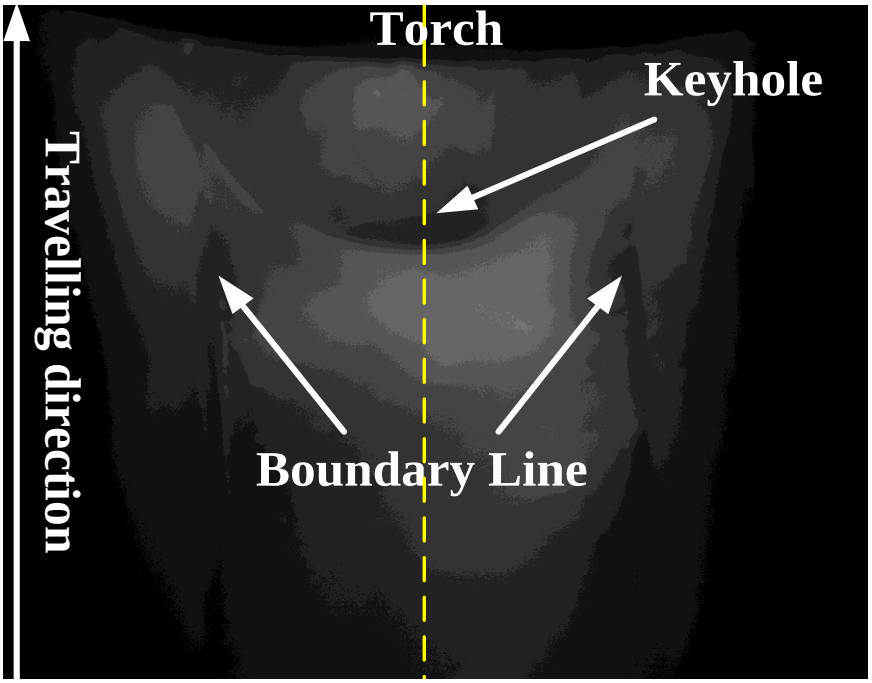

(a) Fusion zone image of following weld line

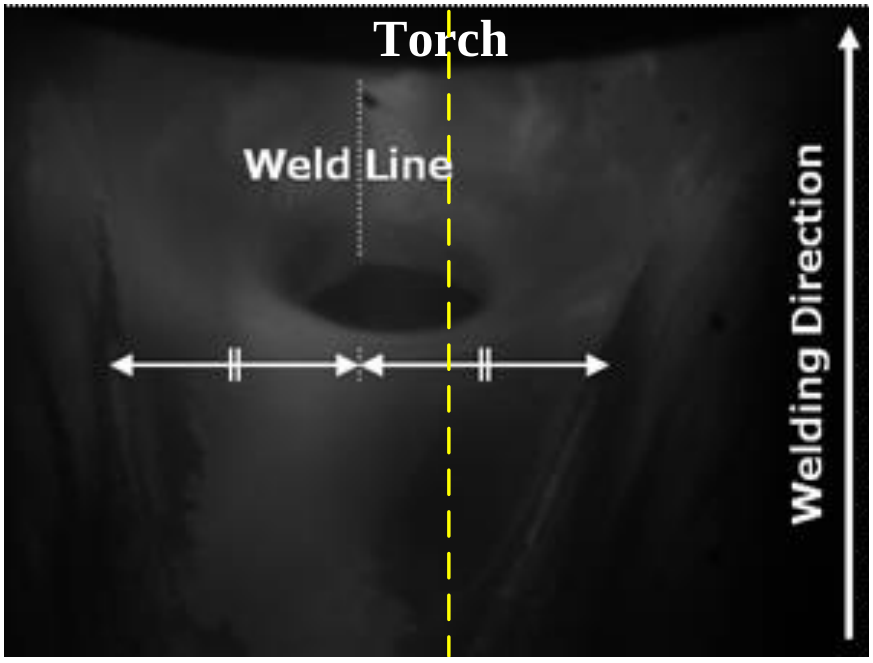

(b) Fusion zone image of wrong teaching

Fig. 3.6 Typical image of no-tracking

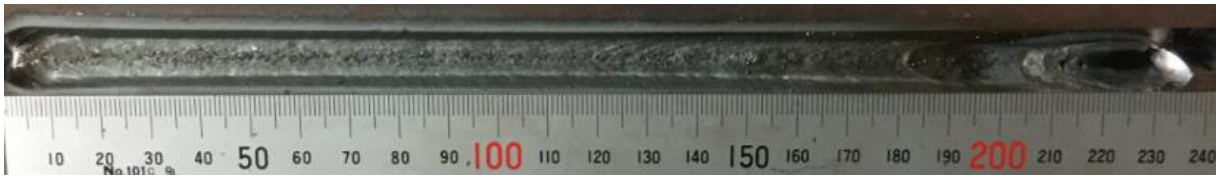

(a) Topside weld bead with wrong teaching

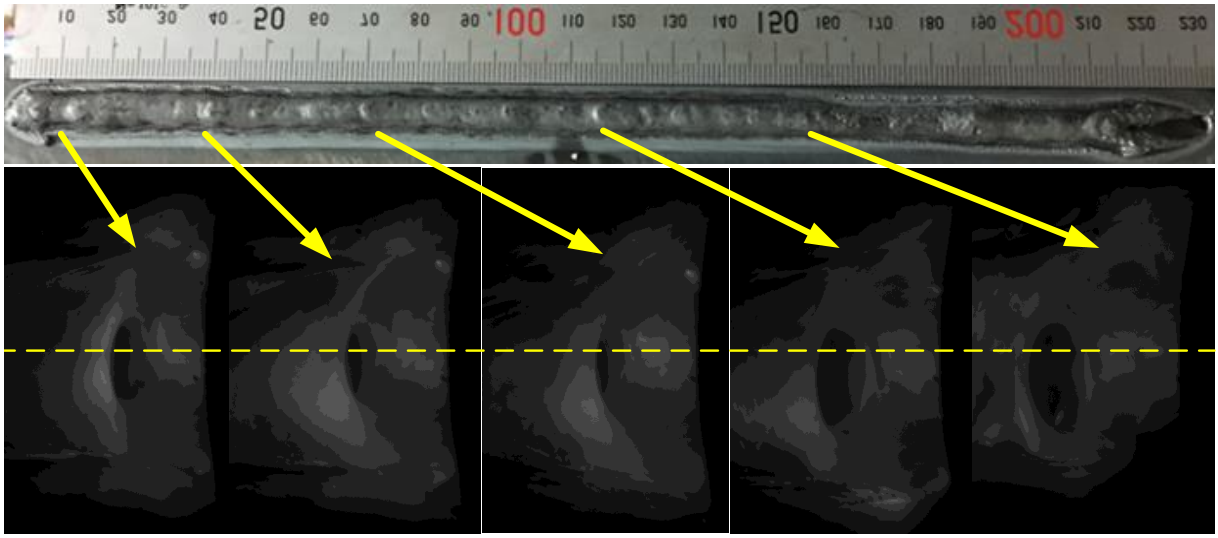

(b) Bead appearance on the rear side and corresponding images of the fusion zone with wrong teaching

Fig. 3.7 Experimental results of placing the endpoint at 3 mm

apart from weld line.

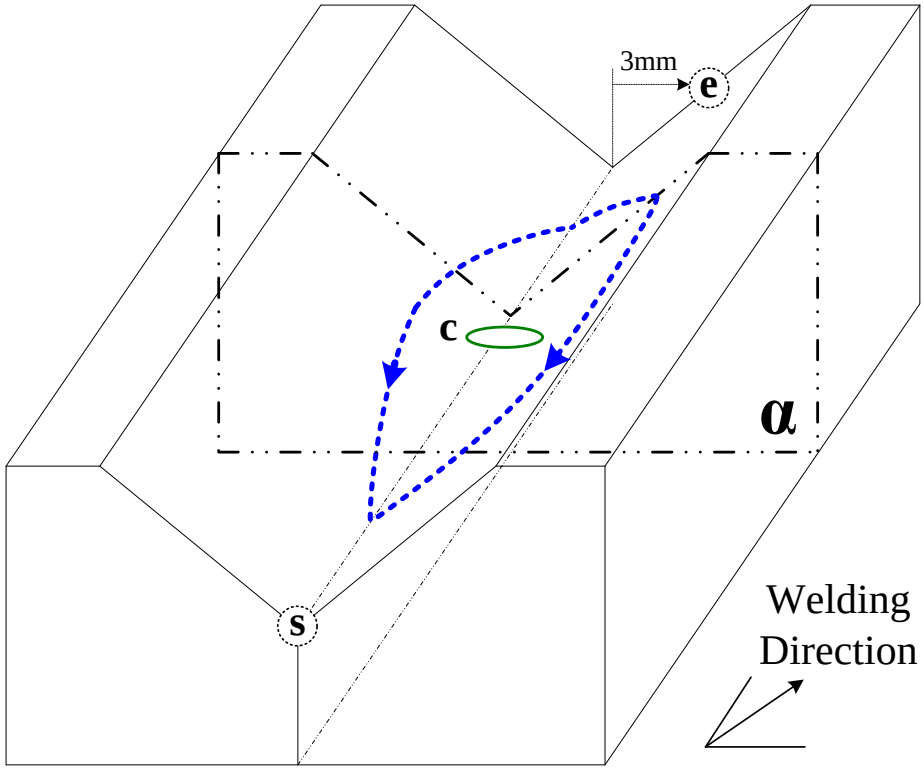

(a) Model of welding state with wrong teaching

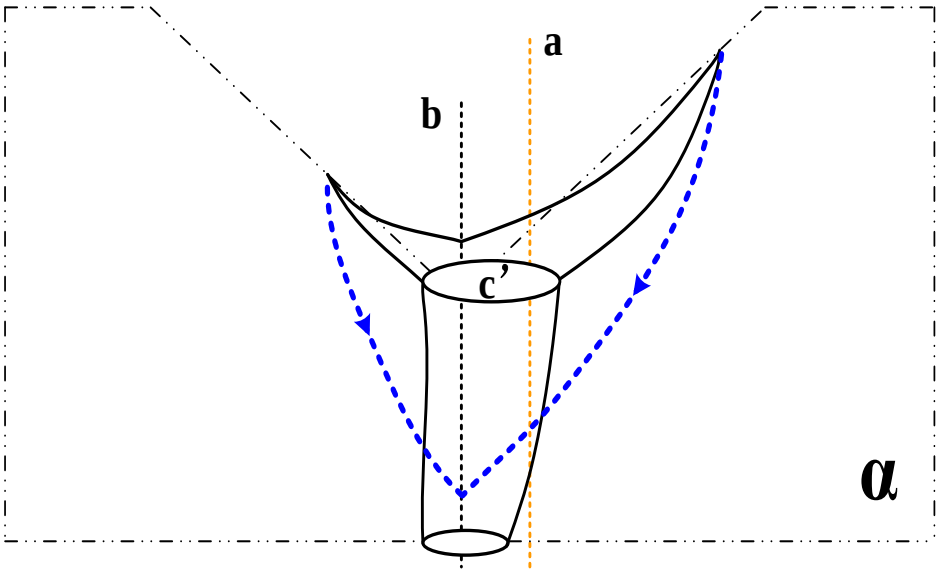

(b) Projection of fusion zone in cross section

Fig. 3.8 Typical model of fusion zone with wrong teaching

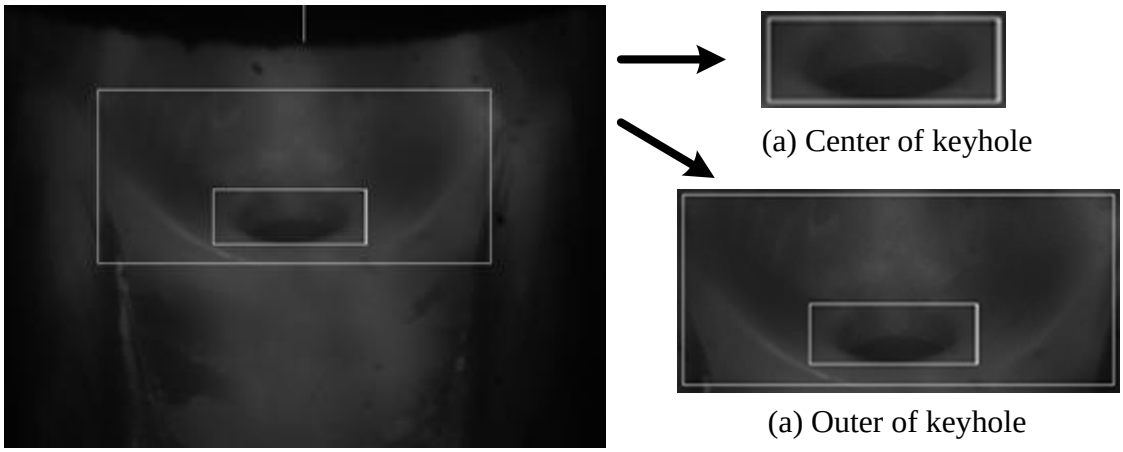

Fig. 3.9 Template matching for recognition of keyhole

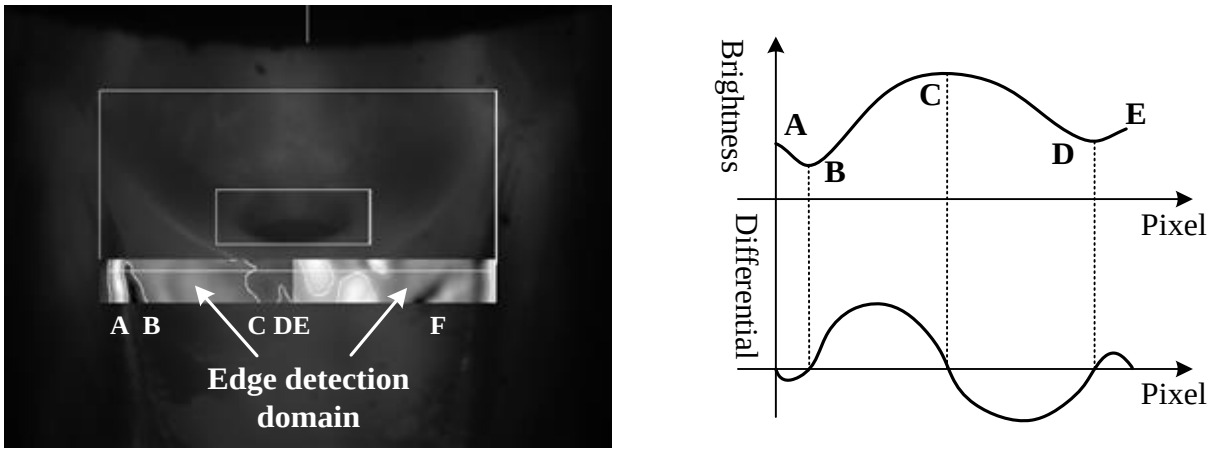

(a) Edge detection in both sides (b) Determination of boundary line

Fig. 3.10 Boundary acquisition by using differential filter of Gaussian function

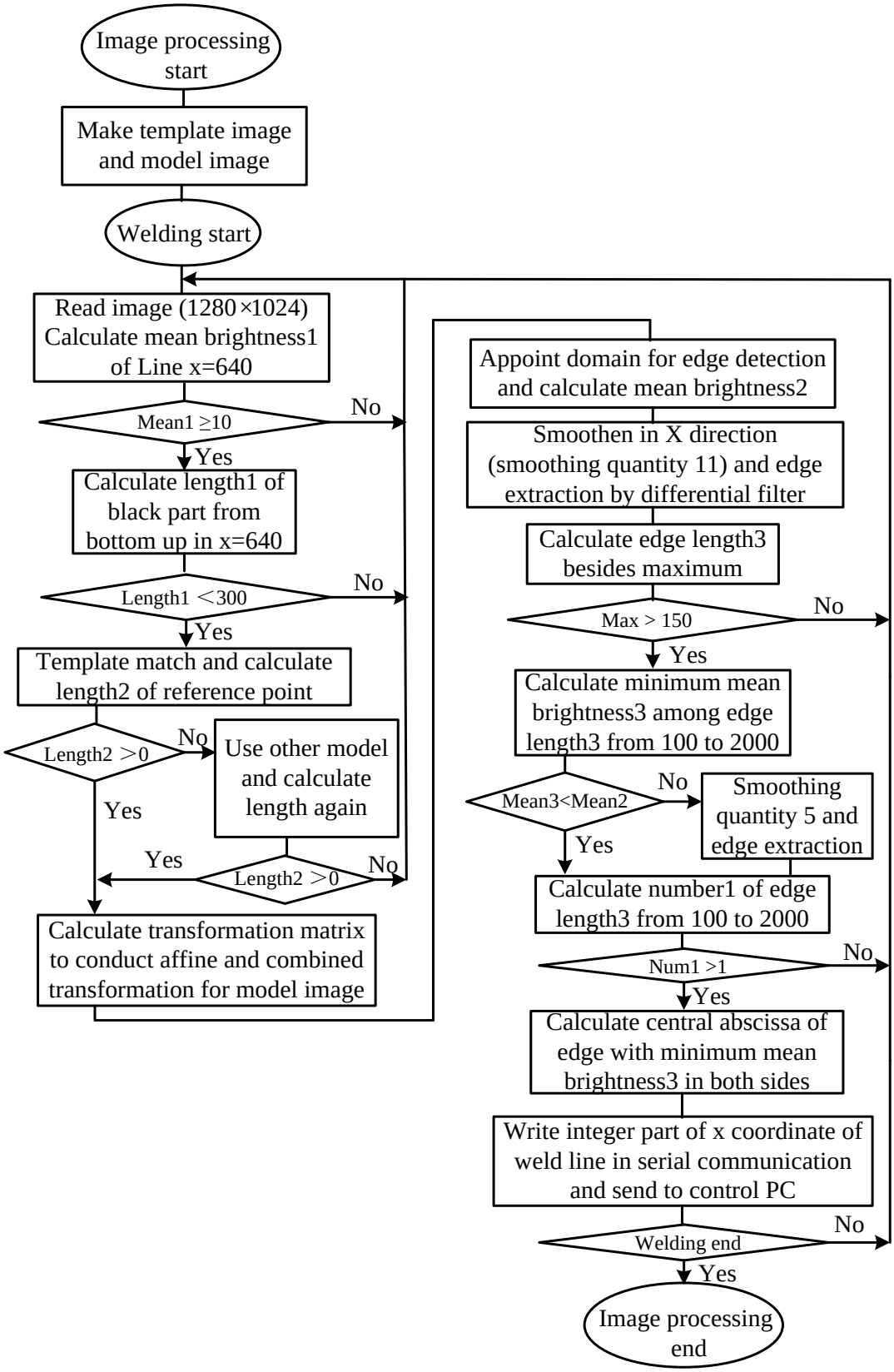

Fig. 3.11 Flowchart of image processing algorithm

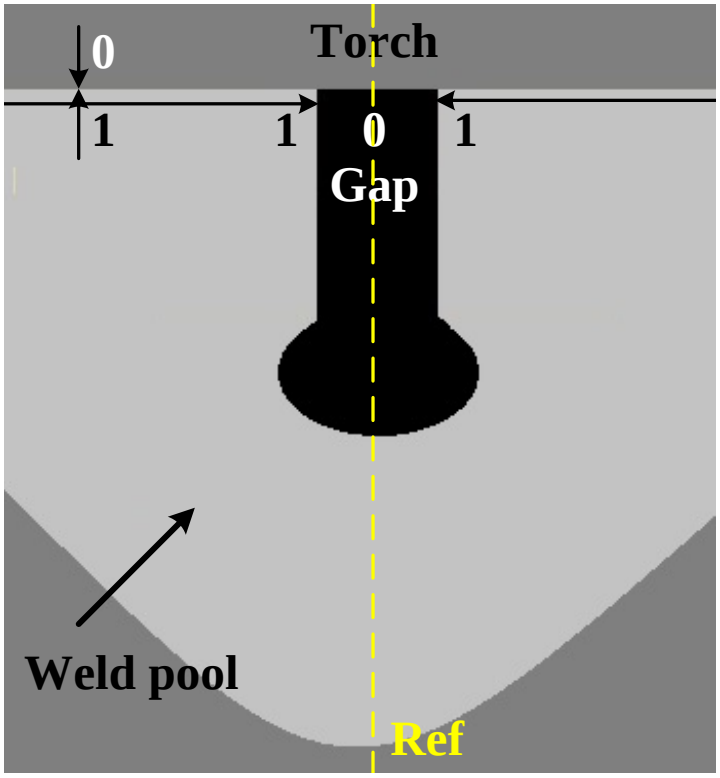

Fig. 3.12 Principle of image processing

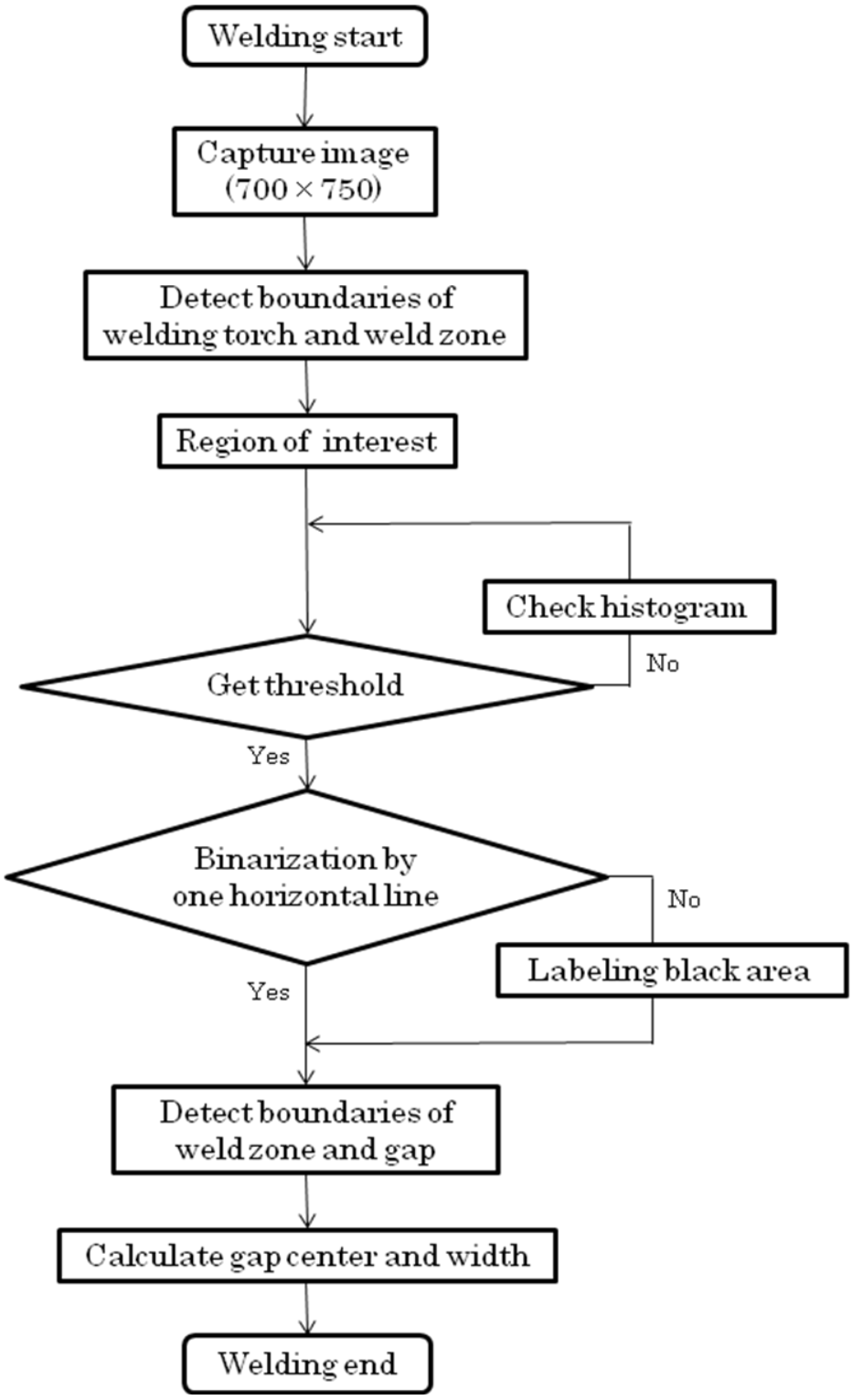

Fig. 3.13 Flowchart of the image processing algorithm

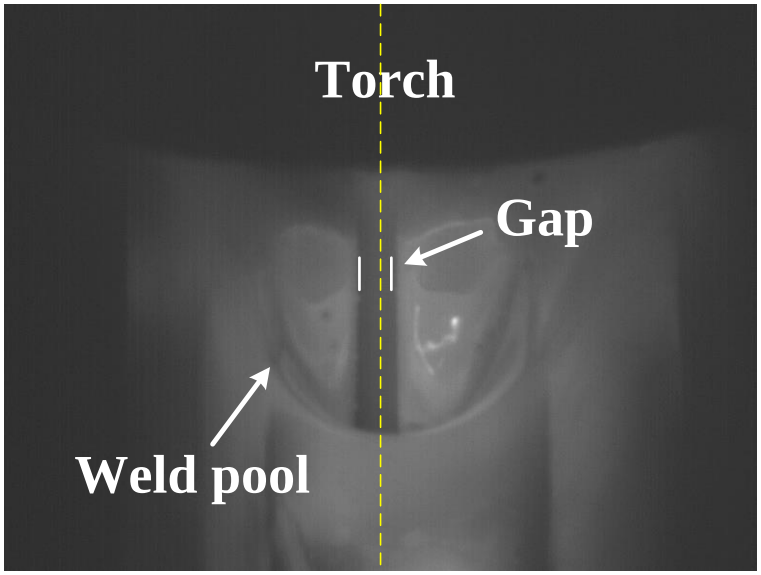

Fig. 3.14 Image processing result

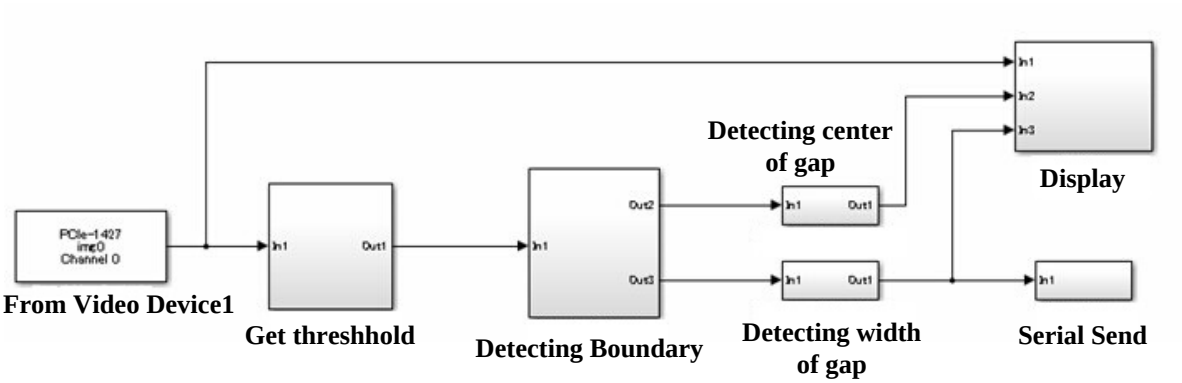

Fig. 3.15 Block diagram of the image processing

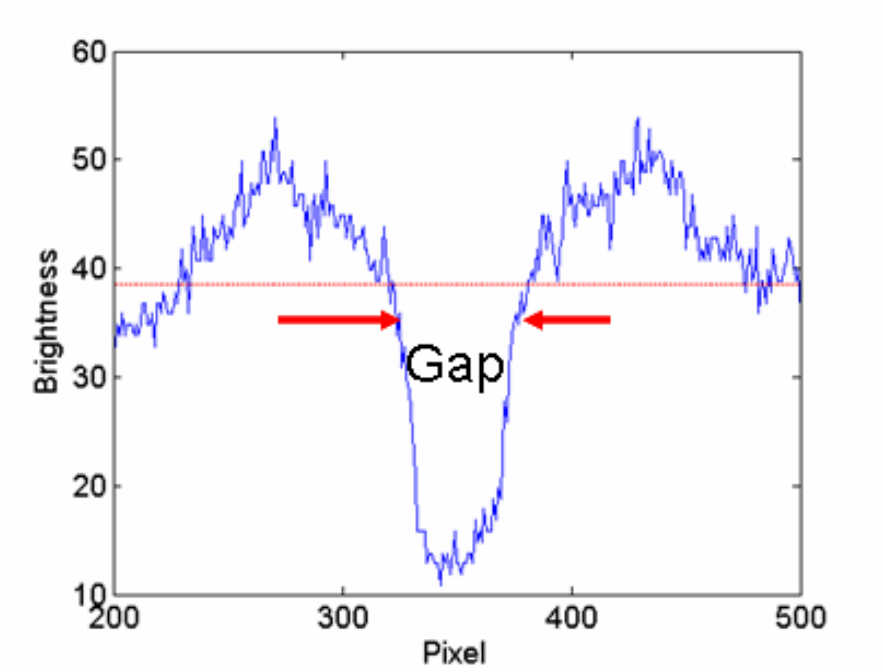

(a) Brightness distribution

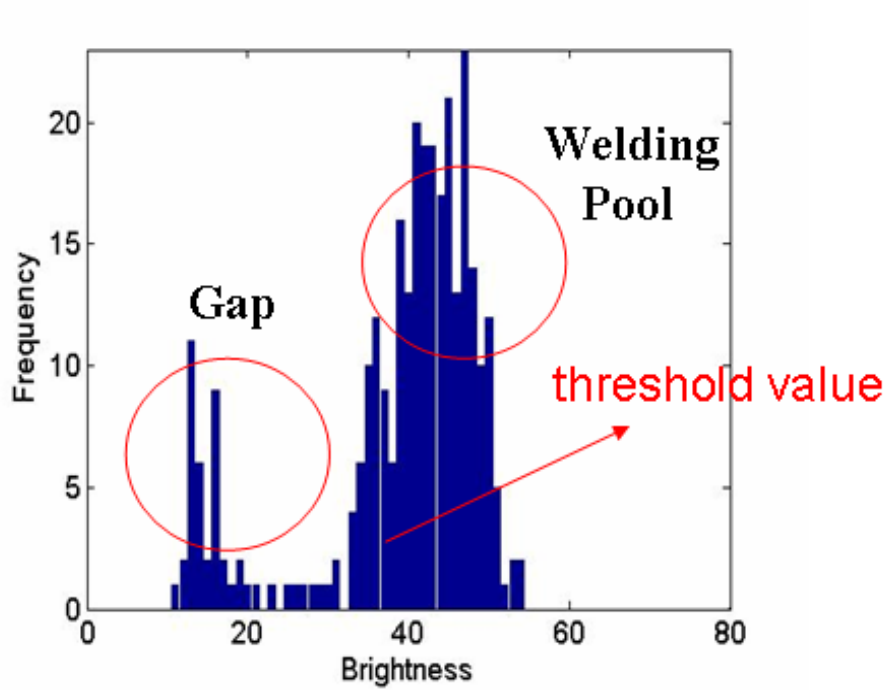

(b) Histogram of horizontal line

Fig. 3.16 Image processing under normal conditions

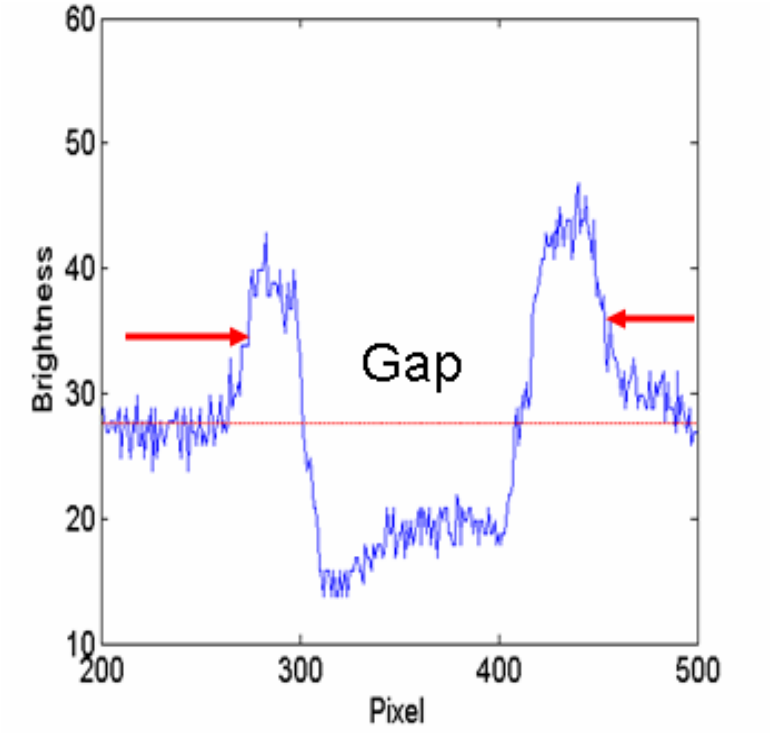

(a) Brightness distribution

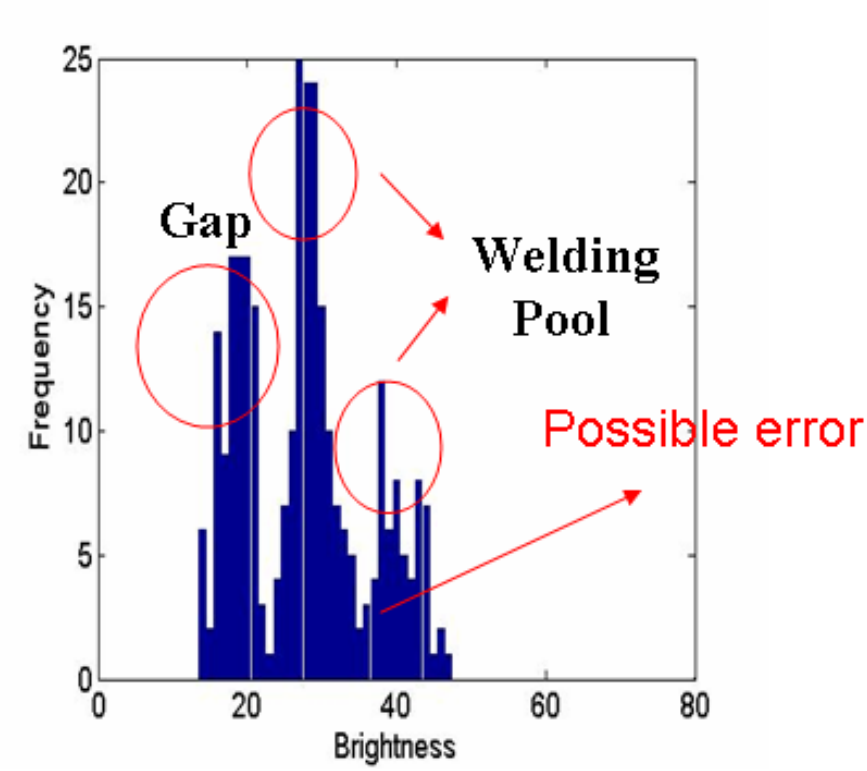

(b) Histogram of horizontal line

Fig. 3.17 Image processing under decreased brightness

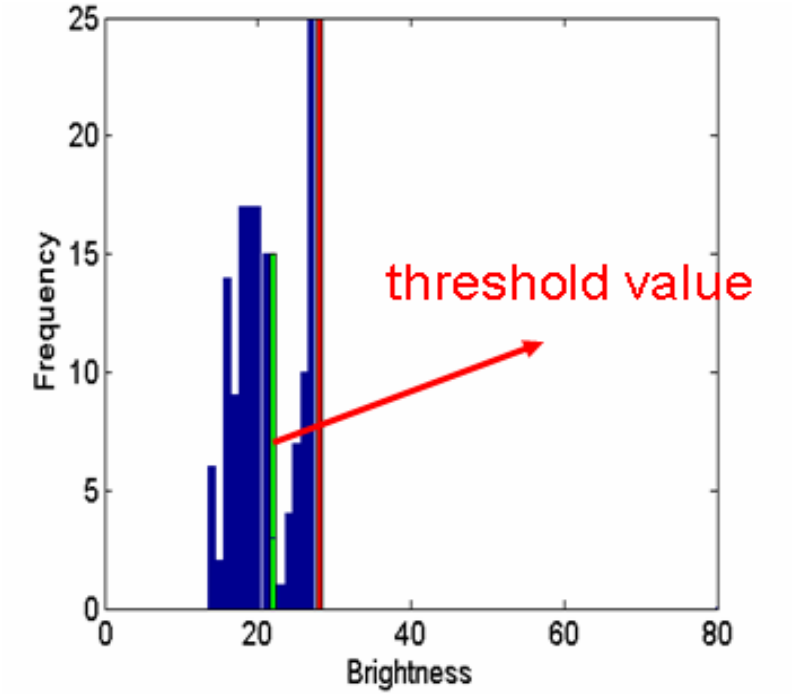

Fig. 3.18 Determination of threshold in the declining brightness case

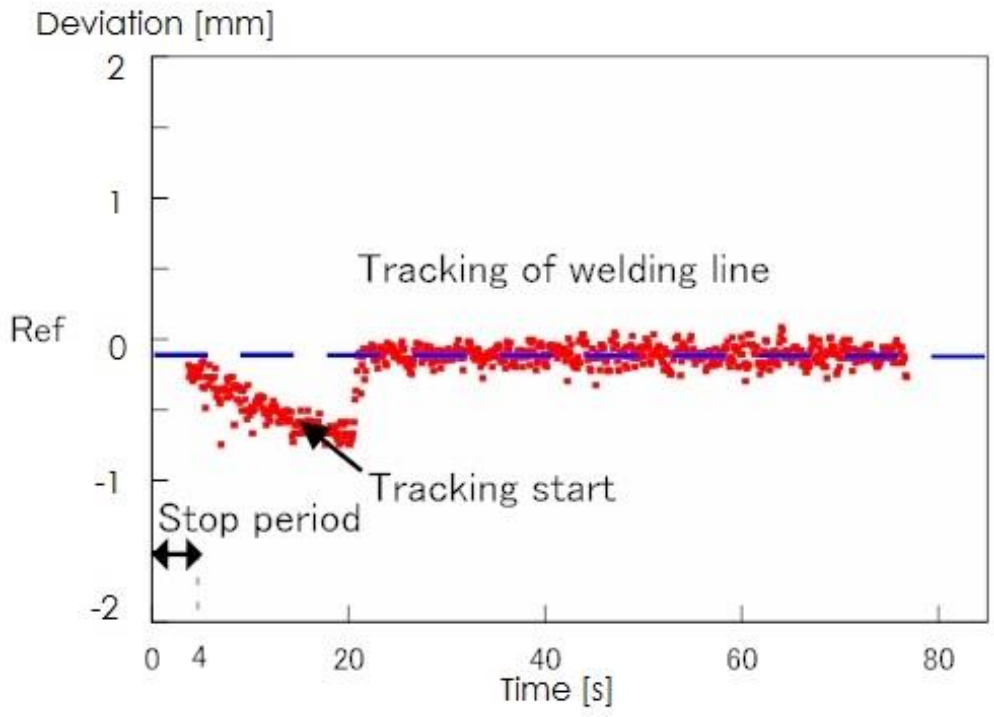

Fig. 3.19 Tracking result of template matching

(a) Photograph of the topside weld bead

(b) Back bead of base material

Fig. 3.20 Weld bead of base material under normal conditions

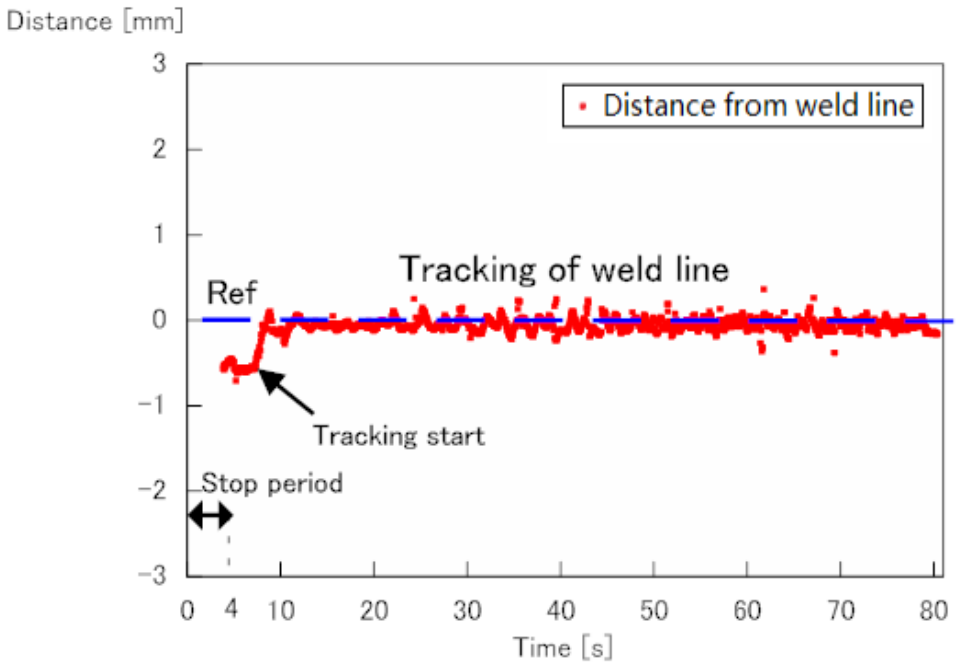

Fig. 3.21 Tracking result of weld line

(a) Photograph of topside weld bead

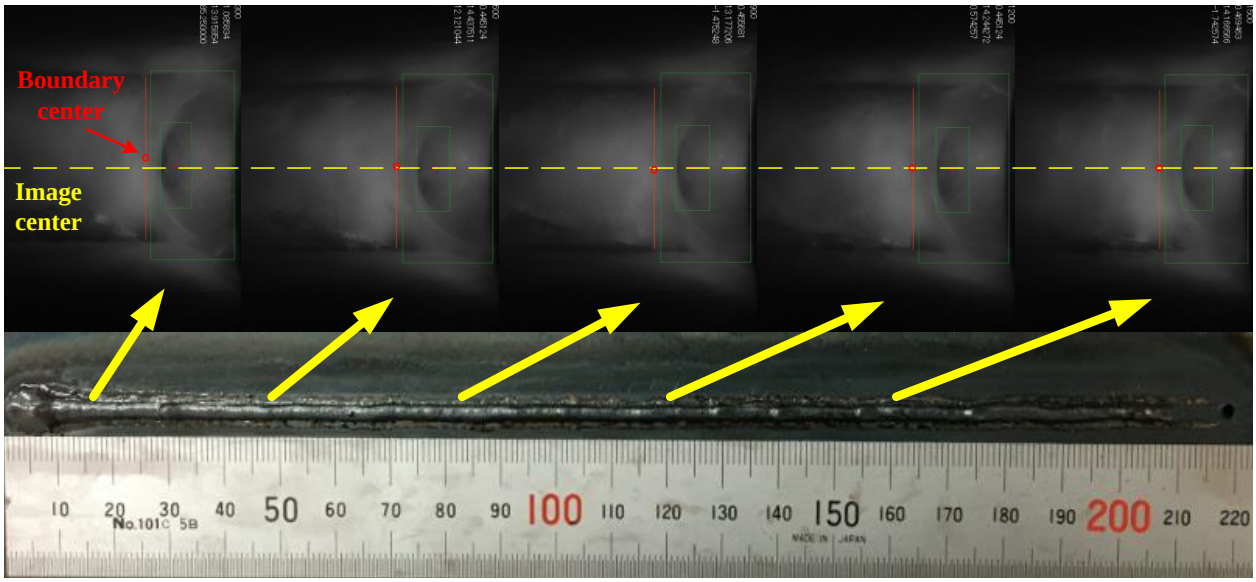

(b) Bead appearance on the rear side and corresponding images of fusion zone

Fig. 3.22 Experimental results after rough learning of weld line by the robot

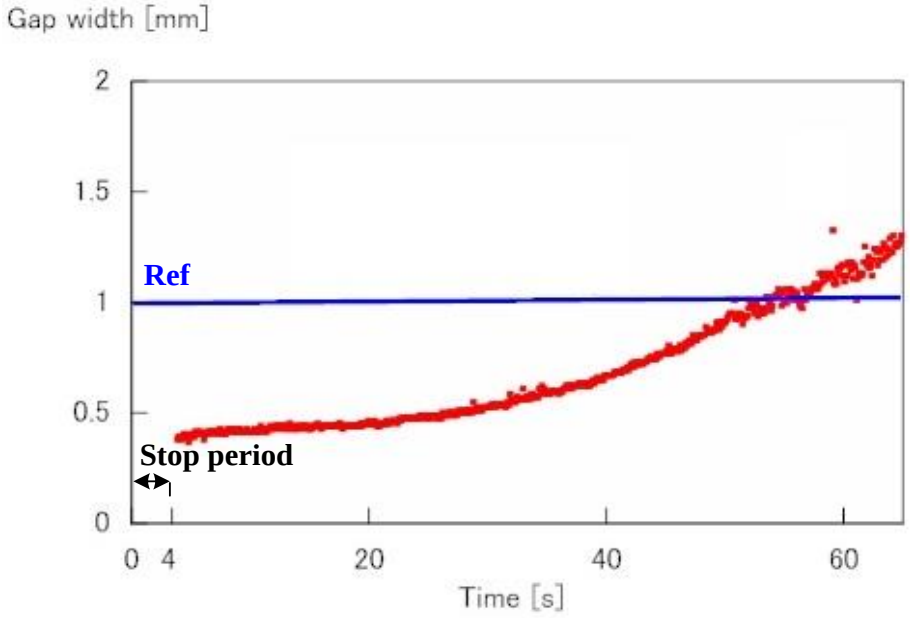

(a) Variation of gap

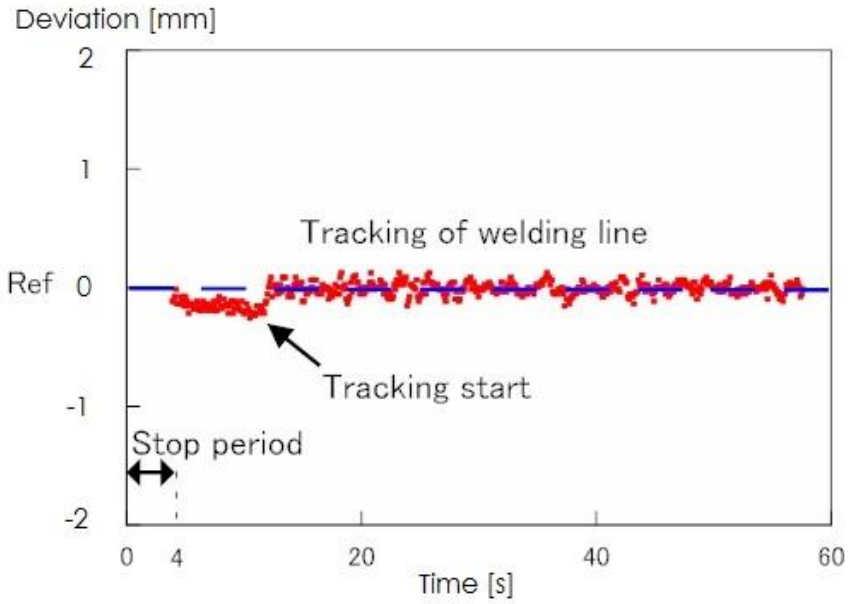

(b) Tracking result

Fig. 3.23 Tracking performance in the presence of a welding gap

Fig. 3.24 Photograph of the topside weld bead on the base material

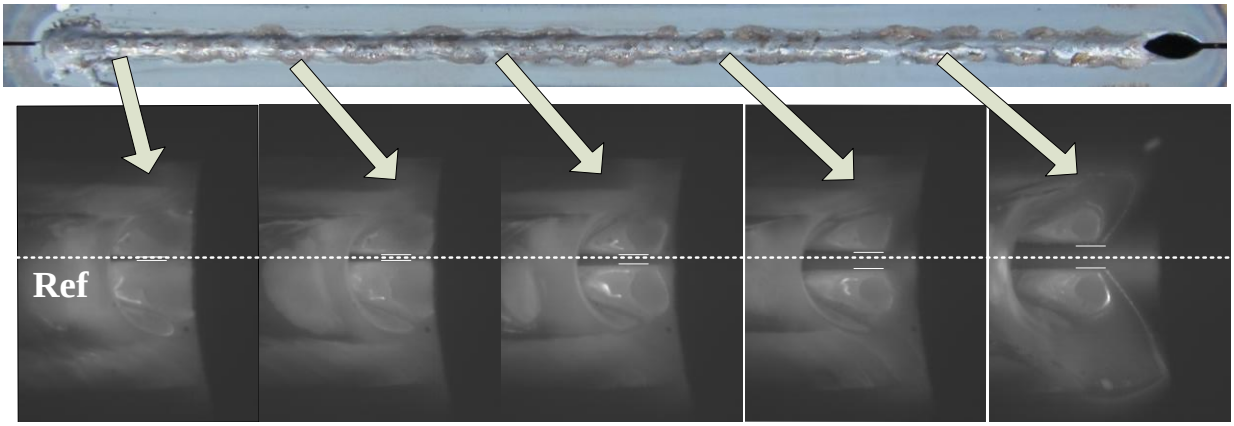

Fig. 3.25 Correspondence between back bead and gap of the weld pool

CHAPTER 4. COMBINATION SYSTEM OF PLASMA AND GMA WELDING

4.1 Introduction

Since inert gas has been employed as shielding gas in the MIG welding for steel, it is thought to obtain a good quality of welding result. However, cathode spot will become unstable due to no oxide film existing on the surface of base metal. And in MIG welding, metal transfer commonly depends on the stability of MIG arc. Additionally, several researchers have reported to achieve stable arc under the inert shielding gas in MIG welding, including the combination of laser and MIG, TIG and MIG, and plasma-MIG, which have been proposed to improve the stability of MIG arc.

Hybrid welding, such as laser welding combined with MIG welding has been developed to get a high efficiency [39, 40]. Although MIG arc became stable due to keyhole of the laser welding, the laser welding equipment is thought to be expensive. A combination of TIG welding with MIG welding has been developed. In this method, MIG arc maintains stable under the influence of TIG arc in this method [41]. Furthermore, there comes up with a special method of plasma-MIG

welding in which consumable electrode is used as the plasma electrode. And regrettably, it is cannot achieve a keyhole welding [42, 43].

As a result, a brand new PAW system integrating plasma arc welding (PAW) and gas metal arc welding (GMAW) has been proposed. In this system, PAW is leading torch with high current density and GMAW tailing torch using consumable electrode has been developed to improve the welding quality at a higher level. The welding system has used the interaction between the arc of PAW and GMAW. So the distance between welding torches and angel of GMAW torch from PAW torch have an influence on the welding results. When the distance between welding torches becomes small, the fusion zone under both electrodes will form one weld pool. Because the heat input becomes concentrated, it is promising to increase the travelling speed. Due to much molten metal, it is difficult to maintain the surface tension on back bead. If the weld pools join with each other, the flow of molten metal becomes unstable. As a result, in order to conduct a stable welding, it makes the flow of molten metal in each fusion zone independently. The torch configuration is shown in Fig. 4.4.

Combination of PAW with MIG welding to obtain a better welding quality was discussed in this chapter. And in the welding system, the plasma welding to

carry out the keyhole welding is selected as leading electrode, since the keyhole welding is selected to achieve a deep penetration. Moreover, the deposited metal was supplied by MIG welding as tailing electrode. Two kinds of different welding are processing on the same base metal. The polarity of the electrode in the conventional plasma welding is negative. But, the polarity of the electrode in the conventional MIG welding is positive. It is necessary to investigate the polarity of both electrodes.

If the polarity of two electrodes is the same, the current flow is the same direction. Electromagnetic force between two electrodes was upward due to the magnetic field. Positive was used as the polarity of MIG welding to prevent droplet from flying to upper side and failing to form the weld pool. Besides, pulsed current has been used in PAW. The current of MIG welding was synchronized with the current of PAW. Welding phenomena were observed by using high-speed video camera to analyze the phenomena in this study. Interference between the two electrodes has been investigated with respect to weld pool and metal transfer. The pulsed current waveform was adjusted to obtain smooth droplet transfer by using the analysis results. Furthermore, welding conditions are discussed so as to get the stable back bead in groove welding.

4.2 Fundamental principle of dual-electrode welding

High quality welding has been achieved under pure Ar as shielding gas in steel welding, There is a few oxide firm on the weld zone, whereas cathode spot under Ar shielding gas becomes unstable in GMA welding. On the other hand, in the case of active gas like CO_2 or O_2 used as shielding gas, cathode spot become stable owing to impurities such as the oxide firm. However, if oxide exists in welds, mechanical strength of weld joint becomes weak.

Keyhole welding was together with the MIG welding. As a consequence, a welding system with dual-electrode was proposed in this study. In this system, the leading torch is plasma torch and the tailing torch is MIG torch. On the other hand, through the welding system of PAW and GMAW, it is available to obtain a full penetration weld kept by keyhole in PAW and deposited metal weld owing to MIG welding.

The condition like polarities of welding power supplies for PAW and GMAW and electrode distance between both welding should be taken into consideration to build a welding system of PAW and GMAW. The influence of polarities of welding power sources to the welding phenomena was investigated by using high-speed video camera. If the same polarity of power supplies used,

the direction of current flow is the same. Electromagnetic force between two electrodes turns upward due to the same direction of current flow. Droplet of MIG welding flew to plasma tip. As a result, the weld bead was not formed.

On the other side, influence of electrode distance between PAW and MIG welding was investigated as well. If there is a short distance between the two electrodes, two weld pools under leading torch and tailing torch join together, one pool was formed. Hence, bead on the rear side of base metal became unstable due to much molten flow. If the distance between two electrodes was long, the back bead became stable. However, the interference between dual-electrode of PAW and MIG welding became weak. As a result, the stability of arc becomes weak in the MIG welding.

Appropriate welding conditions were found to make a stable metal transfer and stable back bead by carrying out the fundamental experiments.

4.3 System configuration

Welding system of PAW and GMAW with dsPIC of 16-bit digital signal processor is shown in Fig. 4.1. Besides, leading torch is the plasma welding. On the other side, tailing torch is MIG welding controlled by PC controller. Power source of MIG welding has been controlled according to the power source

characteristic, and pulsed welding current is used to achieve one droplet per one pulse. And the PAW current is synchronized with MIG welding.

Author has taken advantage of the power source characteristic to make a control of the pulsed MIG current. Power source voltage E(i) is equal to voltage drop of reactance L of the welding circuit and torch voltage v_t as in Fig 4.2

$$\frac{di}{dt} = \frac{E(i) - v_t}{L} \tag{4.1}$$

If v_t was higher than the voltage *E(i)* of power source, $E(i) - v_t$ becomes negative and current *i* decreases. Power source characteristic is composed of the rising characteristic and drooping characteristic as shown in Fig. 4.3. The no-load voltage is 55V and carrier frequency of inverter is 15kHz. Moreover, The output is controlled by Pulse Width Modulation (PWM), and *E(i)* is found from the welding current i and characteristic of power source, so as to get the average output being equal to $E(i)$. Operating point of voltage v_t and current *i* is on the drooping characteristic during base current, as illustrated by the dash line, i.e., the base current is 150A. If the voltage v_t is lower than $E(i)$, current *i* increases until operating point reaches the drooping characteristic of power source characteristic. Increment rate of current depends on the difference between voltage v_t and power

source voltage $E(i)$ due to Eq. 4.1. If power source characteristic changes to the dash line from solid line, torch voltage v_t becomes higher than power source characteristic $E(i)$. The welding current decreases until the current becomes base current.

4.4 Effect of polarities of PAW and MIG welding on transfer of droplet

The electrode polarity of conventional PAW is negative. If the electrode polarity were positive, the electrode would be worn out. Hence author has investigated the influence of polarity in MIG welding through using high-speed video camera. Configuration of two electrodes has been shown in Fig. 4.4. In the first place, polarity of MIG welding is set to negative and because the polarities of both electrodes are same as each other. As power sources are independent, the directions of current flow become the same. Upward magnetic force due to the same current direction acts on the droplet as illustrated in Fig. 4.5. As a consequence, droplet has transferred upward from the electrode and been deposited onto plasma tip, that is, the bead formation is impossible.

On the contrary, the polarity of MIG welding changes to positive in configuration of welding torch illustrated in Fig. 4.6. In this case, polarity of plasma electrode is different from that of MIG welding power source. Although

the MIG welding current may flow from the PAW power source through arc, two welding currents has interfered each other. Magnetic force generated by plasma current acts on droplet according to Fleming's left-hand rule, and the direction of magnetic force is rearward so that droplet is deposited on the weld pool. The peak of pulse current is synchronized with that of plasma current all the time. As a result, relationship between droplet and welding current taken by high-speed video camera is shown in Fig. 4.7.

Metal transfer becomes stable due to the interference of welding currents, although shielding gas is pure Ar and there is no oxide firm existing under MIG electrode. As mentioned above, in dual-electrode welding, PAW starts before MIG welding to make a keyhole in advance. After stable keyhole generating, MIG welding starts. The arc of PAW is discharged backward as illustrated in Fig. 4.8. The arc of MIG welding was interfered with that of plasma arc welding. The arc of PAW was discharged forward as a result.

If PAW and MIG welding start simultaneously, it will be difficult to make a keyhole as shown in Fig. 4.9. Deposited metal of MIG welding deposit on the weld pool generated by PAW according to the plasma jet of MIG arc. Deposited metal is available to fill the keyhole. Since the jet of PAW is strong in the case of no

keyhole, spatters as small particles fly out from the weld pool. No bead remains on the rear side of base metal. The keyhole generated by PAW is important to improve the spatter and bead as illustrated in Fig. 4.10.

4.5 Effect of the distance between two electrodes to arc stability

Metal transfer of MIG welding becomes stable in steel welding due to the arc interference of PAW. Influence of the distance between two electrodes to stability of back bead was investigated. If electrode distance is short, the two weld pools joins with each other as shown in Fig. 4.10. Metal transfer becomes stable but bead on the rear side becomes unstable. Since the keyhole welding of a deep penetration is carried out, and the arc pressure in the MIG welding is strong enough, much molten metal flows to the rear side through keyhole. A large volume of molten metal appears on the rear side of base metal, molten metal decreases on face bead. There was the burn through in base metal as shown in Fig. 4.11. The back bead will become unstable. Regrettably, one weld pool is not suitable to make stable back bead.

The distance between two electrodes has been made larger than one weld pool to separate the weld pool as shown in Fig. 4.12. For this purpose, the distance between two electrodes has changed from 15mm to 35mm. In this case, keyhole

welding is performed by leading PAW torch to maintain a deep penetration, and bead height can be obtained by MIG welding. However, if the distance between two electrodes becomes too large, there will be no arc interference of PAW and metal transfer turns unstable. Hence, synchronization of pulse peak current and distance between two electrodes are important.

In addition, relationship between the distance and stability of back bead of base metal has been investigated by using high-speed video camera. Fundamental experiments have been carried out under several kinds of distance. In the experiments, the thickness of base metal is 9mm and diameter of the electrode wire is 1.2mm. Traveling speed is 2.5mm/s and feed rate is 90mm/s. Typical welding phenomena by taking high-speed video camera is shown in Fig. 4.13.

4.6 Occurrence and discussion of welding defect

It confirms that the arc of MIG welding becomes stable under the interference of PAW, by using the welding system of PAW and GMAW. There're a lot of indistinct parts due to the complexity of welding conditions due to the combination of PAW and GMAW. If the welding condition is improper the welding results become welding defects.

It has effectively acquired the appropriate welding condition to make an improvement of the welding defects by analyzing the cross section of weld bead, corresponding waveform and arc condition photograph by high-speed video camera in the welding process. During the combination of PAW and GMAW, it is available to perform the keyhole welding and building up of groove at the same time, which leads to an improvement of high work efficiency and welding quality. By using inappropriate welding condition, welding defect may occur during the welding process. Whether the blowhole coming into being inside fusion zone or undercut forming at the toe of weld bead, both lead to a decrease of mechanical strength.

In general, blowhole is caused by the disorder of weld pool and shield gas. Since the gas like air is entrapped in the molten metal, and remained as pore. Moreover, the pit takes place in this dual-electrode welding. Pit is a kind of small hole on surface of the bead as shown in Fig. 4.14a. The blowhole formed as relatively large pore in central part of base metal as shown in Fig. 4.14b. Additionally, not only blowhole and pit, but also the recess called undercut appeared. From viewpoint of practical use, the origin and improvement of these welding defects have been concretely analyzed.

4.6.1 Blowhole forming near the surface

When blowhole is forming near the surface in weld zone, the current waveform of MIG welding becomes unstable as shown in Fig. 4.15. In this case, the arc of MIG welding also becomes unstable such as arc cutting and short circuiting. The arc cutting is mainly due to the magnetic arc blow, and the short circuiting is on account of the touch of feeding wire without the arc.

Arc reproduces after short circuiting occurs. The weld pool becomes disordered state by analyzing the image of high-speed video camera. This kind of blowhole especially appears at the beginning of the welding. Therefore a large number of small pores took place in the cross section of fusion zone or sags in the face bead. In other words, the blowhole depends on unstability of MIG welding.

4.6.2 Blowhole forming in central part

On the other hand, blowhole is forming as relatively large pore in central part of base metal. In this case, the occurrence of arc cutting and short circuit is hardly found out from the current and voltage waveform. However, peak current as indicated by the part circled in the Fig. 4.16, MIG base current became small. The power source characteristics of MIG power supply was shown in Fig 4.2. This power source includes two segments as constant-current characteristic and

constant-voltage characteristic. However, if MIG current is less than 150A, operating point of the voltage characteristic and current is on the constant-current area in the power supply characteristic to refrain from arc cutting.

Besides, by using pulse current, keyhole size changed along with variation of current value. Keyhole became smaller compared to the situation without blowhole by analyzing the image of high-speed video camera. If the keyhole size is not kept an enough size during the period of base current, amount of plasma gas is increased to expand the size of the keyhole.

4.6.3 Undercut

The occurrence reason for undercut, is the position deviation of MIG welding, excessive fusion of base metal by arc, shortage of melting amount, and so on. If the welding conditions are not appropriate, the undercut takes place as shown in Fig. 4.14b.

4.6.4 Effect of MIG peak current to welding defect

The behavior of the MIG arc became unstable due to the interference from the current of PAW as shown in Fig. 4.17. MIG current decreases and voltage increases from the figure A to B in Fig. 4.17. With the variation, since the

brightness in front of MIG electrode becomes high in the high-speed video image, arc in MIG welding is in contact with the arc of PAW.

The arc direction in the MIG welding is changed from vertical to front. That is, the practical arc length in the MIG welding becomes long. The current was reduced according to the power source characteristic. The melting rate is in proportion to the MIG current. If the phenomenon takes place, melting rate of MIG wire decreases, and it will be impossible for an appropriate metal transfer.

4.7 Result and improvement

By using the welding system of PAW and GMAW to carry out the welding experiment, it confirms that undercut (sample *1, 2, 3, 5*), blowhole (sample *4, 5, 6*), and the abnormal dropping of MIG current (sample *7*) has taken place. Characteristic welding section and corresponding welding condition has been shown in Tab. 1 and Fig. 4.18 at the same time. In this chapter, it is going to sum up the examples of weld defect and concrete improvement method.

4.7.1 Improvement of undercut

As it is shown in Fig. 4.18, undercut has occurred on the left side in sample 2, and it is found to be the deviation of welding position. However, on the same terms in sample *1*, undercut occurring on the both sides is thought to be the

shortage of melting amount. As a consequence, melting amount of sample *3*, sample *4* has been increased compared to sample *1*. Although the undercut remains on one side in sample *3* due to deviation of position, it is well improved in the case of sample *4*.

Generally speaking, in order to prevent from the occurrence of undercut, it is normally to increase the melting amount, but with using two electrodes of PAW and GMAW in this welding system, heat input becomes superabundant which may possibly result in an easy formulation of undercut. In sample *5*, undercut and blowhole take place at the same time, yet undercut cannot be seen in sample *6* and sample *8*, which is due to fast travelling speed and the reducing of deposited metal. And at a relatively high travelling speed of 24 cm/min, and nearly 1.5 times melting rate, undercut doesn't occur in sample *8*.

4.7.2 Improvement of blowhole

As blowhole has taken place in this dual-electrode welding, which due to the formation it is classified into one type in the surface part of base metal and the other in central part of base metal. And it is sample *4* that blowhole is occurring in the surface part of base metal with its waveform shown in Fig. 4.15. Though it is a small portion of the waveform during the welding, setting deficiency of power

supply characteristic and wire feeding speed is thought to serve as a reason. In consequence, arc cutting and short circuit of the MIG current take place now and then, and the plasma gas is involved into the weld pool instead of the metal gas at the same time, which is needed to adjust MIG power supply characteristic to achieve the stable state.

On the other hand, it is sample *5* and sample *6* that blowhole is occurring in the central part of base metal, which acting as a representation, the waveform of sample *6* has been shown in Fig. 4.16. Since continuous lowness of MIG base current can be distinctly discovered, it is possible to overlook the problem of PAW. When experimental condition of PAW is not appropriate, especially at the moment when base current value is small, the blowhole is likely to occur. When welding current decreases and cannot maintain the size of keyhole, plasma gas becomes hard to pass through the keyhole. It will be blown backwards and drawn into the weld pool, which results in huge blowhole. Experimental result with the reconsidered PAW condition is sample *7*. Furthermore, with the same melting rate, it has increased the travelling speed in sample *8*, which are using the direct current or pulse current of about 50A difference between peak and base, it is thought to be available to maintain the size of keyhole.

As mentioned before, the state of MIG current reducing continues, it will give rise to the blowhole. The corresponding welding condition is sample *7* with pure Ar. The waveform and image photographed by high-speed camera are shown in Fig. 4.17. MIG current decreases and voltage increases from the figure A to B. With the variation, since the brightness in front of MIG electrode becomes high in the high-speed video image, arc in MIG welding is in contact with the arc of PAW. Therefore, it has adjusted the MIG power supply characteristic to increase the welding current in this case and the welding result has been effectively improved.

4.8 Conclusions

Although a stable metal transfer under pure Ar shielding gas is difficult to join the steels, welding system of PAW and GMAW has been proposed. As a result, PAW torch is leading torch and MIG welding torch as tailing torch. An observation of the welding phenomena was done by using high-speed video camera and an analysis was performed. The following summary has been obtained so as to get a suitable welding result.

Welding defects like blowhole, undercut and some others was investigated, and the author proposed the welding conditions to avoid the defects. The study can help engineers to make a clean welding despite of welding defects leading to a

decrease of mechanical strength. It has also well improved the efficiency and stability of one-electrode of GMAW, and effectively eliminated the bad influence on welding quality in the case of different kinds of welding defects.

1. Polarities of the plasma and MIG welding are set as negative and positive respectively. Electromagnetic force will turn upwards in case of the same polarity of power supplies to be used. A stable metal transfer becomes difficult due to upward force.

2. The spatters as small particles are going to emit from the weld pool due to plasma jet of PAW without a keyhole.

3. Since deposited metal in MIG welding is possible to flow to the weld pool of PAW. As a consequence, it is desired that MIG welding began after generating the keyhole.

4. Weld pool under torch of PAW is separated from that of MIG welding. If the weld pool of plasma and MIG welding join together with each other, molten metal flows to the rear side of base metal.

5. Blowhole took places due to the reduction of MIG current. By prevention of arc cutting and short circuit, it can effectively prevent the occurrence of blowhole.

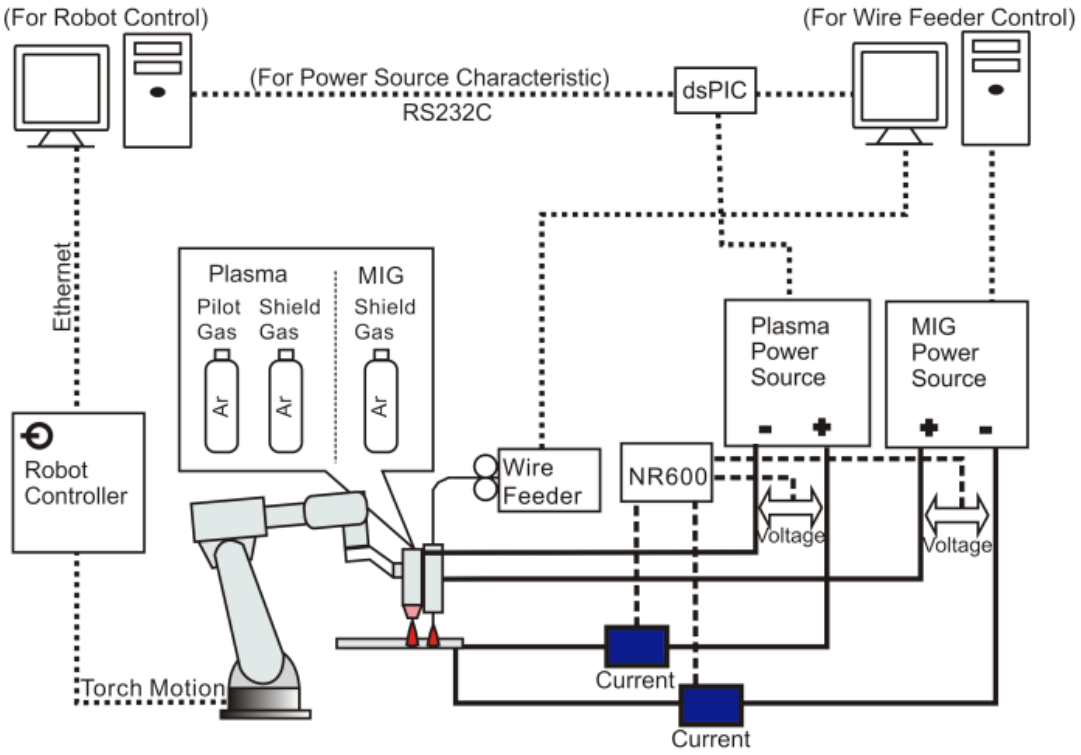

Fig. 4.1 Plasma MIG robotic system.

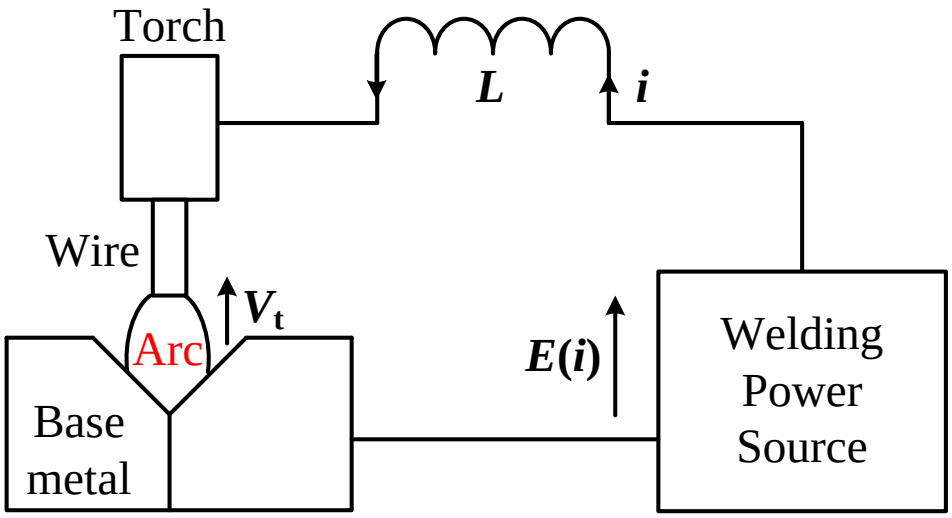

Fig. 4.2 GMA welding circuit.

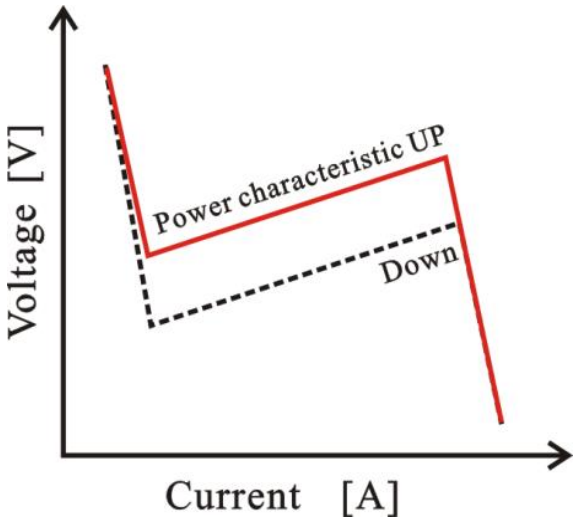

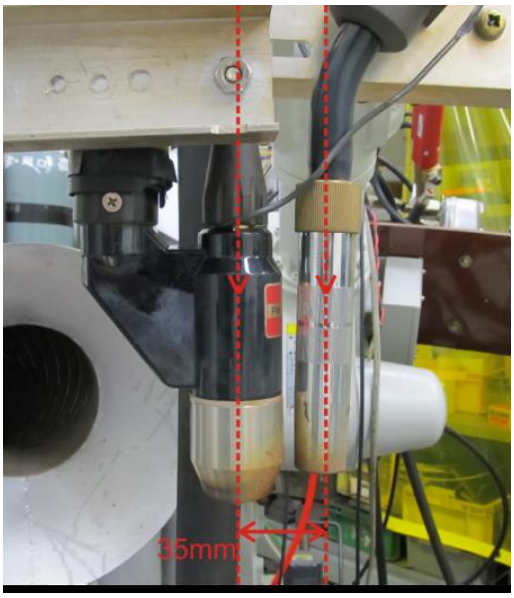

Fig. 4.3 Power source characteristic

Fig. 4.4 Configuration of two electrodes.

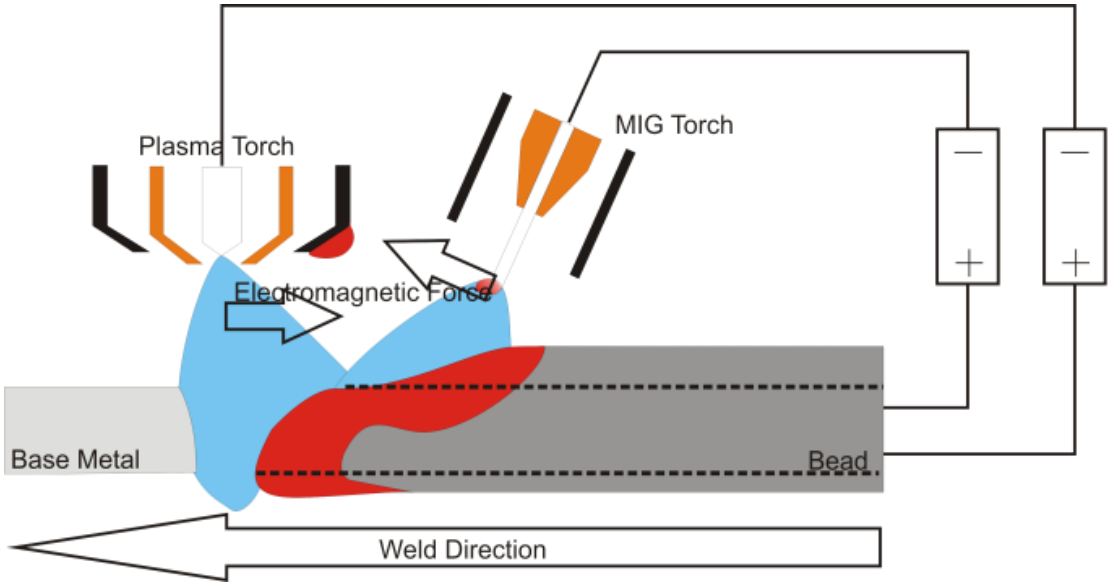

Fig. 4.5 Same polarity of the welding power sources.

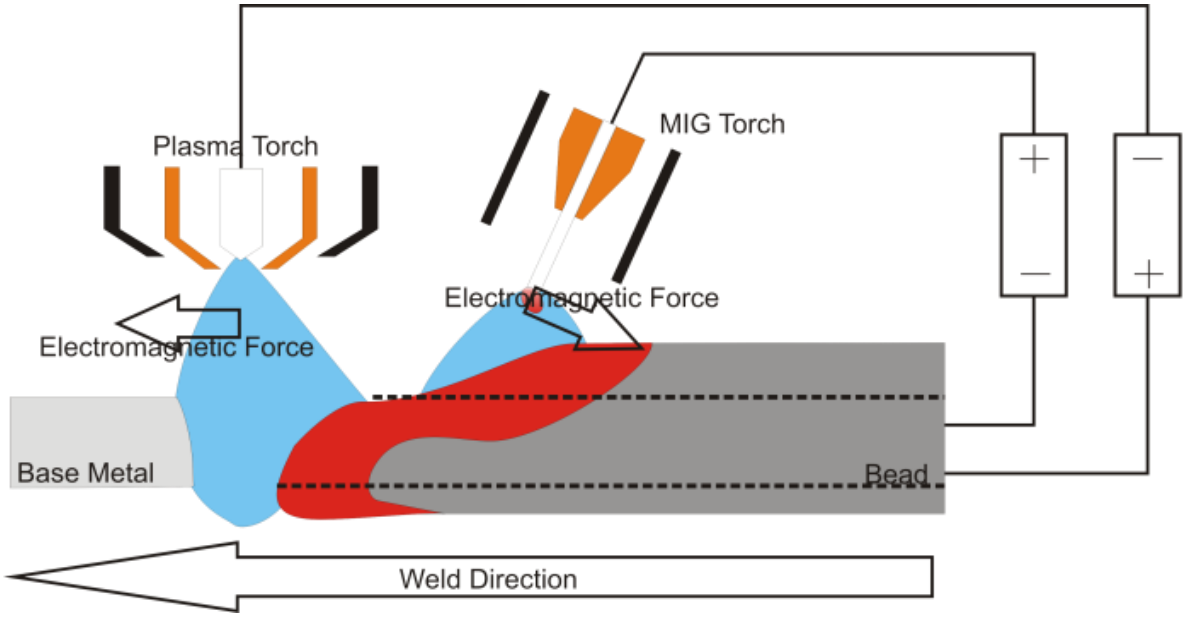

Fig. 4.6 Opposite polarity of the power sources.

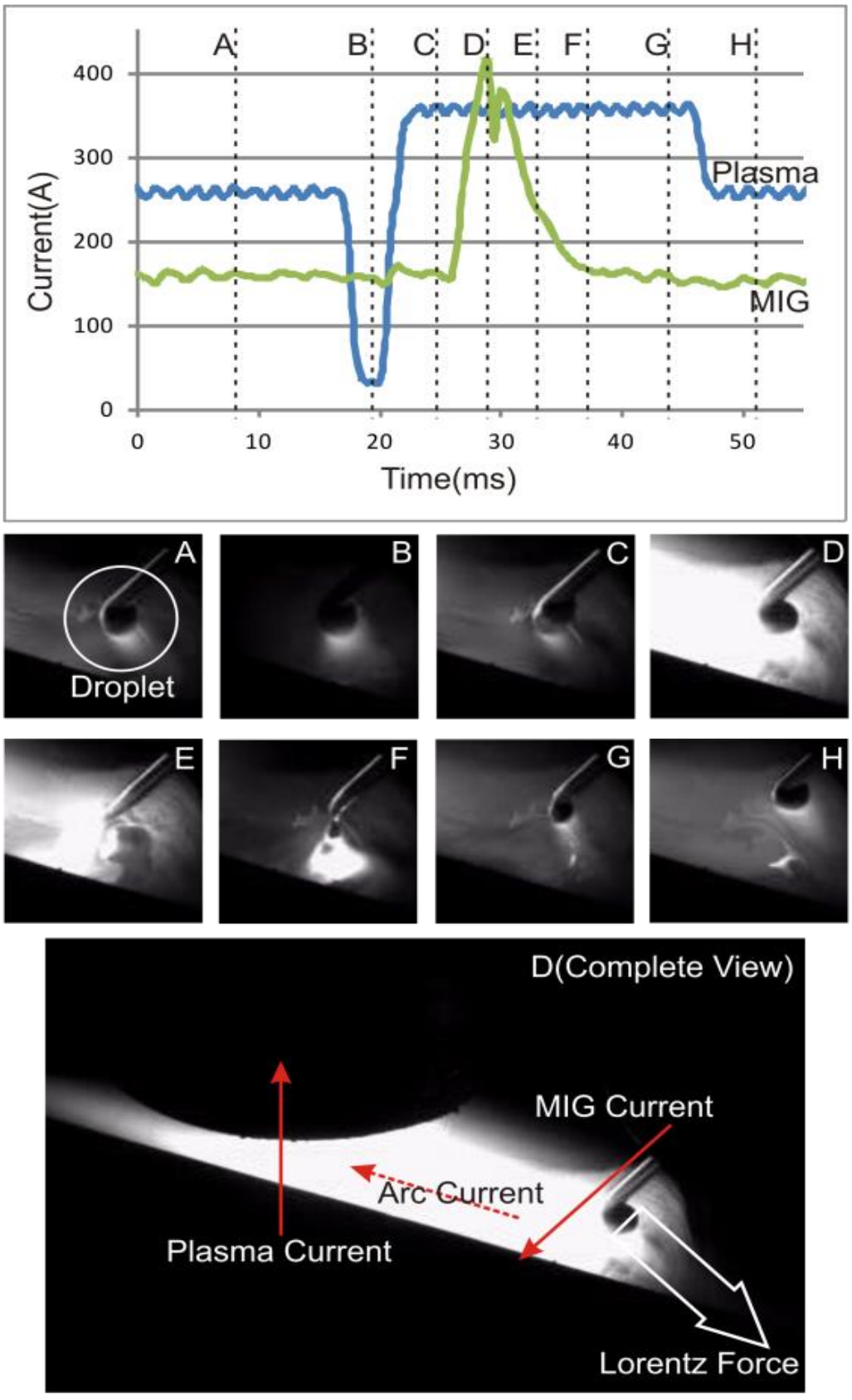

Fig. 4.7 Relationship between the droplet and the current

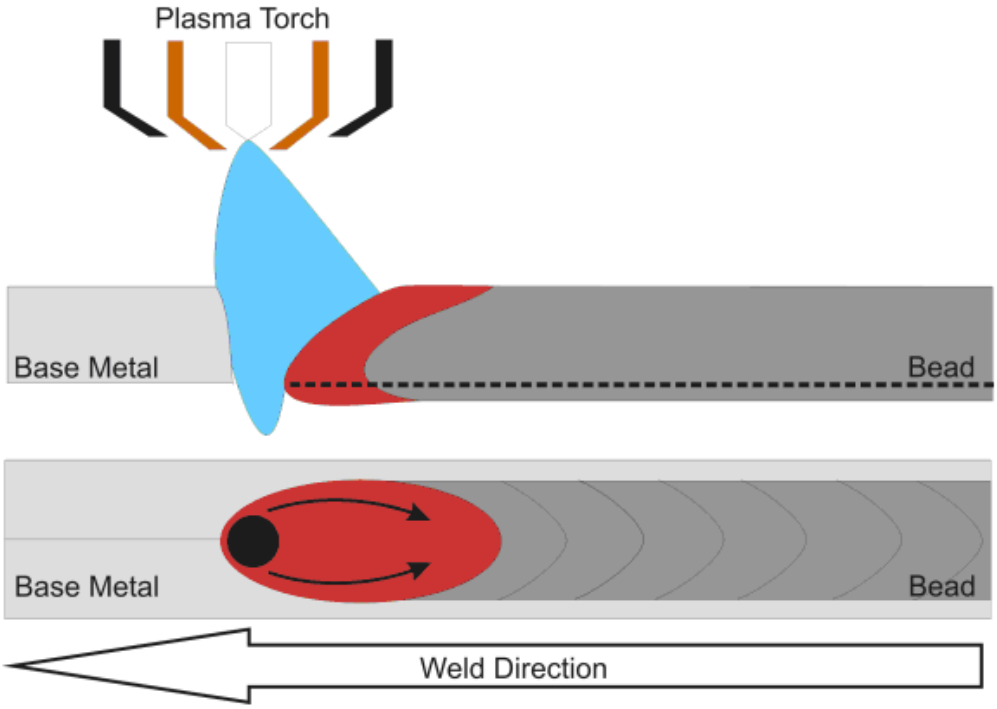

Fig. 4.8 Plasma arc welding.

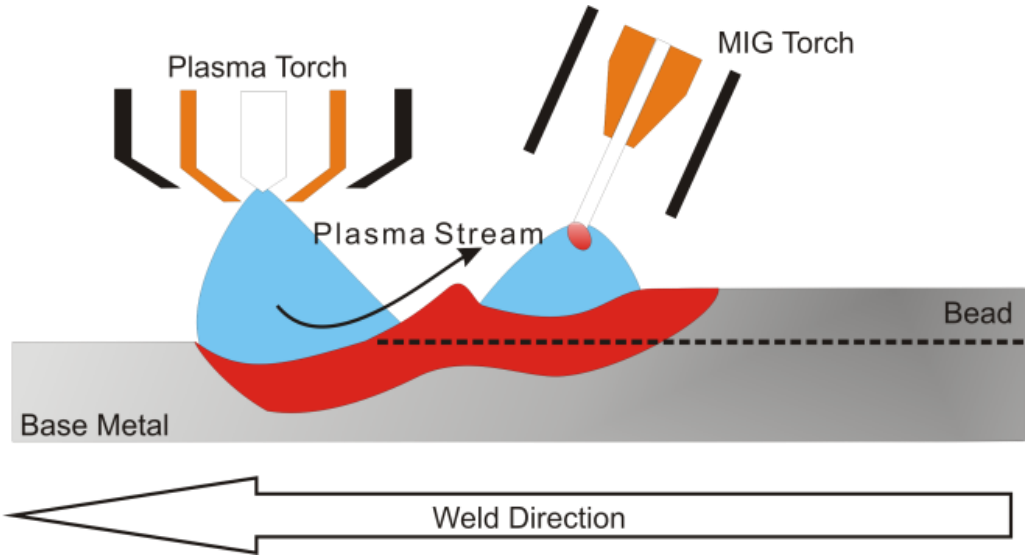

Fig. 4.9 No keyhole welding.

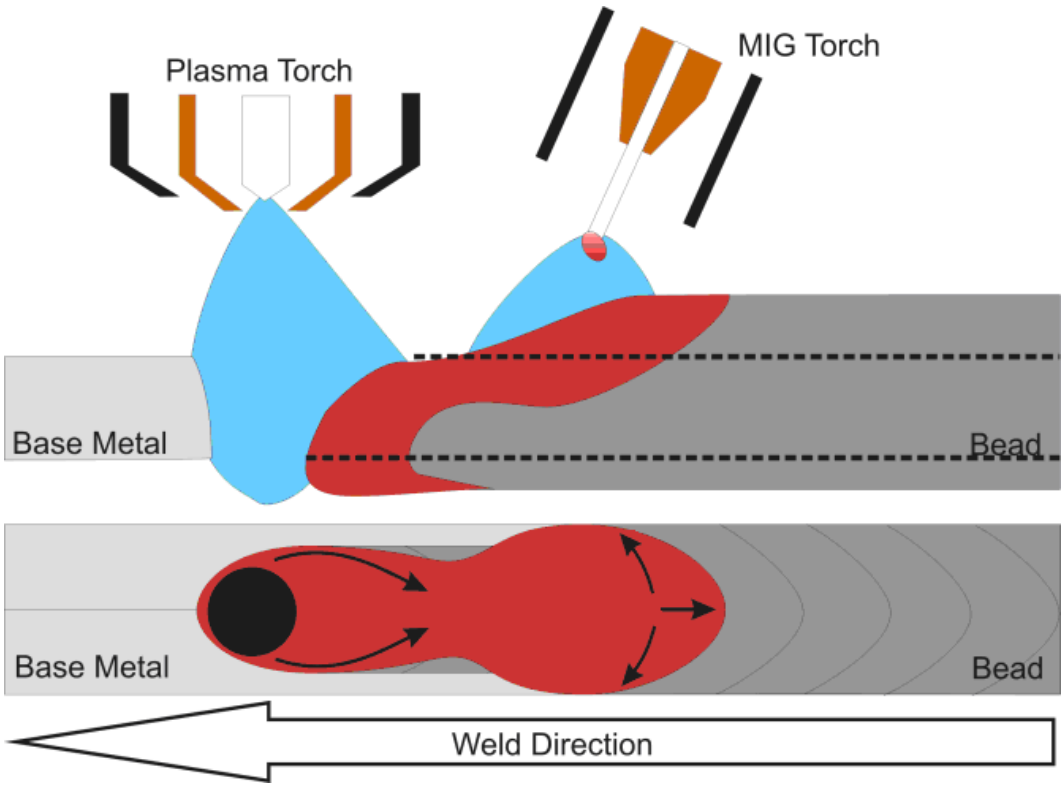

Fig. 4.10 Weld pools joined under the plasma and the MIG welding.

Fig. 4.11 Burn-through appearance of weld bead

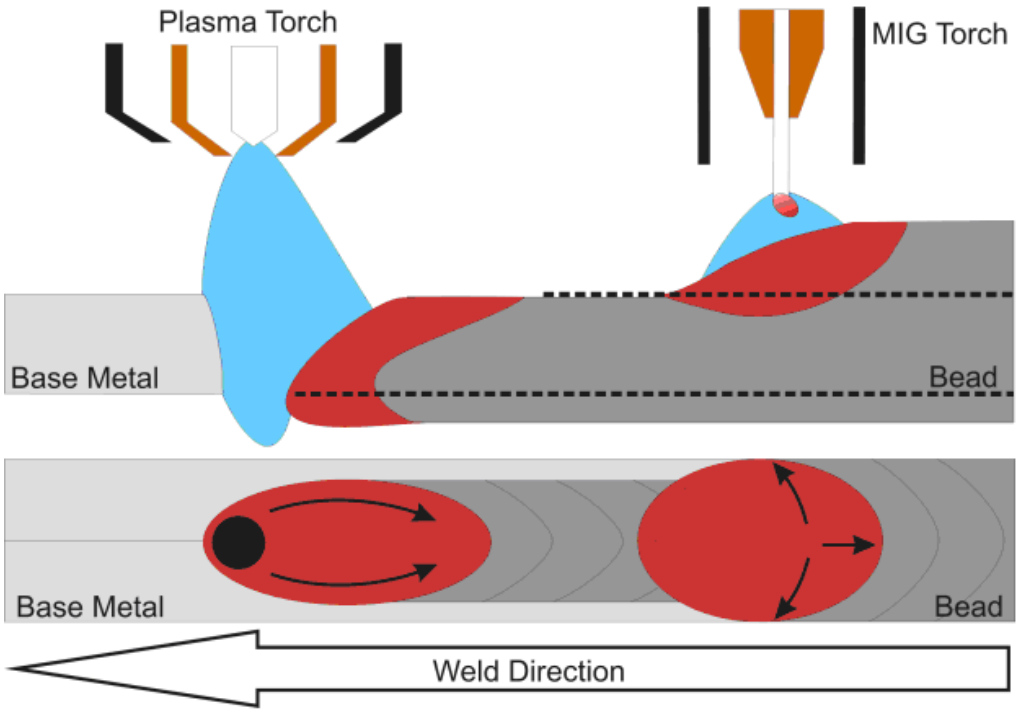

Fig. 4.12 Separation of the weld pool in dual-electrode welding.

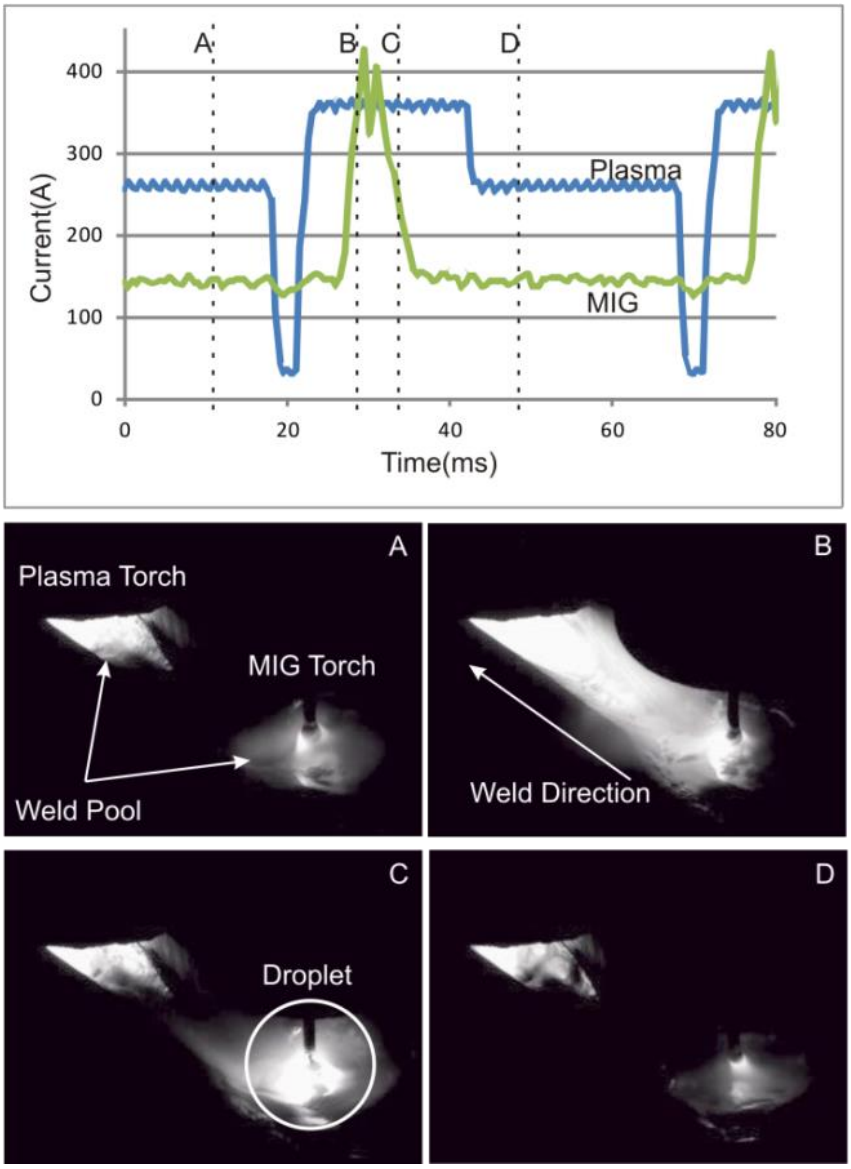

Fig. 4.13 Metal transfer in dual-electrode welding.

(a) Forming near the surface (b) Forming in central part

Fig. 4.14 Two kinds of blowhole in cross section of weld bead

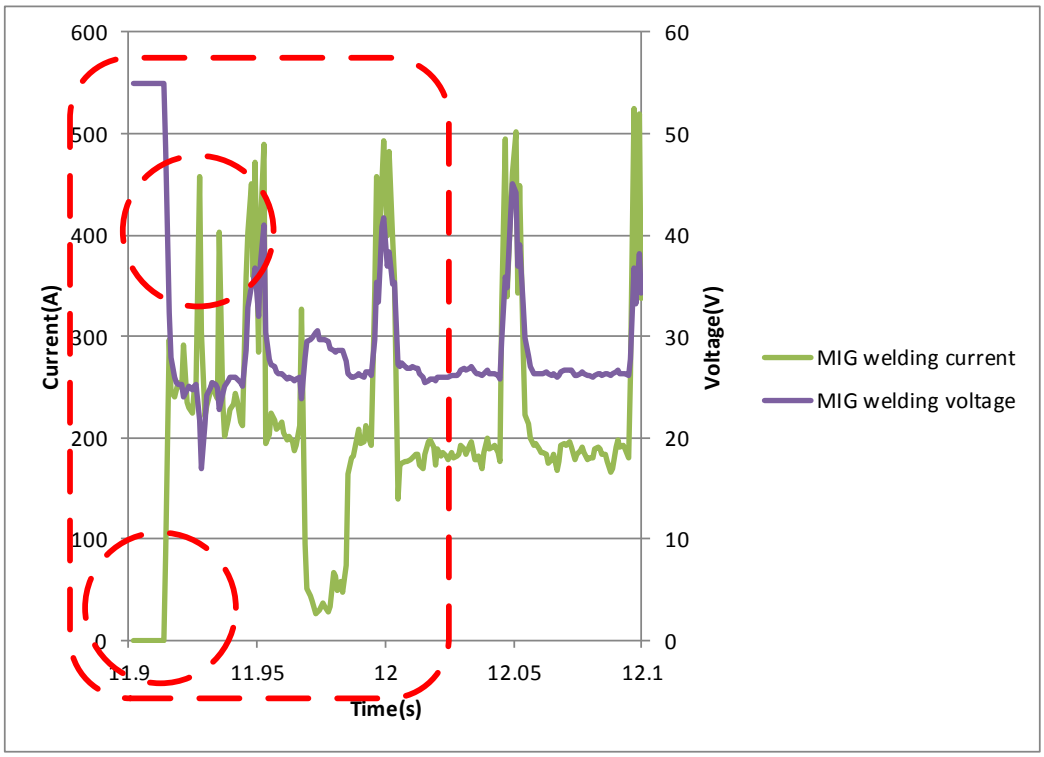

Fig. 4.15 Arc cutting and short circuit has taken place

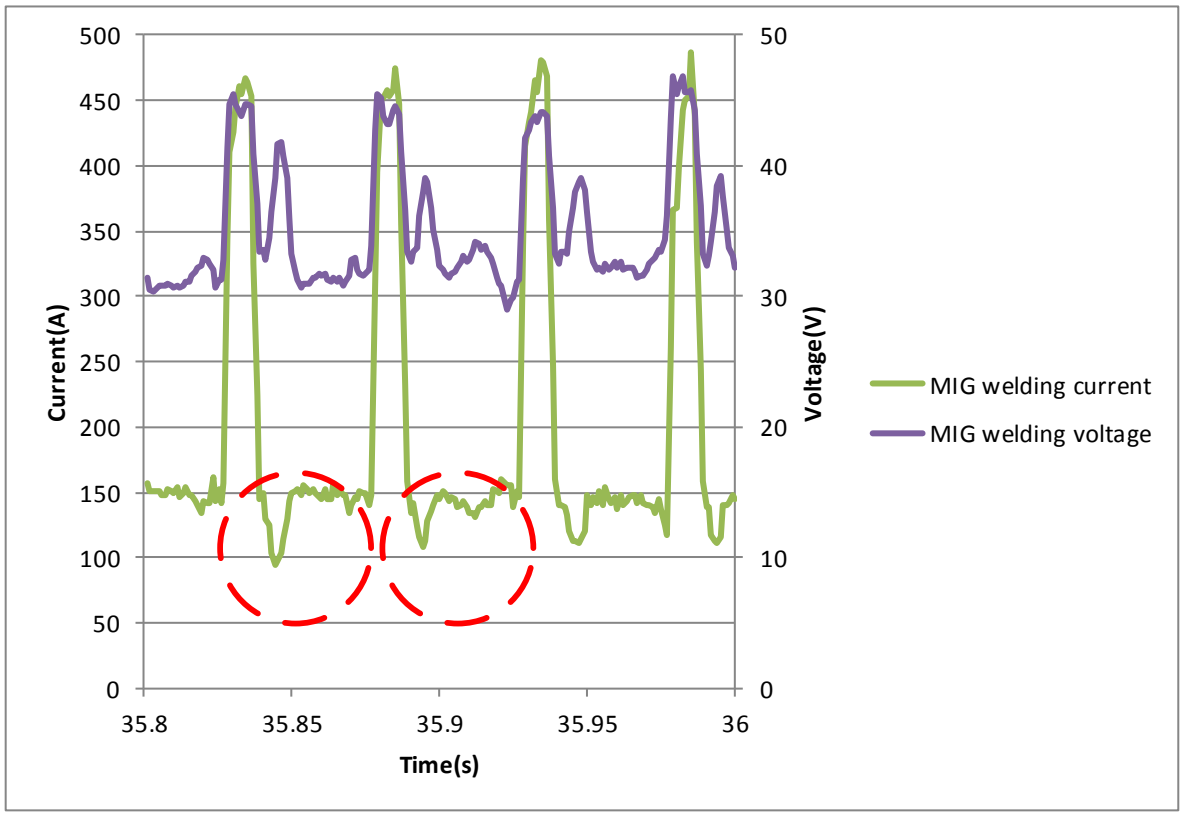

Fig. 4.16 Base current of MIG has reduced

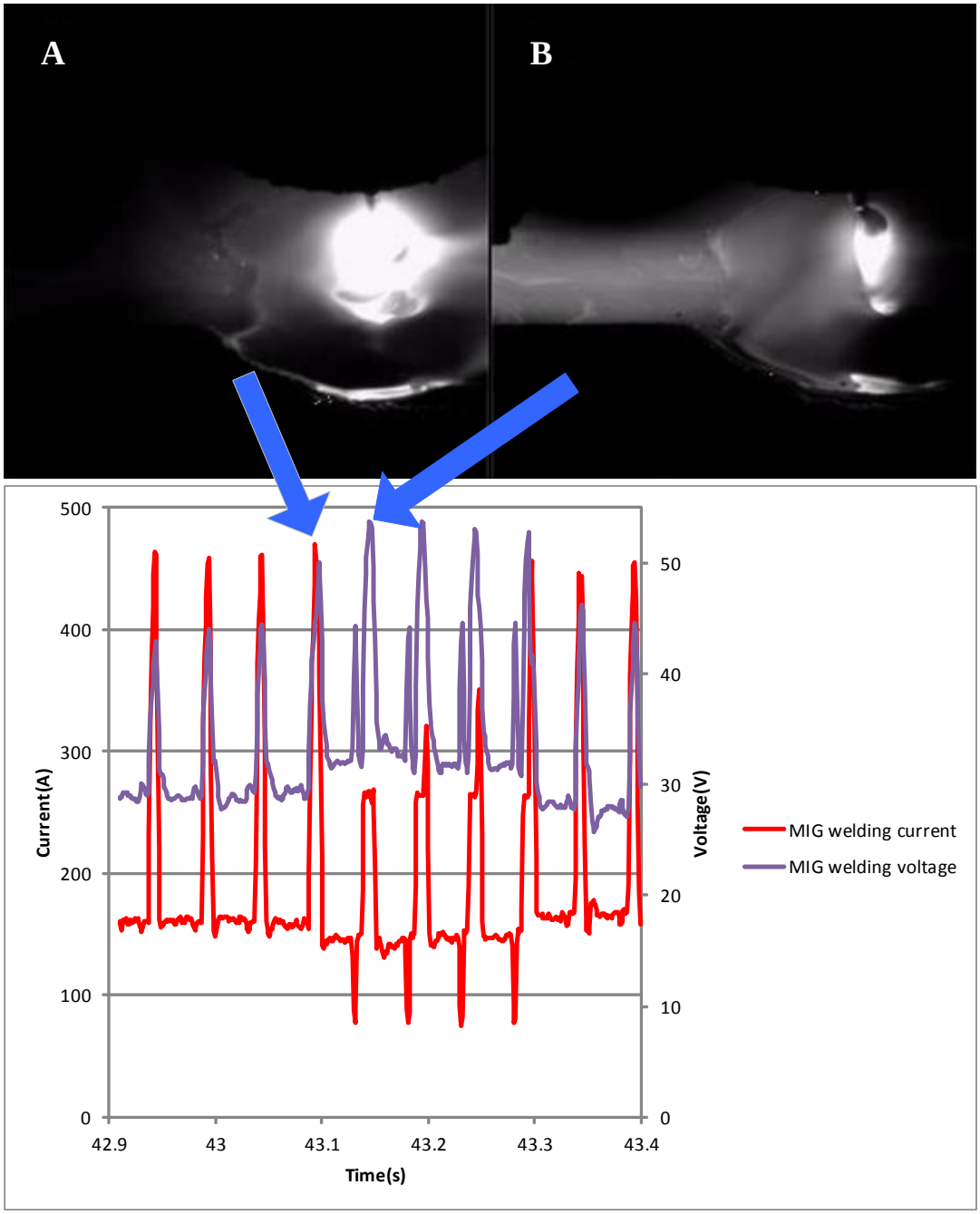

Fig. 4.17 Reducing of the MIG peak current

Table 1 Experimental data of dual-electrode welding

<table>
<tr><td></td><td colspan="4">Plasma arc welding</td><td colspan="3">MIG Welding</td><td></td></tr>
<tr><td>Number</td><td>Peak
(A)</td><td>Base
(A)</td><td>Frequency
(Hz)</td><td>Pulse
width
(ms)</td><td>Pulse
width
(ms)</td><td>Wire
Feeding
(mm/s)</td><td>Sheild Gas</td><td>Travelling
Speed
(cm/min)</td></tr>
<tr><td>1</td><td rowspan="5">350</td><td rowspan="2">250</td><td rowspan="5">20</td><td rowspan="3">20</td><td>4</td><td>85</td><td rowspan="8">Ar</td><td rowspan="3">15</td></tr>
<tr><td>2</td></tr>
<tr><td>3</td><td>200</td><td rowspan="2">8</td><td>110</td></tr>
<tr><td>4</td><td>170</td><td>15</td><td rowspan="2">115</td></tr>
<tr><td>5</td><td rowspan="2">200</td><td>20</td><td>6</td><td>25</td></tr>
<tr><td>6</td><td>25</td><td>9</td><td rowspan="2">100</td><td>18</td></tr>
<tr><td>7</td><td colspan="2">220</td><td colspan="2" rowspan="2">Direct current</td><td>5</td><td>15</td></tr>
<tr><td>8</td><td colspan="2">250</td><td>Constant
Voltage
35V</td><td>160</td><td>24</td></tr>
</table>

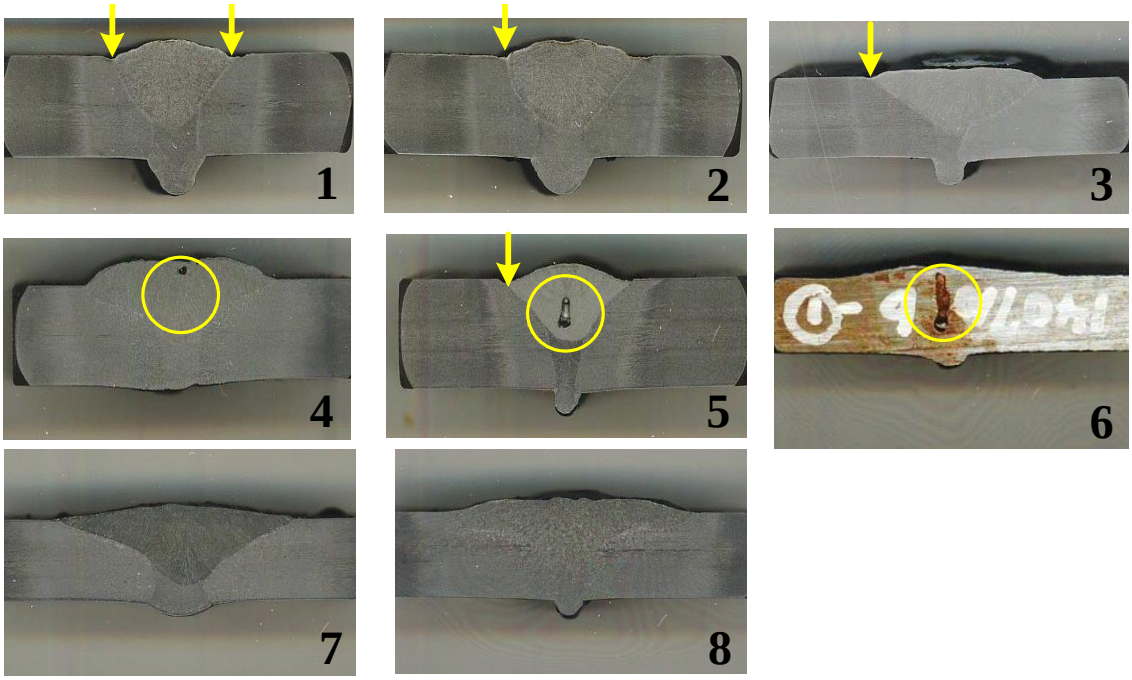

Fig. 4.18 Cross section diagram of the welding bead

CHAPTER 5. SEAM TRACKING AND STANDOFF CONTROL IN PLASMA ROBOTIC WELDING SYSTEM

5.1 Introduction

Since the GMAW is employed as a tailing torch in the welding system of PAW and GMAW, it is difficult to observe the fusion zone from the rear of consumable electrode to realize a seam tracking. Consequently, a CCD camera has been set on the jig in front of plasma torch and operating together. It pays attention to the front part of fusion zone known as the fusion zone of keyhole at a constant angle.

During the welding process, plasma arc is constricted to the slope on V-type groove. Base metal in groove is melted and tore down along the surface so that molten metal solidify once more and form the back bead in base metal. Since the weld line has the worst pyroconductivity, it is easier to be melted than other zone under the plasma arc. Downstream of molten metal fluid will almost descend along the groove centerline. By analyzing the taken image, it is available to consider that the tip of fusion zone boundary falls on the centerline area of groove.

Preceding research has been carried out in author's lab [44]. In this case, the image processing was developed to detect the top of the molten zone with the torch

position estimated by processing the taken image. However, the performance of the digital controller was unstable because of the image processing mistake and electronic noise. And, the study carried out only seam tracking of the weld line without a standoff control.

To solve these problems, a program of boundary detection between base metal and tip of fusion zone has been designed by image processing for the seam tracking and standoff control in this chapter.

5.2 Image processing by binarization

In the actual image processing, above all, the taken images compose of 750×700 pixels. Then, a line in vertical direction, at 375th pixel center, was taken across the image as shown in Fig. 5.1a. And a threshold T_F to identify the boundary is found from the brightness distribution on this line. Since histogram is divided into two peaks, the threshold level T_F of brightness on the boundary is commonly decided according to the medium value between two peaks of histogram shown in Fig. 5.1b.

Taken image includes fusion zone and non-melted side, and the brightness of fusion zone of keyhole is higher than non-melted side. By using the threshold T_F, it is available to process binarization to the image. That is, pixels having

brightness below threshold corresponds to non-melted side and the other pixels are taken as fusion zone.

Otsu method is a method widely used to regard the point with separation degree having a largest value. In this method, threshold is found in the histogram. But due to the electrode reflection and non-melted parts included in the image, it becomes unable to detect the boundary in bulge or dent towards fusion zone exactly by using this method, as shown in Fig. 5.2.

Since it needs to remove the tiny points and unevenness in the image, the median between original threshold decided by Otsu method and peak value of higher brightness was selected as the new threshold shown in Fig. 5.3b. In addition, the area right under the electrode is in high brightness due to electrode reflection, while the tip of fusion zone appears dark, i.e., brightness distribution is not same in the fusion zone. It is to determine the brightness above the threshold as 1, and under the threshold as 0.

For instance, two sample lines in vertical direction were taken in the image as shown in Fig. 5.5a, which line ② is near the tip and line ① is away from the tip. As it is shown in the Fig. 5.4, the threshold-1 near the tip of fusion zone will

become smaller. Multiple thresholds valid to raise the precision of detected boundary.

The image is divided into 5 equal parts in vertical direction, whose vertical coordinates of parting lines are (Y_1, Y_2, Y_3, Y_4) shown in Fig. 5.5b. The new threshold (T_1, T_2, T_3, T_4) corresponding to each parting line by binarization was calculated. It is possible to cope with varying brightness due to the molten condition in fusion zone. Moreover, closing and opening processing has been applied to remove the tiny points and unevenness near boundary.

5.3 Boundary detection of fusion zone

The edge of fusion zone in vertical line of $Th1$ is detected. And its horizontal ordinates are recorded as (X_1, X_2). Furthermore, it processes binarization round the calculated threshold (T_1, T_2, T_3, T_4) once again. The detection of boundary was performed from the starting point (X_1, Y_1) and (X_2, Y_1), which left side make a detection in anti-clockwise and right in clockwise.

Fig. 5.6 shows the situation of right side. Above all, the pixel of start put at point A in the center of 3×3 matrix, and the pixel of fusion zone was detected according to binarization in the clockwise. The point with the brightness beyond threshold was selected as the center of new matrix. In this way, the boundary of

fusion zone was found. Boundary detection of the tip by each 300 point was done from both starting point.

Since the detection of boundary starts from the both sides, two different tips were found out in front of the fusion zone. In this case, it is needed to calculate an average coordinate of the two tips recorded as (X_T, Y_S). It takes about 0.14s from taking image to calculation of the tip coordinate, and then the coordinate was transmitted to PC for motion control through RS-232C.

5.4 Tracking of weld line and standoff control by image processing

As mentioned before, the CCD camera and plasma torch is working together. It will make a setting that the center of torch should be at center in the vertical line, 350th pixel, of taken image in a horizontal projection plane before the welding starts. And because of strong pressure of plasma arc during the welding process, the keyhole was generated and plasma arc and torch are almost in a straight line. Since the image was taken from the front of the travelling direction, the weld line is almost the vertical center line of taken image.

Setting of the jig and the camera is shown in Fig. 5.7a. Since the weld line has the worst pyroconductivity, it is easier to be melted than other zone under the plasma arc. And the tip of fusion zone calculated by image processing is confirm

to locate in the weld line. In other words, make the electrode of vertical center line, 350th pixel, in taken image trace the horizontal ordinate X_T of the tip of fusion zone by image processing to realize the seam tracking.

On the other hand, standoff of plasma torch has been set to 5mm determined by lots of basic experiments. A standoff control is required to make the welding stable. Plasma torch and CCD camera are fixed on the same jig. If standoff becomes lower, the camera moved forwards along the tip of fusion zone being backwards and vice versa as shown in Fig. 5.7b. In this way, the standoff can be detected by the vertical coordinate Y_S of the tip.

In addition, the flowchart of image process is shown in Fig. 5.8. As it is shown, visual sensor took the image of fusion zone after the welding start. Since the brightness distribution is not same in the fusion zone, the image is divided into 5 equal parts in vertical direction to get the thresholds, respectively. It processed binarization to the image to determine the brightness above the threshold as 1, and under the threshold as 0. Moreover, closing and opening processing has been applied to remove the tiny points and unevenness near the boundary. Since the detection of boundary starts from the both sides, it is needed to calculate an average coordinate of the two tips. The average coordinate is going to match the

ideal tip coordinate (X_T, Y_T) to realize the seam tracking and standoff control at the same time.

5.5 Control result and discussion

12mm thick plate of mild steels compose of butted part of 5mm and groove angle of 90 degree. Moreover, pure argon has been used, and other welding conditions are as shown in table 5.1.

Table 5.1 Experimental data of plasma arc welding

Diameter of nozzle	3.2mm
Electrode setback	3.5 mm
Flow quantity of orifice gas	3.2 l/min
Flow quantity of Shielding gas	10 l/min
Standoff	5 mm
Pulse frequency	20 Hz
Duty ratio	40 %
Peak current	350 A
Base current	250 A

Author makes a control of the welding robot through image processing. Tracking of the weld line and standoff control of the torch standoff was carried

out. Plasma torch has been roughly taught in an appropriate position to check the control performance.

Deviations $e_t[i]$ and $e_s[i]$ are the difference between references R_t and R_s, and tip position (X_T, Y_s) of fusion zone of keyhole and given by Eq. 2.3. Command pulse of the target position is calculated by Eq. 2.8, and sent to the robot. R_t and R_s are determined as 350th pixel in vertical direction and 400th pixel in vertical direction, which will be shown by crosswire as the image processing results. The cross point is the best position of tip for automatic torch guidance. Meanwhile, 1mm of the deviation corresponds to 72 pixels in the image.

Image processing result is shown in Fig. 5.9. Automatic control is done after 10 seconds since the welding begins to investigate the control performance. As it is shown in Fig. 5.9a, the standoff has automatically adjusted to the best welding height after the control start. Tip of the fusion zone of keyhole are the cross point of R_t and R_s. They almost achieved an invariant position so as to keep the back bead stable. Back bead appearance and fusion zone images corresponding to the torch position are shown in Fig. 5.9b.

The end point of the welding was at a 3mm apart from weld line to evaluate the performance of the controller. As it is shown in Fig. 5.10a, standoff has still

well adjusted to the best welding height and weld line has exactly matched the reference line of R_t to achieve a good trace result regardless of the end point. In this way, an image processing and the usefulness of tracking and standoff control have been well confirmed.

5.6 Conclusions

In this chapter, an image processing for automatic tracking of the weld line and self-regulated standoff of the torch has been developed in plasma robotic welding. During image processing for automatic tracking, multiple thresholds was applied so as to raise the precision of boundary detecting and improve the welding quality.

As a result, the efficiency of welding work was improved. Some other consequences are shown as follows:

1. Clear weld pool images have been taken by using CCD camera on camera link transmission.

2. Detection of tip position of fusion zone corresponding to the weld line and torch height has been achieved by image processing, which is carried out by MATLAB/Simulink.

3. Control system has been designed to track the weld line and adjust the torch standoff.

4. Validity of image processing and control system has been verified by the welding experiment.

5. This method can be applied to Plasma-MIG welding.

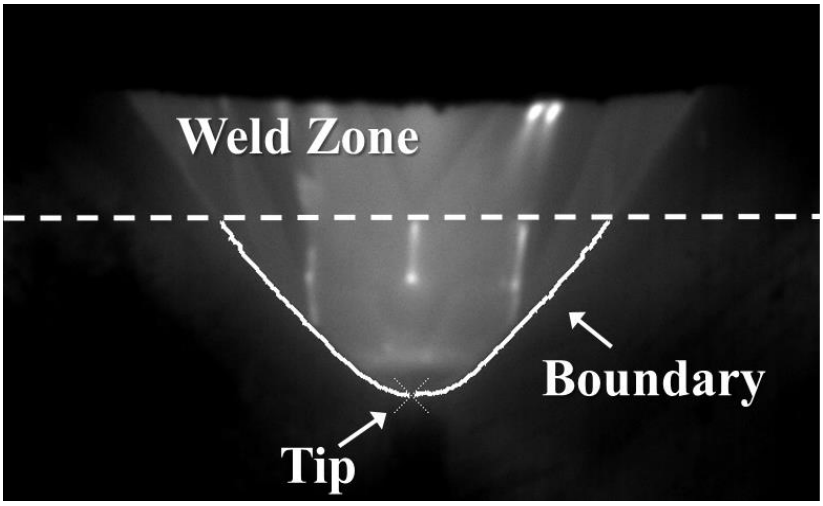

(a) Typical fusion zone image.

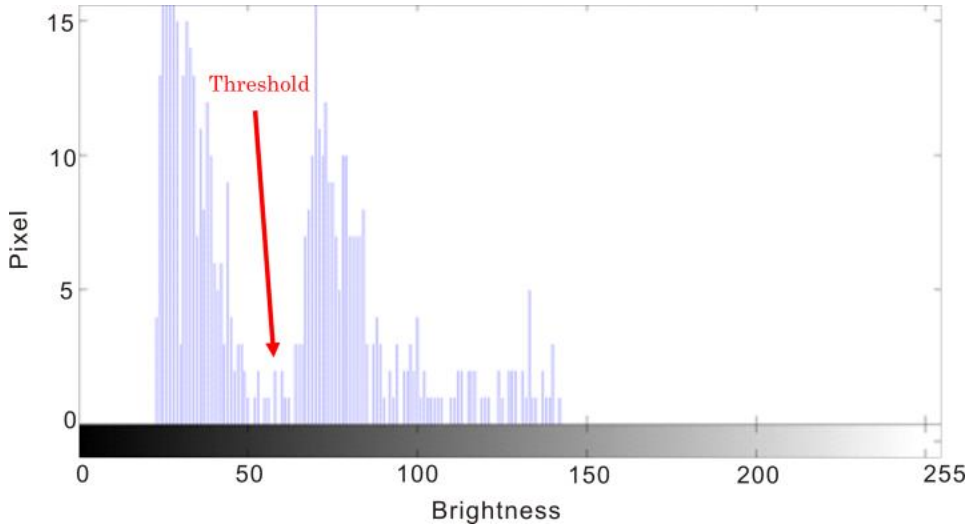

(b) Histogram of horizontal line.

Fig. 5.1 Relationship between histogram and fusion zone image.

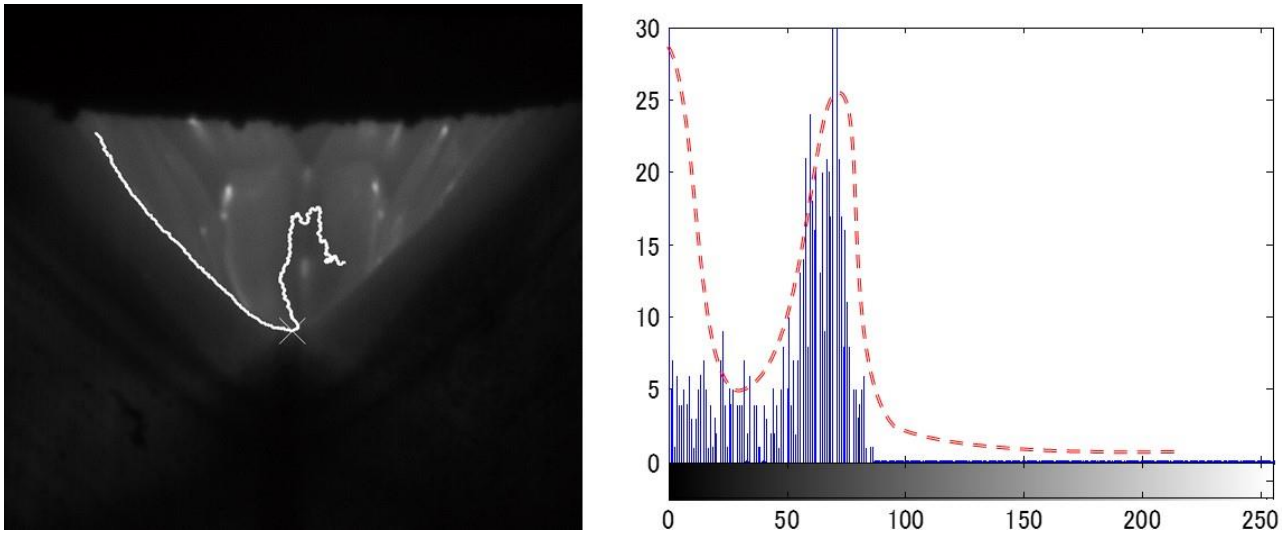

(a) Fusion zone image (b) image histogram

Fig. 5.2 Unsuccessful detection of fusion zone boundary

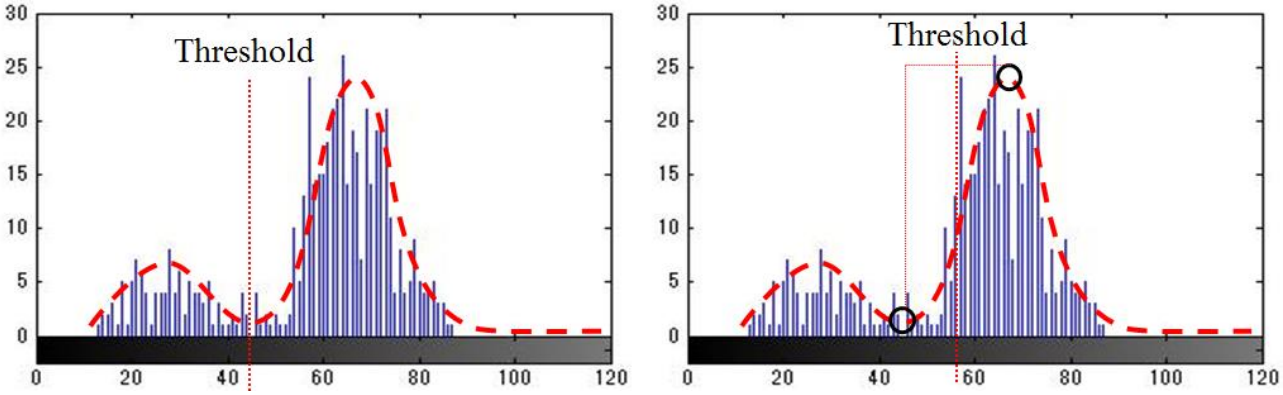

(a) original threshold decided by Otsu (b) new threshold

Fig. 5.3 Threshold definition method

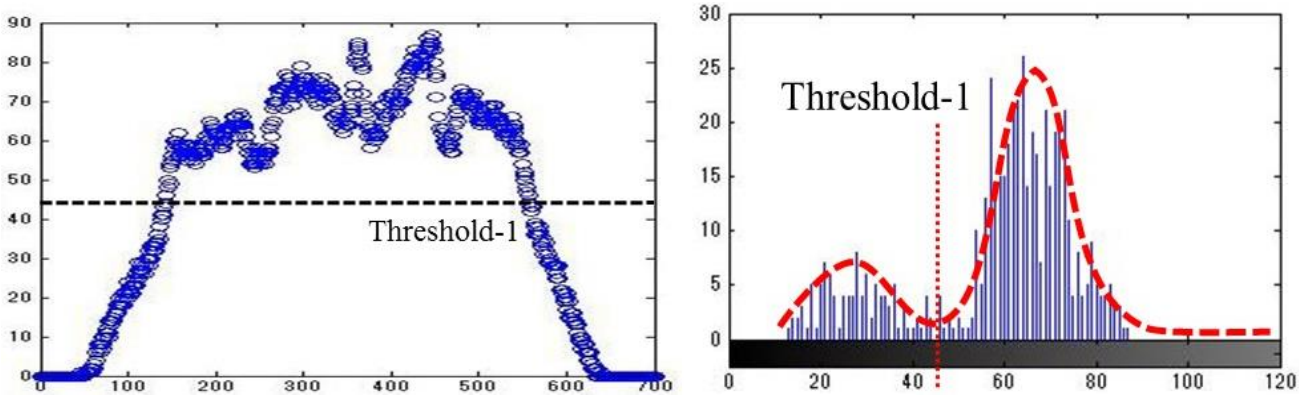

(a) Line away from tip

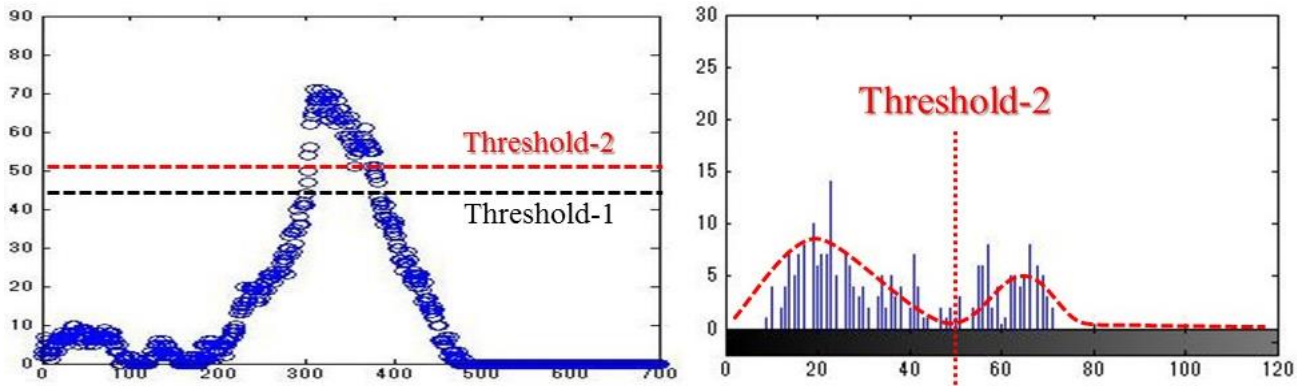

(b) Line near the tip

Fig. 5.4 Threshold of two sample lines

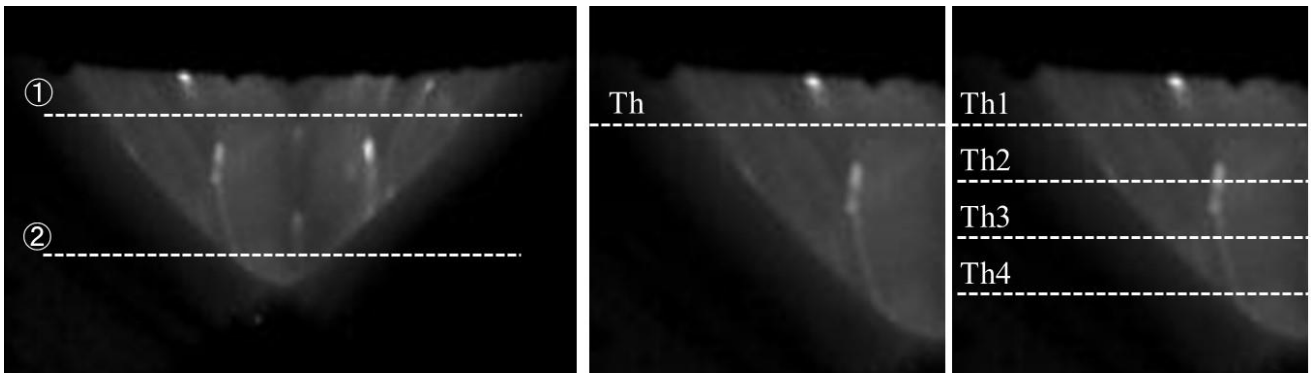

(a) Sample lines (b) improved threshold method

Fig. 5.5 Get the threshold of five parts coping with the varying brightness

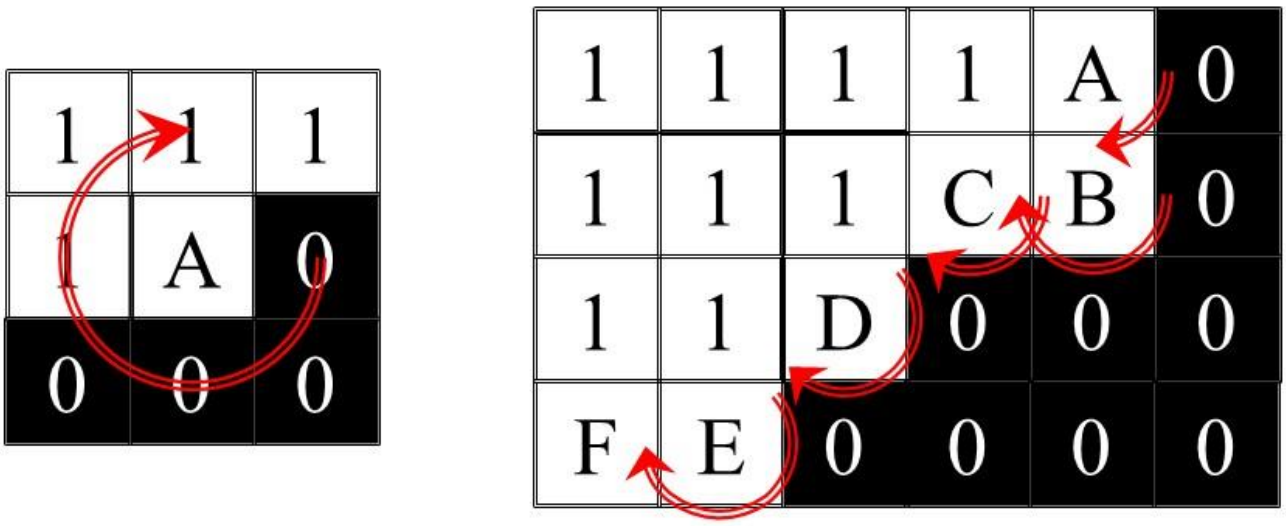

Fig. 5.6 Method of boundary detecting

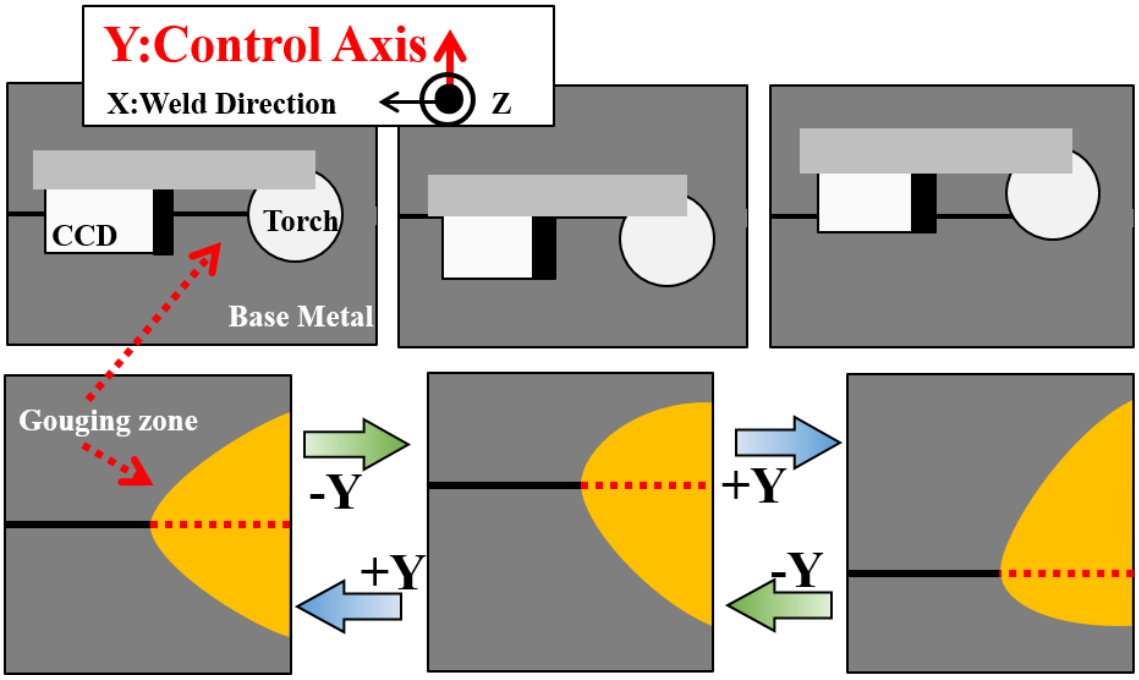

(a) Top view and lateral deviation

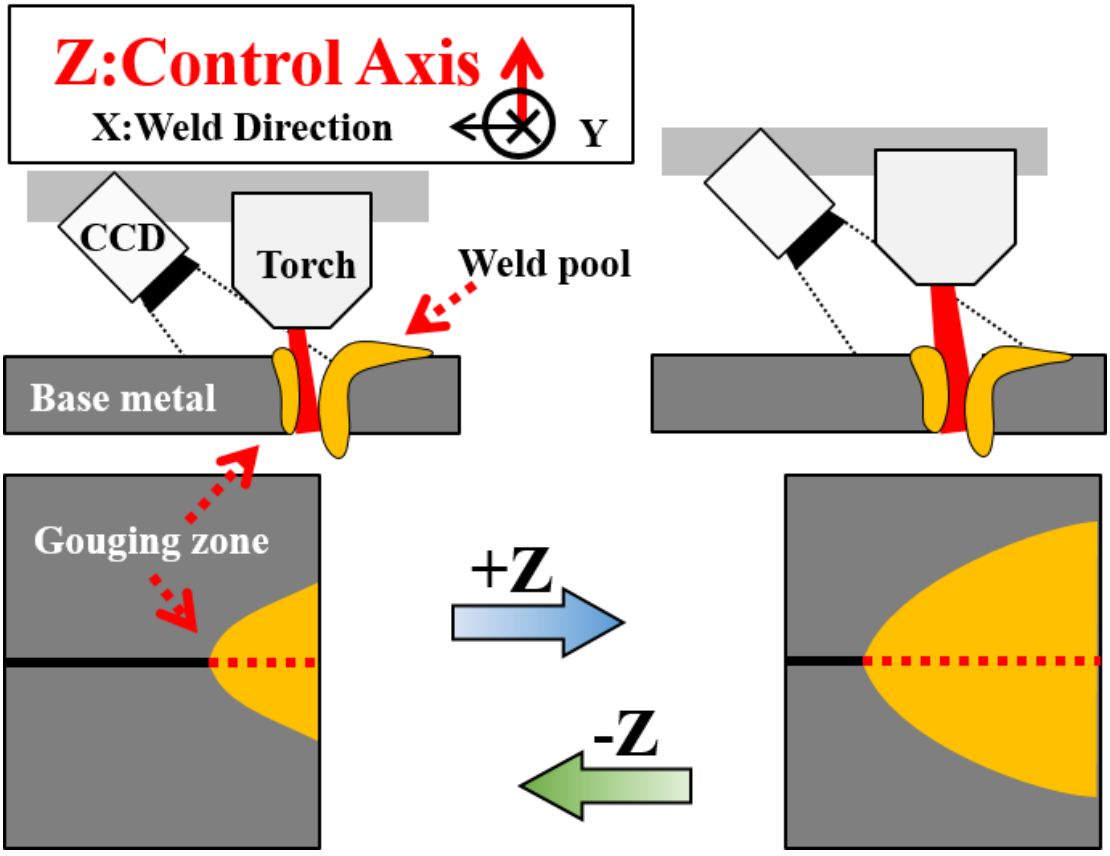

(b) Side view and vertical deviation

Fig. 5.7 Visual difference of fusion zone image by torch position

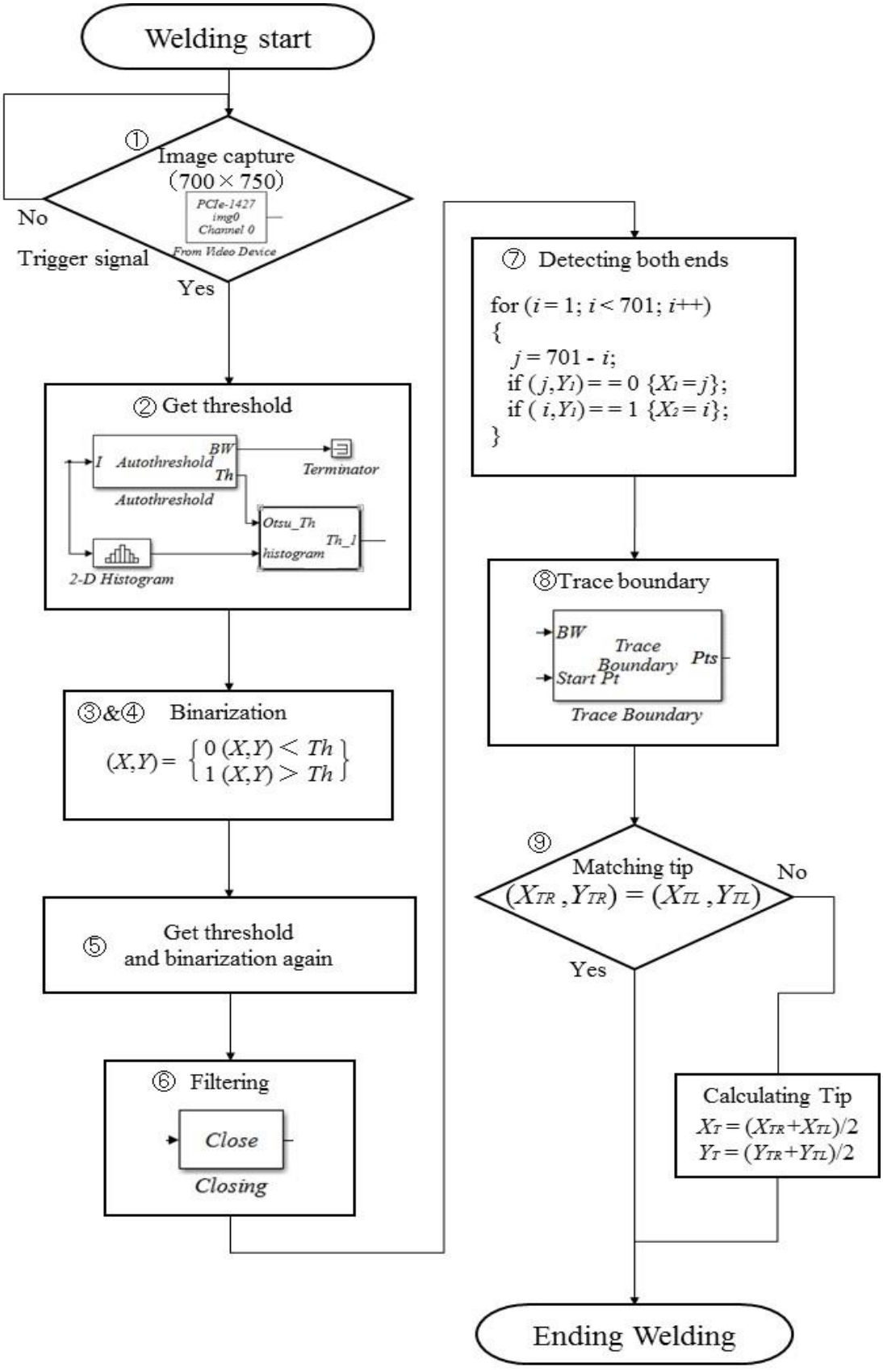

Fig. 5.8 Flowchart of image processing algorithum

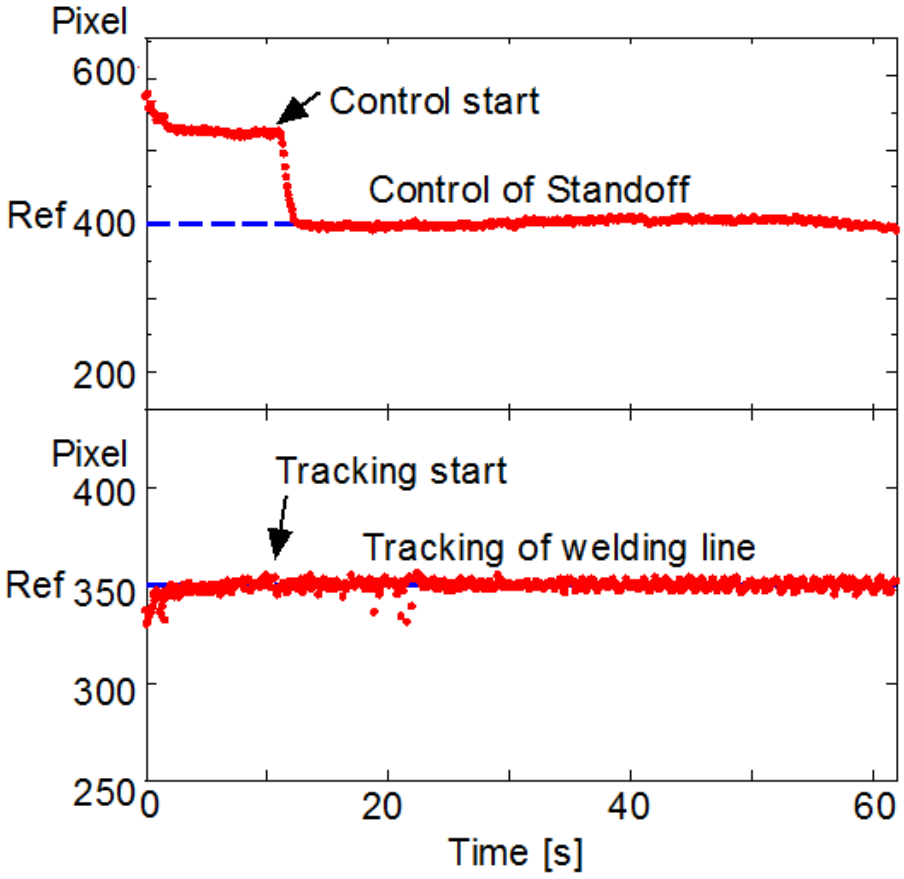

(a) Behavior of the tracking and the standoff control

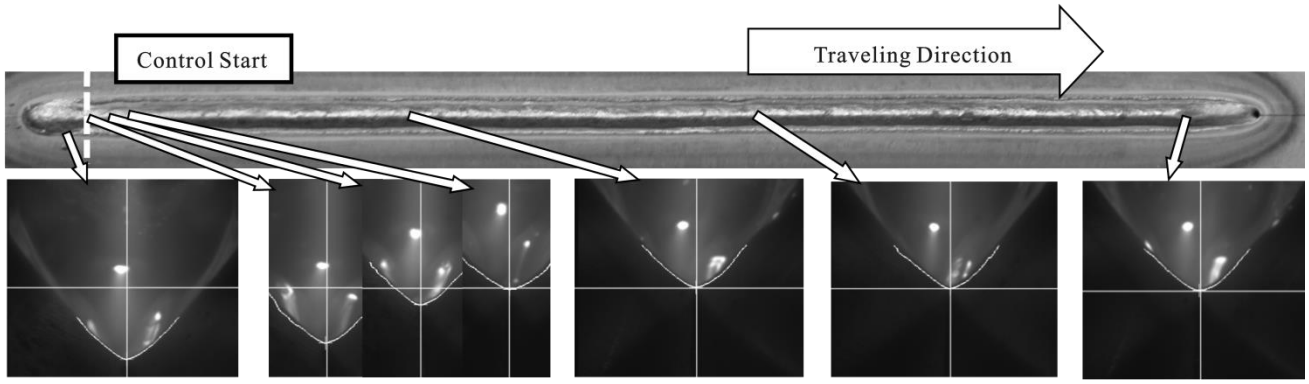

(b) Relationship between the bead appearance on the rear side and weld pool images.

Fig. 5.9 Experimental result if the weld line was roughly taught to the robot.

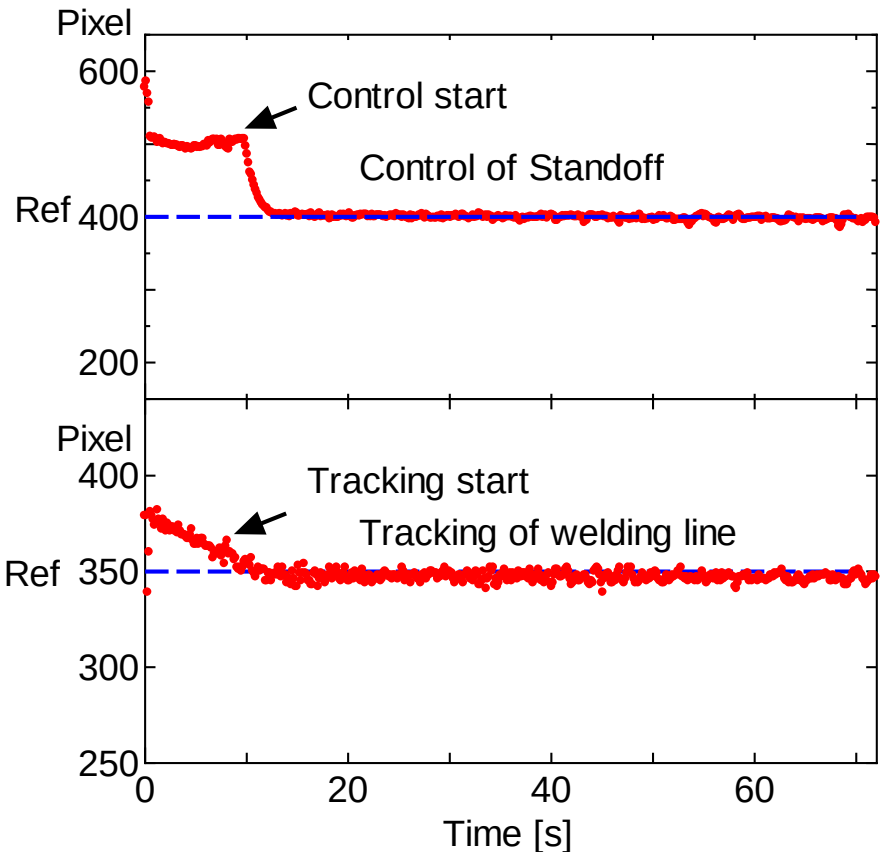

(a) Behavior of the tracking and the standoff control

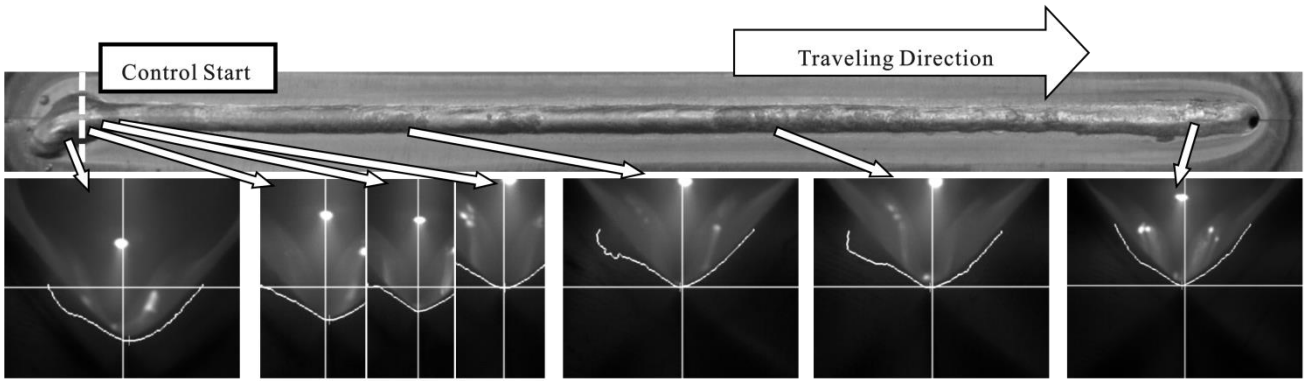

(b) Relationship between the bead appearance on the rear side and weld pool images.

Fig. 5.10 Experimental result if the endpoint was at 3mm position apart from the weld line.

CHAPTER 6. CONCLUDING REMARKS

This thesis treats the problem which is concerning the development of high efficiency plasma robotic welding system with several image processing.

The problems include controlling of the welding torch and tracking of the weld line. It is difficult to teach the weld line to the robot and trace the weld line exactly during the welding process, since plasma electrode hides in the plasma torch. Arc length in PAW is almost kept constant due to keyhole. The conventional arc sensor isn't available to be applied.

Real time control of the welding robot is useful to achieve high efficiency of the welding. For this purpose, visual sensor is very useful to make an exact observation of welding conditions. Therefore the intelligent welding robot has been constructed with visual sensing system with a variety of applicable image processing. As a consequence, successful tracking has been achieved in the welding results that has well improved the efficiency of welding work, and effectively ensure the welding quality.

A welding system on the basis of PAW and GMAW has been developed in this study to achieve high deposited rate of the molten metal. But, welding defects

such as blowhole and undercut depends on the welding conditions. The welding phenomena was analyzed to avoid the defects and optimum welding conditions was proposed. This study can help engineers to make a clean welding despite of welding defects leading to a decrease of mechanical strength. Furthermore, the seam tracking method in this welding method has been discussed.

From this research, we summarized as follows:

(1) template matching is a technique used digital image processing for finding small parts of welding characteristic image which match the template image, serving as a part of quality control in general case and boundary detection method effectively detect the existence and boundary of the welding gap, and make real-time tracking and analysis of variable gap to ensure the welding quality in particular case.

(2) Welding quality in PAW depends on the performance of tracking results and keyhole is required to make an assurance of welding quality. The monitoring of the real-time status of keyhole area is needed. In the study, numerous fundamental experiments and analyses have been carried out for the acquisition of characteristic to detect the weld line from keyhole area. According to this, to ensure the keyhole the automatic tracking was achieved.

(3) Since arc under 100% Ar shielding gas becomes unstable in the mild steel welding, by using the welding system of PAW and GMAW, it confirms that the arc of GMAW is going to be stable under the interference of PAW. Because two kinds of different welding are processing on the same base metal in the meantime, it has discussed the concrete system structure, especially the polarity and distance of both electrodes. Through high-speed video camera, it is available to make a clear observation of welding phenomena, and the interference between two electrodes has been investigated with respect to weld pool and metal transfer, which has become smooth.

(4) Because of the combination of PAW and GMAW, there're a lot of indistinct parts due to the complexity of welding conditions, which has resulted in several welding defects due to the improper welding condition. By using data processing method with the analysis of cross section of weld bead, corresponding waveform and arc condition in the welding process, it has effectively confirm the appropriate welding condition to make an improvement of the welding defects. During hybrid optimization process for the combination of PAW and GMAW, it is available to perform the keyhole welding and building up of groove at the same time, which leads to an improvement of high work efficiency and welding quality.

(5) The visual sensor can be fixed in front of plasma torch to monitor the fusion area of plasma keyhole in welding system of PAW and GMAW. Multiple thresholds was proposed to raise the precision of boundary detecting. The welding quality, and standoff control method effectively keep the standoff of plasma torch in a constant value determined to maintain the keyhole.

ACKNOWLEDGEMENT

The author would like to thank Associate Professor Satoshi Yamane of Saitama University for supervising this thesis. His constant encouragement and invaluable comments have greatly helped to complete the work of this thesis.

The author wishes to express gratitude for Professor Hiroshi Kadono and Professor Yasuyoshi Kaneko of Saitama University for their significant comments and suggestions.

The author also would like to express his thanks to Kazumichi Hosoya, Toru Nakajima, and Hikaru Yamamoto of Hitachi Construction Machinery Co., Ltd for the aid in the experiments of this thesis.

The author's thanks must also go to all the member of Professor Satoshi Yamane's Laboratory for their direct and indirect aid in making it possible to write this thesis.

PREFERENCE

[1] Gage Robert M (1957) Arc torch and process, U.S. Patent # 2806124A https:// www.google.com/patents/US2806124

[2] Yu. D. Shchitsyn, D. S. BelininV. Yu. ShchitsynS. D. Neulybin (2016) Plasma Welding of Aluminum Alloys with the Use of Two Direct ARCS on Reverse-Polarity Current. Metallurgist 59: 1234–1237

[3] B. L. BozhenkoV. N. Shalimov (1991) Physicochemical interaction of gas and liquid phases in plasma welding. Journal of engineering physics 61: 815–819

[4] Hsuan-Liang Lin, Tong-Min WuChing-Min Cheng (2014) Effects of Flux Precoating and Process Parameter on Welding Performance of Inconel 718 Alloy TIG Welds. Journal of Materials Engineering and Performance 23: 125–132

[5] A. A. SychevA. V. ElpatovV. G. ProvotorovO. N. Polozenko (1984) Experience in the introduction of plasma arc welding of commercially pure aluminum. Chemical and Petroleum Engineering 20: 263–265

[6] T. Ishida (1987) Interfacial phenomena of plasma arc welding of mild steel and aluminium. Journal of Materials Science 22: 1061–1066

[7] Tanju Teker, Niyazi Özdemir (2012) Weldability and joining characteristics of AISI 430/AISI 1040 steels using keyhole plasma arc welding. The International Journal of Advanced Manufacturing Technology 63: 117–128

[8] Zhonglin Gao, Shengsun Hu, Fengliang Yin, Rui Wang (2008) Modeling of arc force in plasma arc welding. Transactions of Tianjin University 14: 157–163

[9] T. Q. LiC. S. Wu (2015) Numerical simulation of plasma arc welding with keyhole-dependent heat source and arc pressure distribution. The International Journal of Advanced Manufacturing Technology 78: 593–602

[10] Hyeong-Soon Moon, Sung-Hoon Ko, Jeong-Cheol Kim (2009) Automatic seam tracking in pipeline welding with narrow groove. Int J Adv Manuf Technol 41:234-241

[11] Hong Luo, Xiaoqi Chen (2005) Laser visual sensing for seam tracking in robotic arc welding of titanium alloys. Int J Adv Manuf Technol 26:1012-1017

[12] Paul A. Fleming, Christopher E. Hendricks, D. M. Wilkes, George E. Cook, Alvin M. Strauss (2009) Automatic seam-tracking of friction stir welded T-joints. . Int J Adv Manuf Technol 45:490-495

[13] Shen Hongyuan, Huang Xixia, Lin Tao, Chen Shanben (2009) Weld formation control for arc welding robot. Int J Adv Manuf Technol 44:512-519

[14] Zhou L, Lin T, Chen SB (2006) Autonomous acquisition of seam coordinates for arc welding robot based on visual servo. J Intell Robot Syst 47:239–256

[15] D. N. Trushnikov, V.Ya. Belenki'y, G. M. Mladenov, N. S. Portnov (2012) Secondary-Emission signal for weld formation monitoring and control in eletron beam welding (EBW). Materialwissenschaft und Werkstofftechnik 43:892-897

[16] D.N. Trushnikov E.G. Koleva, G.M. Mladenov, V. Ya. Belenkiy and E.S. Salomatova (2013) Weld Formation Control at Electron Beam Welding with Focal Spot Scanning. Middle-East Journal of Scientific Research 16: 1062-1068

[17] Zhang GJ, Chen SB, Wu L (2005) Intelligent control of pulsed GTAW with filler metal. Weld J 84(1):9–17

[18] Fan CJ, Chen SB, Lin T (2006) Visual sensing and image processing in aluminum alloy welding: 2006 International Conference on Robotic Welding, Intelligence and Automation, Lecture Note in Control and Information Sciences 362:275–280

[19] C.S. Wu, L. Wang, W.J. Ren, X.Y. Zhang (2014) Plasma arc welding: Process, sensing, control and modeling. Journal of Manufacturing Processes 16:74-85

[20] Zu Ming Liu, ShuangLin Cui, Zhen Luo, ChangZhen Zhang, ZhengMing Wang, YuChen Zhang (2016) Plasma arc welding: Process variants and its recent developments of sensing, controlling and modeling. Journal of Manufacturing Processes 23: 315-327

[21] Guokai Zhang, Chuan Song Wu, Xinfeng Liu (2015) Single vision system for simultaneous observation of keyhole and weld pool in plasma arc welding. Journal of Materials Processing Technology 215: 71-78

[22] Zuming Liu, Chuan Song Wu, Jinqiang Gao (2013) Vision-based observation of keyhole geometry in plasma arc welding. International Journal of Thermal Sciences 63: 38-45

[23] Di Wu, Huabin Chen, Yiming Huang, Yinshui He, Minghua Hu, Shanben Chen (2017) Monitoring of weld joint penetration during variable polarity plasma arc welding based on the keyhole characteristics and PSO-ANFIS. Journal of Materials Processing Technology 239: 113-124

[24] ZuMing Liu, ChuanSong Wu, ShuangLin Cui, Zhen Luo (2017) Correlation of keyhole exit deviation distance and weld pool thermo-state in plasma arc welding process. International Journal of Heat and Mass Transfer 104: 310-317

[25] Yan Li, Yanhui Feng, Yafei Li, Xinxin Zhang, Chuansong Wu (2016) Plasma arc and weld pool coupled modeling of transport phenomena in keyhole welding. International Journal of Heat and Mass Transfer 92: 628-638

[26] Guokai Zhang, Chuan Song Wu, Zuming Liu (2014) Experimental observation of both keyhole and its surrounding thermal field in plasma arc welding. International Journal of Heat and Mass Transfer 70: 439-448

[27] M. Yuda, M. Tao (2009) Application of visualize technology for arc welding. Kawada Technical Report 28:106-109

[28] Y. M. Zhang, S.B. Zhang (1999) Observation of the keyhole during plasma arc welding. Welding Journal 78:53s–8s.

[29] MTI Instruments Inc (2014) An Introduction to Laser Triangulation Sensors. http:// www.azosensors.com/article.aspx?ArticleID=523

[30] Z.M. Liu, C.S. Wu, J. Q. Gao (2013) Vision-based observation of keyhole geometry in plasma arc welding. International Journal of Thermal Science 63:38–45.

[31] Z. M. Liu, C. S. Wu, M. A. Chen (2012) Visualizing the influence of the process parameters on the keyhole dimensions in plasma arc welding. Measurement Science and Technology 23:105603.

[32] Aksoy, M. S., O. Torkul, and I. H. Cedimoglu (2004) An industrial visual inspection system that uses inductive learning. Journal of Intelligent Manufacturing 15.4: 569(6).

[33] ZuMing Liu, YueXiao Fang, ShuangLin Cui, Song Yi, JiaYu Qiu, Qu Jiang, WeiDong Liu, Zhen Luo (2017) Keyhole thermal behavior in GTAW welding process. International Journal of Thermal Sciences 114: 352-362

[34] Jiajing Pan, Shengsun Hu, Lijun Yang, Shujun Chen (2016) Numerical analysis of the heat transfer and material flow during keyhole plasma arc welding using a fully coupled tungsten–plasma–anode model. Acta Materialia 118: 221-229

[35] Xiaoxia Jian, Chuan Song Wu (2015) Numerical analysis of the coupled arc–weld pool–keyhole behaviors in stationary plasma arc welding. International Journal of Heat and Mass Transfer 84: 839-847

[36] Xingxing Shen, Wenxing Bao (2014) The Remote Sensing Image Matching Algorithm Based on the Normalized Cross-Correlation and SIFT. Journal of the Indian Society of Remote Sensing 42: 417–422

[37] Yehu Shen (2011) Efficient normalized cross correlation calculation method for stereo vision based robot navigation. Frontiers of Computer Science in China 5: 227–235

[38] H. Nohara (2012) How‐nual Visual Text Book. Shuwasystem, Japan.

[39] 1. J. Matsuda, A.Utsumi (1988) TIG or MIG Arc Augmented Laser Welding of Thick Mild Steel Plate, Joining & Materials, 1:31

[40] Herbert Staufer (2007) Hybrid welding for the automotive industry, Welding Journal;Oct, 86, 10:36

[41] S. Kanemaru; T. Sasaki; T. Sato; M. Tanaka (2012) Basic Study on TIG-MIG Hybrid Welding Process, Q. J. OF THE J.W. S,30,1:29-34;

[42] S.Asai, T.Ogawa, Y.Ishizaki, T.Minemura, H.Minami and S.Miyazaki, Application of Plasma-MIG Hybrid Welding to Dissimilar Joint between Copper and Steel, IIW Doc. No.XII-1972-09

[43] Yan BAI, Hong-ming GAO,Lin WU, Zhao-hui MA, Neng CAO (2010) Influence of plasma-MIG welding parameters on aluminum weld porosity by orthogonal test, Trans. Nonferrous Met. Soc. China, 20: 1392-1396

[44] S. YAMANE, T. GODO, K. HOSOYA, T. NAKAJIMA, H. YAMAMOTO (2013) Detecting and Tracking of Welding Line in Visual Plasma Robotic Welding. Quarterly Journal of the Japan Welding Society, 31: 175-180